ON THE GENERATION OF SHOCK WAVES IN AN INVERSE PINCH

Thesis by

F. Y. Sorrell, Jr.

In Partial Fulfillment of the Requirements

For the Degree of

Doctor of Philosophy

California Institute of Technology

Pasadena, California

1966

(Submitted May 26, 1966)

ACKNOWLEDGMENT

The author wishes to express his appreciation to Professor H. W. Liepmann, who introduced him to this field of study and under whose direction the research was carried out. In addition, the help of Mrs. Geraldine Krentler in typing the manuscript is gratefully acknowledged. He would also like to thank Mr. B. H. Suzuki, who painstakingly converted the original manuscript into English.

The author is indebted to the California Institute of Technology for various forms of financial assistance, and to the National Aeronautics and Space Administration for their fellowship support for one year of study. He is also grateful to the Office of Naval Research, who supported the experiments.

ABSTRACT

A problem inherent in magnetic shock tubes is the difficulty of achieving separation of the driving current sheet and the shock wave. If such devices are to be applied to produce shock waves for experimentation, then separation will usually be a necessary requirement. In the present experiments in an inverse pinch shock tube, preliminary measurements showed that not only was separation not achieved, but under certain conditions the shock was actually found to be located far behind the front of the current sheet. This appeared to be a paradoxical case of the shock wave pushing the piston. Moreover, measurements of the current sheet velocity indicated that the interaction of the current sheet with the gas should be strong enough to sweep up all the gas encountered by the current sheet and thus to produce a shock wave moving ahead of it. In order to find explanations for the absence of separation and for some other puzzling aspects of these early experiments, further measurements were made to study in more detail the processes taking place in the device. These included measurements of the radial electric field with electrostatic probes and of the ionization levels by the technique of spectral line broadening. The results of these measurements show that the degree of ionization is surprisingly low and that the amount of gas leaking

ABSTRACT (cont.)

through the current sheet is significantly high in some cases. The conclusion is then reached that although the so-called "snowplow model" is successful in predicting the current sheet velocity, it does not lead to the correct picture of the physical processes taking place. Finally, conditions for which separation may be achievable are inferred from the experiments.

TABLE OF CONTENTS

TABLE OF CONTENTS (cont.)

LIST OF FIGURES

LIST OF FIGURES (cont.)

LIST OF TABLES

I. INTRODUCTION

1.1 Generation of Shock Waves in Magnetic Shock Tubes

In the field of Fluid Mechanics the study of shock waves has proved to be a very fruitful area of research. Thus, it was natural to extend the range of investigation to the field of very strong shock waves, which promises to produce many new and interesting phenomena. The shock wave itself is not the only object of interest; as the shock wave becomes stronger the shocked gas also exhibits many interesting and unexplored effects. Of these, the processes of dissociation and ionization, the rates at which they occur, and the atomic properties of the gas appear particularly to be of interest.

This has led to the development of a number of new experimental techniques for producing strong shock waves since conventional shock tubes are capable of producing only relatively low Mach number shock waves. For example, if one wished to produce shock Mach numbers larger than 15 in Argon, or 6 in Hydrogen, other methods must be used. Of the various experimental devices that have been proposed, those which use the principle of magnetohydrodynamic acceleration show the best theoretical performance. These devices have no inherent limit on the shock Mach number that can be generated and have application where high Mach numbers are desired in light gases such as Hydrogen or

Helium. Strong shocks in light gases are of interest because these gases generally have atomic properties such as energy levels, spectroscopic data, etc., that are more completely known.

All of these shock tubes are based on the idea of using a sheet of current as the piston to accelerate the gas and thus produce the shock wave. An inherent problem in these devices is that of obtaining separation of the shock wave and the driving current sheet (piston). If the shock wave were to occur somewhere inside the current sheet, it would not be possible to determine which changes in the state of the gas were caused by the shock wave and which were caused by the current sheet. Moreover, it would also be difficult to determine the conditions immediately ahead of the shock. When these conditions are not known, the speed of sound ahead of the shock and thus the shock strength (Mach number) cannot be found. It is also clear that when this occurs there is no uniform region of shock-heated test gas in which experiments can be made. Therefore, if the purpose of the experiments is the study of strong shock waves (or the shock heated gas), separation of the shock wave and the piston is usually essential.

At high Mach numbers the gas is highly compressed and the separation of the shock and piston is small. The diffusing current sheet may then occupy a large part of the

separation distance, making it difficult for the shock to move ahead of the current sheet. In addition, it is clear that an appreciable amount of the gas must not leak through the piston. If gas does leak through the piston, the ideal separation (i.e., the distance between the shock wave and an ideal, impermeable piston) of the shock from the piston will be reduced. When this leakage is large it may preclude the possibility of obtaining separation of the shock and current sheet. All magnetic shock tubes have experienced these difficulties in obtaining separation, and in fact, the author knows of only a single case where there is reason to believe that separation may have been achieved (Ref. 1).

The present work is an investigation of the problem of separation in a specific device, the inverse pinch shock tube. A description of the inverse pinch and the main characteristics of its operation are given in the following part of this section (Sec. 1.2).

Some of the first experiments using the inverse pinch as a shock tube were performed by Vlases (Ref. 2). The experiments gave no evidence of separation, and in addition, some details of these experiments were not completely understood. At that time one of the more puzzling results was the position at which the shock occurred. In particular, for the experiments in Argon the shock appeared to occur at the trailing edge of the current sheet. In analogy with conventional shock tubes, this meant that the piston

actually preceded the shock! In order to understand this phenomenon and also to determine under what conditions separation could be achieved, additional experiments were undertaken to obtain more detailed measurements.

The device in which the present experiments were performed was an improved version of the one originally used by Vlases, and in addition, several improvements in the instrumentation were incorporated (Sec. 2.1). In the first of these experiments, measurements were made to determine more accurately the relative position of the shock within the current sheet and were extended to include a wider range of gases and current sheet speeds. The conditions under which these measurements were made are given in Table 1 (the experiments of Vlases (Ref. 2) were in Argon and Helium at 12 KV). The relative position of the shock was measured accurately and a summary of the results of these measurements is given in Table 3 (these measurements will be described and discussed in section 2.2). The results show a wide range in the relative position of the shock, ranging from the extreme leading edge of the current sheet (Hydrogen, 14 KV, 500 μHg) to the extreme trailing edge (Argon, 14 KV, 500 μHg).

Although separation never occurred in these experiments, it was closely approached in some cases. The anticipation was that if the mechanism which governed the shock position within the current sheet could be determined,

then some insight might be gained about the conditions necessary for the shock to move ahead of the current sheet. Thus, the investigation of what determines the relative position of the shock seemed closely related to determining what must be done in order to obtain separation. Consequently, much of the work was devoted to defining as accurately as possible what controls the shock position within the current sheet.

During the early stages of the experiments described above, it appeared that the diffusion of the current sheet might be largely responsible for the absence of separation (see Sec. 3.1), but this did not explain many of the details. In particular, they did not reveal exactly what had to be done to achieve separation and what determined the relative position of the shock within the current sheet. When the single fluid equations were used to calculate the current sheet widths (Sec. 3.2), the calculated results were in poor agreement with the experiments. Hence, another important unanswered question was what controls the current sheet width. This may be directly related to the problem of achieving separation (Sec. V). For these reasons, a further investigation of the processes taking place in the device appeared necessary.

Section III contains a survey of conditions that may prevent separation. This analysis was carried out in an attempt to determine the factors which may be important in

preventing separation. These factors were then used as a guide in planning the subsequent experiments which are described in section IV. The general approach of these experiments was to investigate the interaction of the current sheet with the gas that is swept up. Measurements of the radial electric field were made with electrostatic probes in order to determine whether the electrons carried the current and to estimate the degree of ionization. In addition, the charged particle number density was measured by using the technique of spectral line broadening.

The results of these measurements led to a much better picture of the interaction process between the current sheet and the gas. In section V a physical model is proposed to explain the observed behavior of the current sheet widths and the relative positions of the shock. While this model shows that separation of the shock wave and current sheet should not have been expected for these experiments, it does indicate a range of operation where it appears reasonable to expect it.

1.2 The Inverse Pinch Shock Tube

Since a detailed description of the inverse pinch shock tube is given in reference 2, only its major features will be described here. A side view of the cylindrical device is shown in the schematic diagram of figure 1. It consists essentially of a glass chamber under vacuum within which are contained two 6 inch diameter electrodes and an insulated center conductor. The conductor and the bottom electrode are in turn connected across a capacitor bank which can be discharged by ignitron switches. In operation, a discharge is initiated between the electrodes and forms into a thin annular current sheet about the insulated center conductor. The Lorentz force between this current sheet and the magnetic field, produced by the current flowing in the center conductor, then pushes the current sheet radially outward like an expanding cylinder. If the gas within the current sheet is highly conducting, the current sheet should behave much like a piston and one would expect a shock wave to form in front of it.

A further explanation of this seems to be in order here. When the gas is considered as a single conducting fluid, the degree which the current sheet interacts with the fluid depends largely on its electrical conductivity. If the gas has a low conductivity, the current sheet tends to be diffuse and is permeable to the gas. Clearly no

satisfactory form of separation can be expected for this case. On the other hand, if the gas is highly conducting, the current sheet should be thin and impermeable to the gas. When this occurs the shock must form ahead of the current sheet. Therefore, the actual operation of the device depends, to a great extent, on the electrical conductivity of the gas.

The advantages of the inverse pinch geometry over other configurations were discussed at some length by Vlases (Ref. 2). Two significant points seem worth repeating here. First is the gross stability and reproducibility of its operation. Dramatic evidence of this is given by the measurements of the current sheet and shock trajectories plotted in figures 6-24. These measurements will be discussed in detail in sections 2.3 and 5. The reproducibility exhibited by the data in these figures is remarkable in view of the fact that each experimental point had to be obtained by a separate firing of the device, i.e., one shot at a time. Furthermore, the data shown in figures 28 and 29 for the line broadening experiments (c.f. Sec. 4.3) indicate that the radiation is also reproducible. Such reproducibility is unusual for magnetic shock tubes, and the inverse pinch appears significantly superior in this respect.

Another advantage attributable to the inverse pinch is that it is simple to operate at constant current sheet

speed. That constant speed is indeed achieved in the experiments is readily evident from the linearity of the trajectories plotted in figures 6-24. Moreover, this speed can be easily predicted theoretically by using the so-called "snowplow" model, in which the current sheet is assumed to be infinitesimally thin and the gas dynamic pressures are assumed to be small compared to the magnetic forces and the momentum of the gas (for a more detailed discussion of this model, see references 3 or 4). Thus, the magnetic force on the current sheet is simply equated to the change in momentum of the gas. In calculating this change in momentum, it is further assumed that all of the gas encountered by the current sheet is swept up into a thin layer on the front of the current sheet and accelerated to the current sheet speed (hence, the term "snowplow"). When the simple momentum equation derived under the above assumptions is solved, it is found that a current sheet moving with constant speed is obtainable with a linearly increasing current. The formula obtained in this case for the constant current sheet speed, U_{sp}, is

$$U_{sp} = \left[\dot{I}^2 \frac{\mu_o}{8\pi^2 \rho_o}\right]^{\frac{1}{4}} \qquad (1)$$

where μ_o is magnetic permeability of free space, ρ_o is the initial mass density to which the chamber is filled, and $\dot{I}$ = constant is the rate of current increase. Note that if

$\dot{I}$ is given, then U_{sp} depends only on ρ_o.

It should be mentioned here than an exact similarity solution using the full equations of motion under the assumption of infinite conductivity has also been given in reference 3. The current sheet speed given by this exact solution agrees closely with that given by the "snowplow" theory.

In the experiments, the rate of current increase, $\dot{I}$, depends only on the external circuit inductance, L, and the capacitor bank voltage V. Enough capacitance is used so that the current continues to increase linearly at the end of the experiment (since the current wave form is a damped sine wave, only the first part of the quarter cycle is used where the current increases almost linearly). The rate of current increase, $\dot{I}$, is then given approximately by

$$\dot{I} = V/L \qquad (2)$$

where V is the capacitor bank voltage and L is the circuit inductance.

All of the experiments were carried out at either of two capacitor bank voltages and with the following circuit characteristics.

14 Kilovolt Operation

Diameter of the device	6"
Dimension between electrodes	4"
Total circuit inductance	0.30 μh
Bank capacitance	30.0 μf

25 Kilovolt Operation

Dimensions as above	
Total circuit inductance	0.35 μh
Bank capacitance	13.6 μf

Using these circuit parameters, the "snowplow" speeds were calculated for the conditions of the present experiments, and are given under the column, U_{sp}, in Table 1. The measured speeds corresponding to these are tabulated in the next column. The calculated and measured speeds are seen to be in excellent agreement (these results will be discussed in more detail in section 2.2).

II. MEASUREMENT OF CURRENT SHEET AND SHOCK WAVE TRAJECTORIES

2.1 Description of Experimental Techniques

The experiments to be described here were the first to be performed in the present work and were carried out in a device similar to that used by Vlases (Refs. 4, 5). However, two modifications were made to improve on the operation of the device. First, the anode was modified in such a way that a charge layer observed on it was removed. Figure 4 shows this modification which amounted essentially to reducing the size of the anode. A complete analysis of this anode layer is presented in appendix E. Second, the center insulator of the device was changed from teflon to fused quartz, when it was discovered that the teflon insulator was prone to ablation in the presence of the discharge and added impurities to the gas. These impurities were detected by a decrease of the current sheet speed in the lighter gases. With the quartz insulator no deviation from "snowplow" speed was observed. In addition, the absence of impurities was verified when time integrated spectra with the quartz insulator showed no impurity radiation for operation at 14 KV, and only two silicon lines for operation at 25 KV.

The range of current sheet speeds possible in this device is presently bracketed at the low end by the speed

at 14 KV, 500μ, in Argon and at the high end by the speed at 25 KV, 100μ, in Hydrogen. The lower limit is fixed by the requirement of a linearly increasing current for the duration of the experiment; and the upper limit by the requirement of a high enough initial pressure such that the impurity level is still low and the mean free path is still small compared to the dimensions of the device.

The objective of these experiments was to determine as accurately as possible the position of the shock wave within the current sheet. This was accomplished by measuring the passage of the current sheet and pressure front using the same basic techniques employed earlier by Vlases (Refs. 4, 5), but with some modifications.

In his experiments, Vlases used a pickup coil enclosed in a glass tube to detect the passage of the current sheet. However, Camac (Ref. 6) has reported finding a difference in such measurements depending on whether the coil was enclosed or left unenclosed. For this reason, both enclosed and open probes whose general construction is shown in figure 3 were used. Both probes gave the same measurement for the arrival times of the current sheet front and of its peak current density. The only difference found between the two probes was in the detection of the trailing edge of the current sheet, which the enclosed probe measured as passing by later in time. This may be explained by the fact that the plasma at the

rear of the current sheet is more highly conducting than at the front, and trapping of the magnetic field by the plasma is stronger here. Consequently, the time required for the field to diffuse into the enclosed coil may become significant in this region of the current sheet, thus accounting for the time lag.

It should be pointed out that the magnetic probes do not measure current density directly, but actually measure the time derivative of the azimuthal magnetic field, $\dot{B}_\theta$. However, the arrival of the current sheet leading edge and the passage of its trailing edge can be taken directly from the probe data. The peak in current density was found to be sufficiently close to the peak in the probe signal ($\dot{B}_\theta$ peak) that the presentation of either gives the same trajectory, within 1 to 3%. For this reason the trajectory designated peak in the figures 6-24 is considered to be both the peak in the probe signal and the peak in the current density. A further discussion of this as well as a description of how the current density is obtained from the probe data is given in appendix F.

The arrival of the pressure front was detected with a piezoelectric pressure transducer identical to that developed and used by Vlases (Ref. 5). However, the circuit was modified by inserting a cathode follower immediately after the transducer to match the transducer and cable

impedances. This reduced the noise considerably and thereby improved the accuracy of the measurement. A diagram of the cathode follower circuit is shown in figure 5. Only the arrival time of the pressure front could be measured with this probe. No attempt was made to measure the actual magnitude of the pressure pulse because the output of the probe appeared to depend not only on the pressure but also on a variety of other conditions such as the age of the probe. Moreover, the output was also found to be oscillatory. This latter behavior can be seen in a typical trace of the probe output given in figure 4, which also shows the low level of the noise. The risetime of the probe was calculated to be 0.2 to 0.3 μsec. There is also a delay of approximately 0.2 μsec in the signal of the probe due to the glass front plate (Ref. 4). The presented data are corrected for this delay.

Some comments will also be made here about the errors that are present in these measurements. The principal errors in the data are those due to timing. In particular, it was difficult to exactly synchronize the firing of the device with the triggering of the oscilloscope used to record the data. This difficulty in synchronization was compounded when more than one oscilloscope was used. The errors from this source exhibit themselves in the greater scatter in the data taken at the higher current sheet speeds for which, of course, higher sweep speeds were used. For

example, from the magnetic probe data for Hydrogen at 100μ Hg and 25 KV, it appears that the beam recording this data was triggering approximately 0.2 μsec early. As one would expect, this error was not significant at the lower sweep speeds. An additional error arose because the beams did not sweep at exactly the same speed. As much as 10% difference in the sweep speeds of the two different oscilloscopes was found at sweep speeds of 0.5 μsec/cm and faster.

2.2 Experimental Results

Figures 6-24 present the current sheet and pressure front trajectories mapped out from the data obtained by the measurements. The pressure probe data, the enclosed magnetic probe data and the open (unenclosed) magnetic probe data are all given on separate plots. These separate plots were necessary to prevent excessive overlapping of the data from obscuring the results. In cases where the measurements of the two types of magnetic probes were the same, only a single set of data is given. There are two exceptions to the above format. For Hydrogen at 25 KV, 500 μHg, no open magnetic probe data was obtained; for Argon at 25 KV, 500 and 100 μHg, the pressure and both magnetic probe data are plotted together in figures 18 and 19.

A number of important quantities are taken directly from these plots. Among these are the propagation speeds of the current density peak. These are tabulated, as previously mentioned, in Table 1 and will be compared to those predicted by "snowplow" theory in the next section. Another is the width of the current sheet which is tabulated in Table 2, and will be used in discussing current sheet diffusion (Sec. 3.2). One of the most important quantities is the position of the shock wave relative to the current sheet. This position may be given either at a fixed time

or at a fixed radial station. The latter is chosen here (expressed in units of time to arrive at the station) because it was found that the relative position of the shock did not vary much with radial position. This behavior can be seen in figures 18 and 19 in which the pressure and current sheet data are plotted together. It may be verified in other cases by superimposing the pressure and current sheet data. Because of this characteristic behavior of the shock in these experiments, it is possible to define a relative shock position R, which is approximately independent of the radial station in most cases. R is defined, at any fixed radial station, as the ratio of the distance of the shock from the leading edge of the current sheet to the total width of the current sheet (distances being measured in units of time). Values of R taken from the plots of figures 6-24 are given in Table 3. However, no value of R is given for the experiments in Hydrogen at 25 KV because it was found to vary considerably with the radial station. The importance of this parameter will be discussed in section V in connection with the possibility of achieving separation.

2.3 Comparison with Theory

As discussed in section 1.2, the exact similarity solution and "snowplow" theory give approximately the same value for the current sheet (or piston) speed. This speed will be compared with the speed of the current density peak. Alternatively, the speed of the current center of gravity could be used for this comparison but the difference between the two is not significant. Both the predicted and measured speeds are tabulated in Table 1, and as can be seen, the agreement between the two is excellent. This agreement holds over a wide range of conditions and could hardly be considered fortuitous.

In view of this excellent agreement, one would usually conclude that the conditions assumed in the theoretical model are actually approached in the experiment. In particular, "snowplow" theory assumes that all of the fluid encountered by the current sheet is swept up (i.e., the current sheet does not leak). On the other hand, if there were appreciable leakage of the current sheet in the experiment, one would not expect the measured current sheet speed to agree with that predicted from this theory. Therefore, one is led to conclude that the current sheet must not leak. This in turn means that the interaction between the current sheet and the gas must be strong, which is possible only if the current sheet gas is highly ionized. Hence,

one is also led to the conclusion that the current sheet gas must be fully ionized.

However, at this point, the steps leading to the conclusions drawn should be more closely scrutinized. First of all, it should be noted that the selection of the speed of the current density peak for comparison with the predicted speed was somewhat arbitrary, particularly in cases where the current sheet is quite diffuse. For example, if this comparison were made with the speed of the shock front, the agreement would not be nearly as good. In fact, in Argon at 14 KV, 500 μHg, the shock speed is 30% slower than the predicted speed and 3% faster in Hydrogen at 14 KV, 500 μHg. Secondly, as was shown in section 1.2, the relationship for the current sheet speed shows that it depends on the initial density only to the negative ¼ power. Because of this weak dependency on density, one should not expect the current sheet speed to vary much even if the leakage through the current sheet is large. Thus, despite the apparent success of "snowplow" theory, the conclusion drawn from it about the possibility of the current sheet leaking may in fact be incorrect.

III. SURVEY OF CONDITIONS THAT MAY PREVENT SEPARATION

3.1 Introduction

Two possible mechanisms which may be preventing separation (i.e., causing the shock to be embedded some where inside the current sheet) are explored here. The first possibility is that the current sheet or piston is not thin but diffusive. The current sheet may be diffusing faster than the shock is separating from the current sheet. The second is the possibility that the current sheet may be leaking. That is, the interaction of the current sheet with the gas may be weak. A third possibility that should be discussed is that the current sheet may not be the actual piston. That is, the current may not act directly on the gas, but interacts with it by some intermediate mechanism so that the gas is accelerated after the current sheet has passed. This type of argument has been forwarded by the author previously (Ref. 7). While additional experiments have shown that the mechanism proposed in reference 7 is not as significant as originally expected, the idea that the current sheet may not accelerate the gas until the major part of it has passed still has validity. This will be considered later in section V, where a description of the interaction of the current sheet with the gas is given.

Also to be discussed here is the problem of layers or sheaths growing on the electrodes or other surfaces.

If such layers are large enough to interact with the moving shock wave or current sheet, they may have a detrimental effect on the performance of the device. Such layers are observed under certain conditions and their effect on the operation of the device should be determined.

3.2 Diffusive Piston

Both Kantrowitz (Ref. 8) and Vlases (Ref. 9) have previously put forth the idea that separation can be prevented because the leading edge of the current sheet is diffusing faster than the shock is separating from the current sheet (i.e., the piston). In order to express this quantitatively, one must calculate the diffusion of the current sheet front from some effective location of the piston. It will simply be assumed here that this effective location is at the center of the current sheet. One must then compare one-half of the total diffusion width of the current sheet to the so-called ideal separation of the shock, which has been defined (c.f., Sec. 1.2) as the distance separating the shock and an ideal, impermeable piston.

The ideal separation of the shock can be calculated with reasonable accuracy. The details of this calculation are given in appendix C, and the resulting values are tabulated in Table 2. The time picked for the comparison is the time at which the current sheet leading edge is about to reach the outer edge (maximum radius) of the electrodes and is also given in Table 2. The diffusion width of the current sheet is usually estimated using the theory of Falk and Turcotte (Ref. 10). This theory can be expected to be valid for conditions in which the

electrical conductivity is high and the single fluid equations are an accurate approximation. It gives the estimate

$$\Delta = \sqrt{\frac{t}{\mu_o \sigma}} \qquad (3)$$

where Δ is the diffusion width, t is the time, μ_o is the magnetic permeability of free space and σ is the electrical conductivity. The value of the electrical conductivity is calculated using the expression given by Spitzer (Ref. 11) for a fully ionized gas (the justification for using the equation for a fully ionized gas is given in section V or reference 11). The temperature used in this calculation is the equilibrium temperature behind a shock moving with the current sheet speed (c.f., Table 1).

Values of the current sheet diffusion width, Δ, calculated from the above formula are tabulated in Table 2. These may be compared with the measured widths tabulated in the preceding column of this table. Considerable differences are seen to exist between the measured and calculated values.

These discrepancies may be partially explained by the fact that a poor estimate of the temperature was used in calculating the electrical conductivity. The gas behind the shock is probably not in equilibrium, in which case the temperature that is used is incorrect. Furthermore, in the theory of reference 10, the shock is assumed to be

completely separated from the current sheet such that there is no interaction between the two; but this is never true in the experiments.

However, even when these factors are taken into consideration, it is still difficult to understand some of the discrepancies. In particular, the calculated widths for Hydrogen are roughly twice those calculated for Argon; whereas the measured widths show the opposite behavior. There is certainly no reason to expect the electrical conductivity to be lower in Argon than in Hydrogen, and probably little reason to expect the magnetic Reynolds number to be lower (Ref. 2). The magnetic Reynolds number is defined as $R_m = \mu_o \sigma r U_{sp}$, where μ_o is the magnetic permeability of free space, σ is the electrical conductivity, r is the radius and U_{sp} is the "snowplow" speed. Hence, based on conductivity arguments alone it is difficult to see why the current sheet is thinner in Hydrogen. Other discrepancies arise when one examines the R-t plots of figures 6-24. The diffusive theory predicts a parabolic spread of the current sheet with time, but the R-t plots exhibit a wide variation of spreading rates ranging from constant width to linearly increasing width. Also the results in Argon indicate that the shock position is quite stable at the rear of the current sheet, and in figure 18, one sees that the shock front actually appears to be moving to the rear of the current sheet. This is primarily because

the current sheet width does not grow parabolically and is certainly not compatible with the idea that the growth is entirely diffusive. It seems clear to the author that under the conditions of the experiment in Argon, the shock will never emerge from the current sheet regardless of how far it is allowed to propagate. For this reason the author believes a comparison of the calculated diffusion width (Eq. 3) to the ideal separation is not a completely valid criterion to be used in predicting separation. These discrepancies in the theory are attributed to the fact that the single fluid equations are not adequte for describing the physical process.

It is pointed out that for the experiments in Hydrogen at 14 KV, the measured current sheet width is only slightly larger than ideal separation. If one-half of the current sheet width is used as a criterion, separation should have been achieved in these experiments. As the shock did occur at the current sheet leading edge and the ideal separation is only slightly larger than one-half of the current sheet width, this does not allow one to conclude that separation will or will not be achieved by a further reduction of the current sheet width.

3.3 Leaking Piston

The amount of fluid the piston leaks can be determined by a measurement of the mass left after the piston has passed. If the gas was a single fluid (i.e., was composed of only one species of particles) then the leakage could be found by a measurement of the number density or mass density of that species immediately after passage of the piston (laboratory coordinates). In these experiments the fluid consists of both ionized gas and neutral gas, and a determination of the total piston leakage requires a measurement of both densities.

The ionized gas number density can be obtained by the line broadening technique to be described in section 4.3, and this was done for all cases where the technique was used to determine number density within the current sheet. No simple means of finding the neutral gas mass or number density was devised, and thus the measurement was not made. Hence, as the degree of ionization is unknown, the measurement of the ionized number density alone does not usually yield any significant information. There is an exception to this, and that is when the ionized mass density is sufficiently large that it implies significant piston leakage even when the neutral mass density is unknown.

The experiments in Hydrogen and Helium are examples

of the former, because the number of ionized particles is low throughout the current sheet and after it has passed. This number density is so low that it alone does not indicate appreciable piston leakage, and until the degree of ionization is known nothing significant can be said about the amount the piston leaks. For this reason a measurement of the ionized number density does not permit any conclusion about piston leakage for either Hydrogen or Helium.

In Argon (14 KV, 100μ) the ionized number density is quite large after the current sheet has passed and this is a case where the measurement of only the ionized number density gives useful information on the amount the piston can leak. Here, even if the degree of ionization is unknown, the amount of mass left behind in this case is appreciable (Fig. 30). The initial filling of the chamber is 3.5×10^{15} particles/cm^3, and this measurement shows that approximately 2×10^{15} ionized particles/cm^3 are left behind the current sheet.

When it is remembered that the current sheet speed is precisely "snowplow" speed, this leakage is so large as to make the validity of the measurement doubtful. Because of this a calculation of the effect of the leakage on the current sheet speed was made, and it is given in appendix D. The calculation shows that the observed amount of leakage

would result in only 6% increase in the current sheet speed. Thus the observation of a large quantity of gas leaking through the current sheet is not in disagreement with the measurement of the "snowplow" speed. Here, clearly, is a case where the current sheet or piston leaks.

3.4 Electrode Layers

Since the electrodes act as a physical boundary for the flow as well as a surface where charge is given or taken from the gas there is the possibility of both a viscous layer and a charge layer or charge sheath on the electrodes. The existence of these layers is investigated here.

The thickness of the viscous boundary layer and the mass contained in it is calculated in appendix E. The results of this calculation show that the thickness of the layer is quite small compared to the electrode spacing, and thus the mass contained in it is also small. This indicates that viscous effects should not cause any layers on the electrodes that could affect the operation of the device.

A theoretical treatment of the charge layers or sheaths that may form on the electrodes is difficult, if not intractable. In these experiments the presence of these layers was investigated by making a survey of the shape of the current sheet along the axis of the experiment. The survey was performed by using the magnetic probes described in section 2.1. When this was done in the early apparatus (Fig. 1), the current was found to vary along the axis of the experiment. Specifically, the current sheet was observed to be relatively thin and well defined on the

cathode, and it remained that way as one moved away from the cathode toward the anode. Within 2 to 4 cm of the anode (depending on the gas that was used in the experiment) the current sheet spread and covered the entire anode. This picture does not change as the current sheet propagates outward. This implies a large charge layer or sheath on the anode. The layer was examined further with pressure probes, and no distinct pressure front was found in it. Others have observed the presence of this layer in similar devices (Refs. 12, 13).

A detailed explanation of the reason for this layer is given in appendix E. The results of this show that the removal of this layer requires a modification of the anode configuration, and the present device incorporates this. All of the data presented in this work were obtained in an apparatus with this modification.

IV. EXPERIMENTAL INVESTIGATION OF THE CURRENT SHEET BEHAVIOR

4.1 Objectives

The results of the early experiments not only left unanswered the question of why separation was not achieved but raised other perplexing questions as well. Because of the remarkable agreement between the measured current sheet speed and that predicted by "snowplow" theory, it did not appear likely that the current sheet was leaking. Therefore, the idea that separation was prevented because of current sheet diffusion (diffusive piston) seemed very reasonable; the expectation being that the shock would eventually move ahead of the diffusing current sheet ultimately resulting in separation. Basing their approach on this idea, other investigators (Refs. 9, 10) have built larger devices in the hope that the longer test times will allow separation. However, it was shown in the last section that the measured current sheet widths did not agree with those calculated from diffusive piston theory and also that the current sheet did not spread parabolically in time in accordance with this theory. Moreover, it was difficult to explain on the basis of this theory the result in Argon where the shock was found to occur at the very rear of the current sheet.

In the light of these experimental findings, it seemed that the more logical approach to take was to gain a better

understanding of the processes taking place in the existing device rather than to simply build a larger one. The reasoning was that with additional knowledge an improved device could be designed with a higher probability of achieving separation. (A case in point is the development of the modified anode described in section 3.4 for the removal of the anode layer.) Consequently, further experiments were conducted to obtain more detailed information about the current sheet-gas interaction. It is a rather formidable task to perform these experiments over the complete range of conditions at which the early experiments were made. The early experiments are described in section II and the operating conditions for these are given in Table 1. Hence, the range of conditions at which the more detailed investigations were carried out was necessarily reduced. As the experiments in Argon and Hydrogen at 14 KV exhibit a complete range in the variation of the shock position within the current sheet, this more detailed investigation was carried out for operation at 14 KV only. In addition, the measurement of the number density required considerably more effort than that for the radial electric field, and hence, the range of conditions at which the number density measurement was made was further reduced. The purpose of this section is to describe these measurements and discuss their significance

relative to predicting how the current sheet interacts with the gas.

4.2 Radial Electric Field Measurements

In order to understand the current sheet-gas interaction, it is important to know whether the ions or electrons carry the major part of the current. Since the mobility of the electrons is much greater than that of the ions, the assumption that the electrons carry most of the current would seem justified. However, two effects could make this assumption doubtful. The first occurs when $\omega\tau$ for the electrons is much greater than unity, in which case the mobility of the electrons across the magnetic field may be seriously impaired. The other effect arises if the cathode cannot emit electrons freely enough to supply the current, thereby limiting the number of electrons available to carry current.

While the calculation of $\omega\tau$ (see Appendix A) for the electrons indicates that their mobility is not materially reduced due to the first effect at the front of the current sheet, $\omega\tau$ can become of the order of 10 at the rear of the current sheet. This could possibly force the ions to carry some of the current. The second effect has been proposed by some authors (Refs. 12, 13, 14) who have then concluded that the ions must carry the current. However, this appears to be open to question because the present author knows of no experimental or theoretical work that gives positive evidence that this occurs.

In view of these uncertainties, it seemed worthwhile to determine experimentally if the electrons actually do carry the current. A method for making this determination has been suggested by Lovberg and Burkhardt (Ref. 15). It is based on the idea that if the electrons carry the current, the Lorentz force, $\vec{J} \times \vec{B}$, must act directly on the electrons accelerating them to the current sheet speed. The ions in turn will also be accelerated to the same speed by the Coulomb forces which arise due to the charge separation of the ions and electrons (similar to ambipolar diffusion). The radial electric field arising from this charge separation could then be measured and would confirm that the electrons are actually carrying the current.

The magnitude of this radial electric field will depend on the degree of ionization. If the current sheet gas is fully ionized, every incoming ion (or neutral that is subsequently ionized) encountered by the current sheet is accelerated to the current sheet speed by the Coulomb forces. The total potential drop across the current sheet should then simply be equal to the energy of an ion or neutral moving with the current sheet speed (Ref. 16).

If the gas is not fully ionized, the potential drop across the current sheet will be higher. Its magnitude depends on how strongly the ions interact with the neutrals. If the interaction is very strong, the current sheet will not leak and all the ions and neutrals encountered will be

accelerated to the current sheet speed. In this case the average number of neutrals accelerated by each ion can be calculated from the degree of ionization; and the potential drop must be equal to the sum of the energies of this average number of neutrals plus the energy of an ion, all assumed to be moving at the current sheet speed. Conversely, if the current sheet speed and the potential drop is known, the degree of ionization can be calculated. However, if the interaction between the ions and neutrals is weak and there is appreciable current sheet leakage, then the speed to which the neutrals have been accelerated is unknown and neither the potential drop nor the degree of ionization can be calculated from the knowledge of the other.

The measurement of the radial electric field was carried out with the probes whose construction and operation is described in appendix A. The data from these probes were used to find the total potential difference across the current sheet (c.f., Appendix A) and this value is given in Table 4. In order to calculate the degree of ionization one must know the energy of an incoming ion; this was determined and the values of this energy are tabulated in Table 4. Then,assuming that the current sheet did not leak, the degree of ionization was calculated and also tabulated in Table 4. The errors in this measurement can be large, and this coupled with the lack of repeatibility and possible piston leakage makes the degree of ionization that they give somewhat inaccurate (see appendix A for a quantitative discussion). However, they do indicate a surprisingly low degree of ionization in Hydrogen and Helium which is a significant result, even if the possible error is large.

More important, the presence of this radial electric field is taken to be a verification that the electrons carry the current and pull the ions with them. In fact, the measurement of so few electrons (low degree of ionization) and the presence of the electric field essentially requires that this be the physical picture. These results will be discussed in section V where they are of help in deriving a physical picture of the current sheet-gas interaction.

4.3 Charged Particle Number Density Measurements

Because of the uncertainties in the degree of ionization calculated from the radial electric field measurement, an independent measurement of the electron number density was felt to be necessary. The measurement technique that was applied is based on the principle that a spectral line emitted by the plasma is broadened due to the electric field caused by the charged particles in the plasma (a more complete description of this is given in appendix C). This effect is sometimes called Stark broadening or Holtsmark broadening (the origin of these names comes from the people who first developed the theory, and the history of line broadening will not be considered here). The broadening of the line depends almost solely on the charged particle number density and is insensitive to other properties of the plasma such as the temperature. Therefore, a relation can be found between the number density and the broadening of the line. The number density can thus be determined by measuring the profile (intensity versus wavelength) of the broadened line. The measurement technique and the method of obtaining the number density from the line profile are described in appendix C.

The line profiles of emitted lines were measured at the following three conditions: Hydrogen at 14 KV and 500 μHg, Helium at 14 KV and 400 μHg, and Argon at 14 KV

and 100 μHg. As previously mentioned, the measurements at other conditions were not made because of the long and tedious procedures involved in measuring a single line profile. The values of the number density calculated from the line profile measurement at the various conditions are given in Table 5. In the measurements with Hydrogen and Helium, the number density was found to remain constant, within experimental error, both through the current sheet and behind it. This was not true for Argon and the value of the number density given for this gas corresponds to that at the rear of the current sheet. More will be said about this shortly.

For Hydrogen and Helium the ionized number densities are seen to be of the order of 10^{15} electrons/cm^3. Since the number densities at the initial pressures were of the order of 10^{16} particles/cm^3, this indicates a surprisingly low degree of ionization, particularly when the compression of the gas by the shock is considered. It is pointed out that for the Mach numbers in Hydrogen and Helium the equilibrium degree of ionization is quite low (see Table 1). This is true even for Helium since the shock occurs within the current sheet and is probably weaker (see section VI for a discussion of this), hence the ionization due to the shock is even lower than that given in Table 1. Thus the ionization due to shock is seen to be quite low, and these results indicate that the ohmic heating of the current

sheet is not enough to cause appreciable ionization.

The line profile for Argon could be measured only at the rear of the current sheet because the radiation intensity was extremely low at the onset of the current sheet and rose to a value high enough to permit measurement only at the rear. In order to obtain some idea of the number densities existing in the front portion of the current sheet, the continuum radiation was measured through and behind the current sheet. The intensity of this radiation can be shown (Ref. 17) to be proportional to $N_e N_i / T_e^{\frac{1}{2}}$ (N_e is the electron number density, N_i is the ion number density and T_e is the electron temperature) for Bremnstrahlung(free-free transitions) and $N_e N_i / T_e^{3/2}$ for recombination to bound states. However, this is true only if local thermodynamic equilibrium (LTE) exists and there is no cyclotron radiation (radiation due to electrons orbiting in a magnetic field). Based on the criteria of of Griem (Ref. 18), it is almost certain that the first condition is not attained in the present experiments. On the other hand, cyclotron radiation does not appear to be important for the magnetic fields and temperatures which are present here (Ref. 18).

In spite of the absence of LTE and the fact that the temperature is not constant through the current sheet, an estimate of the charge particle number density was made by assuming the continuum radiation intensity was proportional

to the square of N_e (or N_i). This is admittedly only a rough estimate, but as will be seen it does give some useful information. Since the temperature must certainly increase from the leading edge of the current sheet, the value of N_e at the leading edge inferred by the continuum radiation will probably be too large.

The result of the continuum intensity measurement is shown in figure 30. This measurement was made at a fixed radial position and the square root of the continuum intensity is shown as a function of time at that position. As previously mentioned, this is assumed to be approximately equal to the charge particle number density. The procedure gives the number density variation, but it is not an absolute measurement in that the absolute continuum intensity was not measured, and hence the absolute value of the charged particle number density can not be obtained. In order to fix the magnitude at one time, the number density at this time and radial position was obtained by the use of the line broadening technique. Using the value of N_e at this time the scale on the right of figure 30 was added. An additional line broadening measurement was made at a later time, and this value is included also. The data from the line broadening measurements are indicated by the triangles. The value of the number density obtained from the continuum radiation is in surprisingly good agreement

with the number density given by the line broadening technique at the later time, and thus lends confidence to the idea that the continuum radiation is a useful measure of the number density variation.

Several important conclusions can be drawn from figure 30. One can see that the number of charged particles, and therefore the degree of ionization, is extremely small at the front of the current sheet. Also the location of the pressure front is shown and is seen to occur at about the same place where the continuum radiation has its most rapid increase. This result lends considerable support to the idea that the measured pressure front does actually correspond to the passage of a shock wave. Until this result was obtained, it had been a matter of some concern to the author.

The fact that the width of the observed line as well as the continuum radiation does not decrease after the current sheet has passed means that the charged particle number density did not decrease after passage of the current sheet. As this number of ionized particles is not small in relation to the initial filling number density (see Sec.3.3), it is clear that the current sheet is leaking a sizeable amount of gas. A discussion of this leakage was given in section 3.3.

The implications of these results will be discussed in the next section (Sec. V).

Some of the possible errors in these measurements are discussed in appendix C. In addition, it should be pointed out here that the degree of ionization itself cannot be determined from the measurements, but only the number density of ionized atoms (actually only the number density of charges). The total number density must be given in order to be able to calculate the degree of ionization, but it is unknown due to the compression of the gas both by the current sheet and shock. Because of this uncertainty, only a rough estimate of the degree of ionization can be made. However, these estimates are found to be in approximate agreement with the equally rough estimates obtained from the radial electric field measurements (c.f., Table 4 and 5). This is taken to be further evidence that the line broadening measurements are correct.

V. QUALITATIVE DESCRIPTION OF THE CURRENT SHEET

As a result of the measurements described in the previous sections, a much better picture has emerged of the physical processes taking place in the device. In this section a physical model which is consistent with the experimental observations will be described in an attempt to explain the occurrence of the shock within the current sheet. This model gives a description of how the gas is accelerated by the current sheet. When this acceleration mechanism is considered, the conditions most likely to lead to separation can then be inferred in a qualitative manner. The last section (Sec. VI) is devoted to this.

First, it seems appropriate to review some of the experimental observations. There is considerable evidence that the position of the shock in the current sheet depends to a great extent on the width of the current sheet compared to the ideal separation of the shock from the ideal piston. The experiments have shown (see Sec. 2.2) that in Argon where this width is relatively large, the shock occurs far to the rear of the current sheet; whereas in Hydrogen where it is relatively small, the shock occurs at the extreme leading edge of the current sheet. Furthermore, Hoffman (Ref. 19) has recently studied the corresponding theoretical problem by integrating the appropriate single-fluid equations numerically. His results also indicate that when

the current sheet is wide relative to the ideal separation, the shock should form at the rear of the current sheet. This evidence indicates that it is important to establish the physical mechanism which governs the current sheet width in order to determine its apparent relationship to the position of the shock.

It has already been seen that the observed behavior of the current sheet width cannot be satisfactorily explained by simple diffusion alone (c.f., Sec. 3.2). The explanation to be given here is motivated by the experimentally observed fact that the gas is not fully ionized and is based on certain assumptions about the interaction process between the ionized gas and the neutral gas. This will be justified later by a detailed consideration of the possible collisional mechanism between the ions and the neutrals leading to such an interaction. In order to do this, it is necessary to examine in detail how the current accelerates the gas it encounters. This will now be done.

One should note that the shock wave is found to occur within the current sheet for all cases, and hence a model is proposed in which there is a local balance of the momentum given the gas and the magnetic force within the current sheet. This is not entirely correct as behind the shock there will be a lower momentum and higher pressure of the gas. To treat this exactly, the magnetic pressure (or forces) must be balanced by both the momentum given the gas directly by the

current sheet and the gas pressure. For the purpose of this argument it will be assumed that the gas pressure is small relative to the momentum change everywhere, and hence simply consider a local balance of the magnetic force and the momentum given the gas throughout the current sheet.

It should be pointed out that this is in contrast to the theory of Falk and Turcotte (Ref. 10) where the shock is assumed to be ahead of the current sheet and the gas pressure behind the shock is large relative to its momentum. In this case the velocity gradients through the current sheet are negligible and the magnetic pressure gradient simply balances the gas pressure gradient. Hence, the entire current sheet moves at a uniform velocity and can only spread by pure diffusion.

Since the gas is not fully ionized, a significant part of the momentum can be carried by the moving neutral gas, and this gas is assumed to ultimately acquire this momentum from the current sheet. Since the neutral gas cannot be accelerated directly by the magnetic and electrostatic forces, it can only achieve momentum by collisions with the ions. Therefore the momentum transferred to the current sheet is governed by collisions as well as magnetic forces.

For a fully ionized gas, once the field profile (and hence the force distribution) through the current sheet is given, the momentum transferred to the gas is determined.

However for a weakly ionized gas the neutrals can acquire momentum by collisions, and one must give the field distribution and also describe the collision mechanism in order to define the overall momentum transferred to the gas.

Usually it is imagined that a uniform (in some sense) interaction exists through the current sheet, such that the presence of the neutral gas does not distort the magnetic field profile. However, it is clear that one is free to prescribe the neutral-conducting fluid interaction in any manner. If this is done so that the leading edge of the current sheet does not appreciably accelerate the neutral gas, and the trailing edge does, then the requirement of a local balance of the magnetic forces with the momentum given the gas will make the leading edge of the current sheet propagate faster than the trailing edge. When this occurs, the current sheet will spread due to the difference in propagation speeds. Conversely, the leading edge of the current sheet may accelerate a large part of the neutral gas, in which case its rate of spreading would be reduced.

This mechanism must certainly hold at the current sheet leading edge, because there is no shock wave and the gas has to be accelerated directly by the current sheet. Behind the shock this may not be exactly true, as it is possible that the gas pressure is of the same order of magnitude as the momentum change. In any case this can explain the increased propagation speed of the leading edge,

and hence the increased width. The important thing to notice is that the manner in which the leading edge of the current sheet interacts with the neutral gas can greatly affect the rate at which the current sheet grows.

If this model is accurate, then for the present experiments the weak interaction of the current sheet leading edge appears to approximate the conditions in Argon, whereas in Hydrogen the leading edge of the current sheet appears to interact strongly with the neutral fluid. A further indication that this is true is given by the spectroscopic measurements. In Argon there is very little line or continuum radiation emitted in the front part of the current sheet; in Hydrogen, however, the radiation "turns on" at the extreme leading edge of the current sheet. This is taken to mean that the current sheet interacts with the neutral gas as described above.

This mechanism will not necessarily require parabolic growth of the current sheet as in the case of pure diffusion, and it is clear that the rate of growth will depend to a large extent on the details of the interaction of the neutral gas with the conducting gas. This is in agreement with the experiments as they show a wide variation in the manner the current sheet grows in width (c.f., Figs. 6-24).

It is important to note that the electrical conductivity of the gas depends almost entirely only on the electron temperature and only weakly on their number

density (Ref. 11). The presence of a neutral gas does not affect this picture until the number of electrons is less than 1% of the overall number density. This is because of the long range nature of the Coulomb force field, which causes the electrons to collide predominately with the ions (Ref. 11). Hence the collisional interaction between the neutral and conducting gas does not affect the electrical conductivity in any manner, and any effects that the conductivity may have on the field profile are independent of those caused by the current sheet interaction with the neutral gas.

As the neutral fluid-conducting fluid interaction must occur by collisions, an examination of the collision mechanism between the two will now be made. One should note that the variation in this interaction can be due to differences in the number density of the various species as well as a difference in the details of an individual collision.

It is necessary to give a physical picture of the collisional mechanism before any conclusion can be drawn about the relative nature of the current sheet interaction with the neutral gas. This picture is derived from the following conclusions which are based on the experimental results. These are that the electrons carry the current and pull the ions with them due to the condition of overall charge neutrality, that the number densities of the ions

and the electrons are small compared to the number density of neutral particles, and that these neutral particles achieve their momentum by collisions with the ions.

Assuming that the ion-neutral collisions account for the momentum transfer to the neutral gas, a calculation was made of the ion-neutral mean free path (MFP). The largest ion-neutral cross-section is that of charge exchange, and the mean free path for charge exchange collisions is calculated in appendix C and tabulated in Table 5. One assumption in this calculation is repeated here, that is that the number of ionized particles is assumed to be 5% of the initial filling number density for the experiments at 500 μHg initial pressure and 10% for the experiments at 100 μHg. The justification for this is given in appendix B. From Table 5, it can be seen that these values of mean free path are of the same order of magnitude as the current sheet width and it seems unlikely that these collisions are capable of the total momentum transfer to the neutral gas. Also there is little difference between the Hydrogen and Argon charge exchange cross-section, and these collisions are not sufficiently different to account for the observed variation in the two gases. Because of this the charge exchange collision process is considered in greater detail.

A charge exchange collision is the exchange of an electron between the atom and the ion. Thus the collision

only changes the name of the colliding particles (i.e., the atom becomes the ion and vice versa) with no momentum transfer between the two particles. Now consider this collision in coordinates moving with the current sheet. For this case one sees the neutral atoms in the ambient gas moving at the current sheet velocity, into the group of particles making up the current sheet. That is, this group of particles that the neutrals move into are all the ions and atoms fixed with the current sheet (in laboratory coordinates those moving with the current sheet). It is assumed that the electrostatic forces are sufficient that all the ions can be considered as fixed with the current sheet.

A neutral is thus seen as entering the current sheet and undergoing a charge exchange collision with the ions. After the collision occurs the neutral is fixed with the current sheet (the neutral was the ion before the collision), and the ion is traveling through the current sheet. It is now assumed that the electrostatic forces are such that the ion is stopped (becomes fixed in the current sheet) before it undergoes another collision of any kind. The final result of the collision is that it brings the neutral to rest within the current sheet, and also leaves the ion at rest. Thus the collision has doubled the number of particles fixed within the current sheet. This means that in laboratory coordinates some of the neutrals are moving

with the current sheet, as well as all the ions. Note that all the neutrals brought to rest within the current sheet by the charge exchange collision do not remain that way because of elastic collisions with other neutrals. Therefore some of the neutrals are forced out of the current sheet by these elastic collisions.

Any neutral which now enters the current sheet may receive momentum from either the neutrals fixed in the current sheet or the ions. The difference between the experiments in Argon and Hydrogen are thought to be the difference in the nature of the collisions between the neutrals entering the current sheet and those that are fixed in the current sheet. In order to explain this, the following collision mechanism is postulated.

In Hydrogen an appreciable number of neutrals (relative to the number of ions) is built up and moves with the current sheet. Because this number is larger than the number of ions, the neutral-neutral MFP will be smaller than that for charge exchange. These neutrals can then account for the collisions that occur at the front of the current sheet. In Argon it appears that not as many neutrals are moving with the current sheet and in addition the effective neutral-neutral cross-section is probably smaller. This allows the neutral-neutral collision to occur further in the rear of the current sheet, and thus the front of the current sheet does not interact with the neutral gas.

The cause of this is probably due to three effects. The first is that the entering neutrals for Argon have a much greater directed energy than thermal energy, and when the neutral-neutral collision occurs the large directed energy tends to drag both neutrals to the rear of the current sheet. This has the effect of lowering the relative number of neutrals moving with the current sheet.

The second effect is due to the size of the neutral-neutral cross-section. While the cross-sections obtained from the viscosity data are expected to be applicable for the experimental conditions in Hydrogen, they are not as applicable for the experiments performed in Argon. Specifically, these cross-sections are probably larger than the actual cross-section because the energy range for the collisions in the experiments in Argon is higher than that for which the viscosity was calculated. The effect of these factors on the size of the cross-section is considered in more detail in appendix B.

The third effect is due directly to the nature of the neutral-neutral collision. As shown in reference 20 and discussed in appendix B, for the experiments in Argon the relative energy in a collision is such that for the neutral-neutral collision, forward scattering should be more prevalent; i.e., the differential cross-section shows a large probability of scattering at small angles. When forward angle scattering is more prevalent, the collisions

are not as efficient in converting the directed momentum of an entering neutral into random motion. Thus, even though the entering neutral has a collision in which it transfers most of its directed momentum to the neutral with which it collided, there is little change in the overall directed momentum of the two particles. On the other hand, if the scattering is more nearly isotropic, each collision is effective in destroying the directed momentum. Thus the predominance of forward angle scattering for the experiments in Argon is assumed to make the neutral-neutral collision less effective in sweeping up the neutral gas the current sheet encounters.

Another factor must certainly contribute to the spreading of the current sheet in Argon, and that is the large variation in ion number density through the current sheet. If one looks at the number density variation shown in figure 30, it is evident that the ion-neutral MFP must be less at the rear than at the leading edge of the current sheet. This implies a stronger interaction with the neutral gas at the rear, and hence the rear would propagate at a slower speed. This difference in propagation speeds of various parts of the current sheet has already been shown to cause an increase in the current sheet width.

So far only elastic neutral-neutral collisions have been considered. When the energy of the colliding particles becomes of the order of 2-3 times their ionization

potential, the collision may become ionizing (Ref. 21). Under the previous assumptions, the ion formed would immediately assume the current sheet velocity and this would move the shock forward. The experiments in Argon are in agreement with this as at 500 μHg initial pressure (energy of an entering neutral is 2.2 times the ionization potential) the shock is further toward the rear of the current sheet than at 100 μHg (energy is 5 times the ionization potential). The experiments in Hydrogen are such that very few ionizing collisions can be expected (14 KV) under all conditions. The experimental results agree with this in that at the higher current sheet speeds the shock forms further toward the rear of the current sheet.

It is readily admitted that the above arguments are rather crude and are considered correct only in a qualitative sense. The calculation of all mean free paths (MFP) was under the assumption of constant conditions through the current sheet; while this appears approximately true for the experiments in Hydrogen and Helium, it is certainly not true in Argon. In particular, in Argon the observed ion number density undergoes a large change through the sheet and thus the MFP must also change. It is probable that the calculated MFP for both collisions may be too large at the front of the sheet and too small at the rear. As previously stated, this can account, to some extent, for the large current sheet width observed in Argon.

It is pointed out that the effect of the initial breakdown of the discharge has been neglected. If the R-t figures (Figs. 6-24) are extrapolated to the t = 0 origin, it is seen that the width of the current sheet just as the experiment starts (breakdown width) is larger in Argon than Hydrogen. One is inclined to think there is only one stable position for the shock (in the current sheet) and that the shock will move to this position regardless of the nature of the breakdown. There is, of course, no definite reason why this must be true and one must admit the possibility that the current sheet width and thus the shock position can depend to some extent on the manner in which the discharge initially formed.

In this model a large part of the difference in the observed current sheet width is attributed to the difference in the interaction between the neutral and conducting gas. If this is correct, an accurate theoretical treatment would require use of the three fluid equations (since the electron collisions do not enter in the momentum transfer between the neutral and ionized fluid, an alternate approach would be to use equations which describe only the ionized and neutral fluid, i.e., two fluid equations where the ions and electrons are considered as a single conducting fluid.)

As the results of these experiments seem to depend to a great extent on the number of ionized particles in the

current sheet, before a comparison can be made with other experiments the level of ionization present in them should be ascertained. For example operating at the same piston speed and a different voltage could yield different results. This is because the degree of ionization is probably controlled not only by collisions, but probably includes other effects such as the current density and voltage at which the experiment is performed.

VI. SUMMARY

Some of the more important conclusions that may be drawn from these experiments are summarized in this section. Perhaps the most remarkable is the extremely low level of ionization that is observed. This is particularly true for the experiments in Hydrogen, because here the shock Mach number is not sufficiently high to cause appreciable ionization, and it appears the ohmic heating in the current sheet also is not large enough to ionize a large portion of the gas. In Argon, the shock Mach number is large enough to ionize the gas, but since the shock occurs near the rear of the current sheet, there is still very little ionized gas through most of the current sheet. Many of the departures from "ideal" or infinite conductivity behavior can be explained by the low level of ionization in the front of the current sheet.

The experiments in Argon showed evidence of a large amount of current sheet leakage. While the gas left after the current sheet is probably moving radially outward, this clearly indicates that the current sheet is not an impermeable piston.

One can see that the single fluid equations are not accurate in predicting the current sheet widths, and this is probably also explained by the low levels of ionization. Another feature is that, in Argon, when the observed current

sheet widths are considered with the piston leakage, the position of the shock at the rear of the current sheet appears entirely reasonable.

For operation as a shock tube an additional problem that may be significant is the presence of charge layers on the electrodes. If charge layers of appreciable thickness are observed on either electrode, they can affect the performance of the device. Such a layer was observed on the anode of the previous device and a complete anode redesign was required to remove it.

In addition to these conclusions several other ideas are added. One should note that the strength of the shock wave given in Table 1 is probably inaccurate if the shock does not occur at the very front of the current sheet. This is because when the shock is within the current sheet the temperature immediately ahead of it is higher due to the ohmic heating. If this occurs the shock is propagating into a gas with a higher speed of sound and must have a corresponding lower Mach number. While the low level of ionization in Argon can be caused by the absence of equilibrium, this lower shock Mach number must have some effect. Due to the difficulty in finding how much ohmic heating there is, it is hard to estimate which of these is the dominate reason for the low ionization.

One may also note that the experiments in Hydrogen imply a relatively strong interaction of the current sheet

at low levels of ionization. While this interaction is not as strong as that desired to produce shock waves, it could be useful in propulsion applications. In this field it has the possibility of given increased propulsive efficiency, as most of the input energy would seem to go into translational motion rather than ionizing the gas. This could have application in any area where it is desired to accelerate a neutral gas to a high velocity.

Finally one may infer what must be done to achieve separation. The manner in which the leading edge of the current sheet interacts with the gas it encounters appears to govern, to a large extent, the possibility of obtaining separation. If it does not interact strongly with the gas, the current sheet becomes wide and diffuse and the shock forms more toward its rear. When this occurs the level of ionization tends to be lower throughout the current sheet, and this appears to contribute to the absence of separation by increasing the possibility of piston leakage. Thus the low level of ionization in the current sheet leading edge appears to be the primary reason for the absence of separation. It is emphasized that this effect is not directly due to low electrical conductivity, but is because of the low ionization and, hence, the small percentage of particles that experience the magnetic body force directly.

The most obvious manner to alleviate this is to use some form of preionization so that the current sheet and

the shock wave are not required to ionize the gas at the current sheet leading edge. If the current sheet was propagating into a fully ionized gas, then all of the gas would experience the magnetic force, and the leading edge of the current sheet would accelerate all of the gas. This mechanism would be more effective in accelerating the gas, because no recourse to collisions would be required.

Therefore, one concludes that experiments performed in a gas that is already ionized to some extent will be much more likely to achieve separation. Indeed, these experiments indicate that without preionization separation can never be expected. Based on the experimental results this seems to be particularly true at high Mach number current sheet speeds.

APPENDIX A

RADIAL ELECTRIC FIELD PROBES

1. Introduction

The probes used to measure the radial electric field are quite similar to the probes first used by Lovberg and Burkhardt (Ref. 15). A drawing of this probe is shown in figure 25. It consists of two electrodes located at equal vertical positions in the device but at different radial positions. The electrodes are insulated from ground potential by use of a pulse transformer, also shown in figure 25. This allows the probe to float at the vertical potential (or value of the E_z field) such that only the difference in the potential of the two electrodes is measured, and hence only the radial field is measured. The output from the pulse transformer is then recorded on an oscilloscope.

There can be some question as to what the actual output of the probe corresponds. If the dimension between the electrodes (L in Fig. 25) is such that it is approximately the length over which there is a field, then the peak output of the probe is the difference in potential over that region. This is approximately the condition under which the probes were used by Lovberg and Burkhardt (Ref. 15).

Another case is when the dimension "L" is small compared to the region in which there is electric field. Under these conditions the value of the measurement should be divided by the distance between electrodes (L in Fig. 25) to give the local electric field. This field is then integrated over the region to give the total potential difference across that region. For these experiments this is not the case, since the probe is never extremely small compared to the region of field. However, it is more closely met than the condition previously described. For the present experiments the probe is a factor of 4.5 to 8 times smaller than the dimension or width of the field, and the latter technique was used to reduce the data.

The data are necessarily taken at a given radial position as a function of time. One procedure would be to do this at several positions and then cross plot the results to get the field at a given time as a function of position. A spatial integration can then be made to obtain the total potential difference across the field. Since the current sheet moves with constant speed, the spatial integration was replaced by a time integral; this can be done if the field is not changing with radial position. One should also note that a one dimensional integration is valid only if the region (width) of the field is small relative to the radius. Both of these conditions are only approximately

true for these experiments; even so, the data were reduced by a temporal integration as follows.

Let the potential across the field be denoted by ϕ, the local electric field by E and the radius by r, then

$$\phi = \int E \, dr \qquad \text{(A-1)}$$

When V is the output of the probe and L is the dimension of the electrode spacing (Fig. 25) the relation becomes

$$\phi = \int \frac{V}{L} \, dr \qquad \text{(A-2)}$$

For a constant current sheet speed U_{sp}, this approximated by

$$\phi = \frac{U_{sp}}{L} \int V dt \qquad \text{(A-3)}$$

Note that V in the equation above is the output of the probe, and hence the total potential across the current sheet can be obtained by integrating the probe output and multiplying by the appropriate constants.

2. Errors

The two electrodes in the radial electric field probes should be approximately at the plasma potential and can therefore be considered as Langmuir probes at the floating potential. Under this condition there is no current to the probe and the sheath is composed of electrons (Ref. 22). As there is no current to the probe, the usual errors due to a variation in electron or ion mobility are not present. The only error that does occur is that due to the electron sheath. The potential across this sheath should be roughly $3.6\ KT_e$ (T_e = electron temperature, K = Boltzmann constant).

An idea of this temperature can be obtained from the equilibrium temperatures given in Table 1. As it is almost certain that equilibrium is not reached, some estimate of how the electron temperature varies from the equilibrium temperature should made. When the gas is in the process of becoming ionized by electron collisions, the electron temperature tends to be lower than the equilibrium value and the ion temperature higher. This has been observed experimentally (Ref. 24), and predicted theoretically (Ref. 25). The conditions in the current sheet are assumed to approximate this and hence the maximum electron temperature is probably that given in Table 1. The shock Mach number given in Table 1 can be higher than that which actually occurs (c.f., Sec. VI) and this means the temperature given in Table 1 is higher than that in the experiment.

The equilibrium temperature in electron volts for the conditions at which the probe was used is given in Table 5. It can be seen that it is small compared to the measured voltage, and when the effects discussed above are considered, it is evident that the error caused by the sheath cannot be large. In addition, only the difference in temperature of the two sheaths can cause error, and this should be considerably smaller than the error caused by a single sheath.

The effect of flow over the probes should not affect the sheath if the probe does not disturb the flow, because the thermal velocities of the electrons are much higher than the directed velocity of the plasma (Ref. 22). Hence if the probe does not change the temperature of the flowing electrons, the effects of the flowing plasma should be negligible. To make sure this is the case, the probe dimensions should be smaller than a gas dynamic mean free path. This condition is not met here.

To investigate this error more fully, two additional probes were made. These probes vary both in size and shape relative to the original probe and are shown in figure 26. Under all experiments in which the probes were used, all three probes gave identical answers to within 10%. In most cases this error is smaller than the variation for an individual probe over a period of several months. This indicates that the error caused by flow over the probe is not large.

Errors were also found to be caused by the circuit which was used in the measurement. The original circuit had an eight foot cable from the probe to the pulse transformer and an additional output cable from the pulse transformer to the oscilloscope (c.f., Fig. 25). In order to keep the noise level down it was necessary to terminate all cables with their characteristic impedance of 75 ohms. Because of excessive noise, the output cable had to be terminated at both ends.

With this circuit it was found that the output of the probe varied with the total resistance of the termination used. Specifically, with lower resistances the signal was smaller. This was because the probe was drawing enough current that it was no longer at the plasma potential. The cause of this was the low impedance of the resistors used to terminate the cables. In order to reduce the current that the probe drew from the plasma, the high impedance circuit shown in figure 27 was employed.

This circuit has the pulse transformer connected directly to the probe. Hence, there is no cable between the probe and the transformer to pick up and transmit noise. The output of the pulse transformer was matched to the oscilloscope cable impedance by use of a cathode follower (this is identical to the one used with the pressure probes, see figure 4). The entire circuit for the probe and cathode follower is also shown in figure 27.

The resistor divider is necessary to prevent over-driving the cathode follower with high voltage. The resistors in the divider are as high as possible to keep a reasonable risetime (0.2 μsec). For this case $R_2 = 8.2 \times 10^3$ ohms, $R_1 = 1.2 \times 10^3$ ohms.

When it became clear that a high impedance for the probe was necessary, it was questionable that the impedance was high enough to avoid these errors. To check this the resistors in the divider circuit were lowered to R = 750 ohms, R_1 = 100 ohms, and this resulted in only a slight, if any, lowering of the signal level. The shot-to-shot repeatability is poor enough such that any change of less than 5% would probably not be noticed.

The attenuation of the resistor dividers and the cathode follower was calibrated using a pulse generator. Pulses of approximately the same frequency and voltage as the measured signal were applied to the input of the pulse transformer, and the total attenuation to the oscilloscope was recorded. This was done for both resistor dividers and the attenuation was found to be 18 for the high ($8 \times 2 \times 10^3$ ohms) impedance divider and 20 for the low (750 ohms impedance divider. The risetime was also noted for these frequency pulses and found to be approximately 0.1 to 0.2 μsec.

It is possible that the pulse transformer could also respond by capacitive coupling to the potential at which

the probe is floating. This so-called common-made response is simply checked by shorting both electrodes at the input of the pulse transformer. When this was done the signal was at least a factor of 50 lower than its unshorted value. It is therefore felt that the output from the purse transformer was only due to a difference in potential of the two electrodes.

A final statement about the general repeatability of these measurements also seems worth mentioning. The shot-to-shot repeatability of the measurements was good for Argon (4% to 8%) to fair for Hydrogen (10% to 15%). The reproducibility over a period of several months was not quite as good. Even using the same probe and circuit the signal seemed to vary somewhat more over an extended period. Typically over a period of a month Argon varied approximately 10% to 15% and Hydrogen varied approximately 15% to 20%. The reason for this is not understood.

Because of all the errors that may be present, and also because of the poor repeatability of the measurements, the author would not class them as having an overall accuracy of better than 40% to 80%.

APPENDIX B

CALCULATION OF RELEVANT PARAMETERS FOR AN INVERSE PINCH

This appendix gives the procedure for the calculation of some of the relevant parameters in the inverse pinch. It is also included to give in detail the assumptions made in the various calculations. Units are MKSQ unless stated otherwise.

1. Equilibrium Conditions behind the Shock

Equilibrium conditions behind the shock are calculated using the measured speed of the peak in current density and ambient temperature to define the shock Mach number. Rankine-Hugoniot relations and a suitable Mollier chart (Refs. 26, 27, 28) are then used to determine the equilibrium conditions behind the shock. The equilibrium temperature and degree of ionization are given in Table 1.

2. Ideal Separation

The ideal separation of the shock from the piston is calculated assuming that the shock and current sheet are both infinitely thin, that the piston does not leak and that there are no boundary layer effects. This can be done by using the estimated compression through the shock and mass conservation, or can be taken directly from the exact similarity solution (Ref. 3). The latter procedure was used here.

As with hypersonic similarity the ratio of the piston speed to the shock speed depends only on the ratio specific heats, γ . Unfortunately the calculations in reference 3 were not done for $\gamma = 5/3$, however this information may be obtained from reference 5. Using the value of the ratio of the piston speed, U_c, to the shock speed, U_s, the ideal separation, δ, is calculated as follows

$$\delta = (U_s - U_c)t \qquad \text{(B2-1)}$$

where t is the time. It is assumed that the piston speed is closely approximated by that given by the "snowplow" theory, U_{sp}, and hence

$$\delta = U_{sp}\left(\frac{U_s}{U_c} - 1\right)t \qquad \text{(B2-2)}$$

The values of U_s/U_c are (Refs. 3 and 5)

For $\gamma = 5/3$ $\qquad U_s/U_c = 1.17$

For $\gamma = 7/5$ $\qquad U_s/U_c = 1.12$

Using these values the ideal separation was calculated and is tabulated in Table 2.

3. Energy of Entering Neutrals

In current sheet coordinates the neutral enters the current sheet with the velocity of the current sheet in laboratory coordinates. Therefore the energy is that energy of a particle with the mass of the neutral particle moving with the velocity of the current sheet, i.e.,

$$E = \frac{m_n U_{sp}^2}{2} \qquad \text{(B3-1)}$$

This is converted to electron volts and given in Table 3. For the inverse pinch at constant voltage

$$U_{sp} \propto (1/m)^{\frac{1}{4}} \qquad \text{(B3-2)}$$

and

$$E \propto m^{\frac{1}{2}} \qquad \text{(B3-3)}$$

Therefore the energy per particle is higher in the heavier gases.

4. $\omega\tau$ for Electrons

The calculation of $\omega\tau$ for the electrons is difficult because the conditions are not known accurately in the device. A rough estimate is made to obtain what is felt to be the upper limit of its magnitude. ω is defined as the electron gyro frequency, i.e.,

$$\omega = e\ B/m_e \qquad \text{(B4-1)}$$

where e is the electron charge, B is the magnetic field and m_e the electron mass. The largest value of the magnetic field encountered is approximately = 0.5 Weber/meter^2. This gives

$$\omega = 1 \times 10^{11}/\text{sec.} \qquad \text{(B4-2)}$$

τ is the collision time, and as the collision time is approximately the same for electron-electron or electron-ion collisions (Ref. 29) either may be used. The electron-electron collision time can be calculated from the relation given in reference 11 for collisions among like particles. Using this expression for the electron-electron collision time, t_{ee}, one obtains (cgs units)

$$t_{ee} = \frac{0.266}{N_e} \frac{T}{\text{Ln}\ \Lambda} \qquad \text{(B4-3)}$$

where T is the electron temperature and is assumed to be $2 \times 10^4\ ^oK$, N_e is the electron number density and is assumed to be 10^{15} electrons/cm^3 and LnΛ is tabulated in

reference 11. The term Ln Λ is a weak function of the electron temperature and number density. The value of t_{ee} is then

$$t_{ee} = 1.2 \times 10^{-10} \text{ sec} \qquad \text{(B4-4)}$$

and

$$\omega t_{ee} = 12 \qquad \text{(B4-5)}$$

This is probably the largest value of $\omega\tau$ that is ever attained. In other places, in particular the front of the current sheet, both the temperature and magnetic field are considerably lower.

5. Energy and Velocity of Electrons Carrying the Current

As the degree of ionization is quite low and the current density is large, it is of interest to know the drift velocity of the current carrying electrons and the energy associated with this velocity. A representative example is given for Hydrogen at 500μ.

If a radius of 2 inches (5.1 cm) is considered, the time the current sheet arrives can be taken from the R-t plot (Fig. 13). This is taken to be 1.8 μsec. The circuit driving current is 5.5×10^4 amps at this time. Using the value for the width of the current sheet (also taken from Fig. 13) the current density is found to be $J = 2 \times 10^7$ amp/meter^2. The electron number density is assumed to be 5×10^{20} electrons/m^3. This gives a drift velocity of 2.5×10^5 m/sec, and corresponds to an energy of 0.2 electron volts or a temperature of 2000^o K. Therefore it is entirely reasonable to assume that the observed number of electrons carry the current.

6. Mean Free Path for Neutrals Encountered by the Current Sheet

The model used here is derived from consideration of the process in current sheet fixed coordinates. The gas encountered by the current sheet can be seen as entering the current sheet with a velocity equal that of the current sheet in laboratory coordinates. The situation is therefore one in which a neutral enters a group of particles (the current sheet) with a known velocity. The major problem in calculating a mean free path for these neutrals is estimating the number density of ions or neutrals in the current sheet and the size of the appropriate cross-sections.

The ion number density in the current sheet is estimated by using the results of the line broadening experiments (Appendix C). Although the information obtained from these experiments is not complete, some idea of the ion number density can be obtained. At the lower pressures the shock Mach number and energy per entering particle are higher, and it seems likely that the degree of ionization is also higher. Using this reasoning and the results of the line broadening experiments, an estimate of the degree of ionization based on the initial filling number density was made. It is assumed that the degree of ionization is 5% for the experiments performed at 500 μHg initial pressure and 10% for those performed at 100 μHg.

Assuming these values for the ion number density within the current sheet, the ion-neutral mean free path can be calculated. The largest cross-section for this collision is that of charge exchange, and the cross-section for the charge exchange collision is taken from reference 30 for Helium and Argon and from an extrapolation of the data in reference 31 for Hydrogen. These values of the ion-neutral MFP are tabulated in Table 5.

It is pointed out that the charge exchange cross-section used for Hydrogen is for collisions between Hydrogen atoms and ions, and this is much larger than for collisions between Hydrogen ions and molecules. The justification for this is primarily from the experimental results, where a comparison with Helium indicates that there is little difference attributable to the diatomic nature of room temperature Hydrogen. Some diatomic Hydrogen ions (H_2^+) may be present and their charge exchange cross-section will be large for collisions with Hydrogen molecules (Ref. 32). Tne neutral-neutral cross-section will also be large for Hydrogen molecules and this can account for the observed short MFP in this collision. Again the experiments in Helium indicate the difference between Helium and Hydrogen is not sufficiently large to warrant this assumption. Unpublished experiments in Nitrogen (whose purpose was a further investigation of the possible effect that a diatomic gas might have) also

indicate little effect due to its diatomic nature.

The neutral-neutral mean free path is calculated in much the same manner. The number density of neutrals moving with the current sheet was assumed to be 5 times the initial filling number density. This is admittedly a rather crude approach, but is included to give an idea of what this MFP will be. The cross-sections for neutral collisions at these energies (4-80 electron volts) are difficult to estimate as there is virtually no information on them in the literature. The most accurate values were assumed to be those obtained from the calculation of viscosity made in reference 33 for Helium and Argon and in reference 34 for Hydrogen. The procedure used here is to invert the equation used to calculate the viscosity so that the cross-section is given as a function of the viscosity. The tabulated values of viscosity are then used to give the cross-sections. Conditions at the highest temperature available(15,000^{o} K) are used.

These cross-sections obtained from the viscosity data are probably accurate for the experimental conditions in Hydrogen, as the energy range for the collisions in the experiments is not appreciably different than those of the viscosity data. However, the energy range of the collisions in Argon is considerably higher than that of the viscosity data. The cross-sections for these experiments could differ from those obtained from the viscosity calculations, and

are expected to be somewhat smaller.

Using the values of the cross-section obtained in this manner and the estimate of the number density described above, the MFP for the neutral-neutral collisions was calculated. The result of this calculation is tabulated in Table 5.

There is another effect which can also be important, and this is the dependence of the differental cross-section on the scattering angle. An indication of this can be obtained by a comparison of the de Broglie wavelength to the dimensions of the scattering body. (It is emphasized that the use of quantum mechanics to give some indication of the angular dependence is not required, since for this range of energies the classical and quantum mechanical description should be approximately the same. The quantum mechanical approach is chosen here merely because of the two, it appeared to be the more convenient.) When the de Broglie wavelength is small relative to the scattering body the differential cross-section should have a large probability of forward scattering, but as the wavelength becomes of the order of the scattering body or larger the scattering tends to become constant with scattering angle (Ref. 20). This is true for center of mass coordinates, but the change to laboratory coordinates (there are equal masses of incident and scattering particles in this case) is the same geometric function for all cases.

Hence the collision which has the largest forward scattering remains that way, and the transformation only shifts the angular dependence more toward forward scattering in all cases.

The de Broglie wavelength, λ , for collisions is given by

$$\lambda = h/MV$$

where M is the reduced mass, V is the relative velocity of approach, and h is Planck's constant. Values of the de Broglie wavelength for the experimental conditions are given in Table 5. From this table it can be seen that the wavelength is approximately the same size as the scattering body in Hydrogen, and is much smaller for the conditions in Argon. Based on this, forward scattering should be much more prevalent for the experiments in Argon. The importance of this is discussed in section V.

No collisional information is given for the experiments performed at 25 KV, as there was no line broadening data taken at these conditions, and thus there is no way to make even a rough estimate of the ion number density.

7. Magnetic Reynolds Number

The magnetic Reynolds number, R_m, for these experiments is

$$R_m = \mu_o \sigma r U_{sp}$$

where μ_o is the magnetic permeability of free space, σ is the electrical conductivity, r is the radius and U_{sp} is the "snowplow" speed. This parameter is a measure of the ratio of the convection to diffusion of the magnetic field and should be large if the experiments are to approximate the ideal model (c.f., Sec. 1.2). For these experiments the range in "snowplow" speed is not large and the major variation in R_m, if any, is probably due to changes in the electrical conductivity.

This parameter is for a single fluid and may have doubtful significance for the low levels of ionization that are observed experimentally. This can be particularly true when inferring the current sheet width.

APPENDIX C

MEASUREMENT OF THE IONIZED NUMBER DENSITY BY LINE BROADENING

1. Introduction

When an atom is in an external electric field its energy levels are shifted due to the effect of the field on the atom. When it is a uniform external field this energy shift is called the Stark effect. In a gas composed of many charged particles, these particles give rise to a random electric field (the plasma microfield), which then shifts the energy levels of an atom that is in the gas. The accumulative effect of the charged particles on many of the atoms makes a spectral line emitted by the atoms appear to be broadened. This is the so-called line or Stark broadening of a line radiated by the gas. When this is considered quantitatively one may use the amount of broadening to infer the number density of charged particles.

To apply the technique, one must have a theory which gives the charged particle number density as a function of the width of a particular line, and be able to measure the line profile (intensity versus wavelength) for that line. A discussion of the theory necessary to do this is given in the first part of this appendix. The procedure for obtaining the line profile is then explained after the description of the theory. In the last part the results of the measurements are given and discussed.

2. Theory

The source of the theoretical part of the technique is reference 18. This has a comprehensive treatment of the theory required to calculate the broadening of a spectral line, and also included in this reference are tables of line profiles for all of the spectral lines used in these experiments. This reference has a complete account of the theory of line broadening, however, some points which are particularly applicable to these experiments are included here.

It is pointed out that this technique is still applicable when the temperature of the plasma is not accurately known, as is the case here. This is because the line profile depends very strongly on the charged particle number density, and only weakly on the plasma temperature. Therefore, in cases where an estimate of the number density is desired, and only a very rough estimate of the temperature is available, the technique of line broadening is still applicable. The use of this technique does not require local thermodynamic equilibrium (LTE), but only a Maxwellian velocity distribution among the electrons. This appears to be a reasonable assumption in these experiments.

It is recognized that for Hydrogen and Helium the temperature of the plasma may be obtained from the ratio of line to continuum intensity (Ref. 18). This was not done, primarily because this measurement assumes LTE, and

if LTE does not obtain, it appears that the errors in the measurement of the temperature could be large. The line width depends so weakly on temperature that these data would not significantly add to the overall accuracy of the density measurements.

For the technique to be accurate the plasma must be optically thin to the particular line observed. That is, the line radiation must not be reabsorbed by the plasma itself. If the plasma is optically thick, it reabsorbs more strongly in the center of the line than in the wings, thus changing the line shape. The optical thickness of the plasma was calculated for each line profile measured (this was not necessary for Helium --see part 4 of this appendix), using the equations of reference 18. The oscillator strengths for the Hydrogen lines were also obtained from reference 18, and the Einstein coefficient for the Argon I 6032 $\mathring{A}$ line was found in reference 35. The calculation of optical depth involves the number density of atoms in the lower state of the transition under consideration. This was estimated by using the Saha equation, with the values of the partition function for Hydrogen and Argon given in reference 36.

The Saha equation does not apply exactly, as LTE is not achieved. However, the optical depth was calculated over a wide range of temperature, and even if the plasma is not in LTE, if the calculation shows it is optically

thin over a wide variation of temperature, it seems reasonable to assume it is optically thin for these experiments.

This calculation showed that the gas was optically thin for the Hydrogen H_β and H_γ lines up to a temperature of 20,000°K, and for the Argon I 6032 Å line the plasma was optically thin up to a temperature of 40,000°K. Therefor it appears that there will be no self-absorption in any of the lines used in these measurements. The optical depth of the Hydrogen H_α line was also calculated, and it was found that this line should be self-absorbed. For this reason H_α line was not used in these experiments.

The intensity of the Argon line radiation was extremely low in the front portion of the current sheet and attained a level sufficient for measurement only toward the rear of the sheet. To obtain some idea of the number density present in the front part, the continuum radiation was measured through the current sheet. A description of this was given in section 4.3, and the results of the measurements are given in figure 30.

3. Experimental Technique

The inverse pinch is shown schematically in figure 1 and its operation is discussed in detail in section 1.2. The high degree of shot-to-shot reproducibility, which is characteristic of this device, is also noted in section 1.2. This is a key feature of the inverse pinch with respect to the present experiments, since a monochromator-photomultiplier system was used, making it necessary to scan a spectral line by measuring different wavelengths on successive shots, through the width of the line.

The monochromator, photomultiplier, and photomultiplier power supply were placed in a shielded screened-room, with the recording oscilloscope. Light from a small region of the inverse pinch was focused onto the entrance slit of the monochromator, through the screening, by means of a system of plane and concave mirrors. This technique virtually eliminated all noise problems.

The inverse pinch was surrounded by a cylindrical Pyrex tube with a glass plate on the top, thus measurements could be made through both the top and side of the device. In addition, for measurements through the top, both a glass and a slotted-metal top electrode were used (the metal electrode has narrow radial slots to permit transmission of the light). In the case of the metal electrode the current path is in the metal itself, whereas in the case of the

glass electrode the current flows in the boundary layer adjacent to the electrode. There were no measurable differences between the line profiles obtained through the top and through the side, and with either the glass or metal top electrode.

The monochromator used was a Jarrell-Ash 0.5 meter Ebert, with an RCA 1P21 photomultiplier tube, typically operated at 850 volts. For all the line broadening measurements both the entrance and exit slits were 0.02 mm (32 Å) wide. Before a line was scanned, its center was located by means of a standard lamp of the same gas. This served to correct for any errors in the monochromator wavelength calibration.

The inverse pinch used for these experiments was 6 inches in diameter. Most of the measurements were made at a radial distance of 1.5 to 1.75 inches from the center of the device. The top and bottom electrodes were 4½ inches apart, with the monochromator focused approximately on the mid-plane of the apparatus.

During the scanning of a line the device was vacuum pumped for 5 minutes between shots. Maintaining this constant purge time helped to minimize the shot-to-shot scatter in the data, especially in Hydrogen. Figure 28 is a typical profile for the Hydrogen H_β line, and figure 29 is the corresponding profile for the Argon I 6032 Å line. A minimum of two shots were made at each wavelength.

The continuum measurements in Argon have already been discussed in section 4.3. For these measurements a portion of the visible spectrum approximately 10 Å wide and centered about 6015 Å was used.

4. Results

Since the measured line profiles were very narrow (see Figs. 28 and 29), it was necessary to correct them for broadening due to the finite resolution of the monochromator. The slits were sufficiently wide that they covered a significant portion of the line. This correction was made by adjusting the theoretical profiles obtained from reference 18.

If the input signal to the monochromator were an infinitely thin line (monochromatic source), the output would be a triangle with a base whose width is determined by the slit width and the monochromator optics. This is due to the finite slit width and does not involve grating dispersion. The base of this triangle was calculated to be 0.666 Å for the 0.02 mm wide slit. To check this, the base of the triangle was measured using the 5789 Å line of a mercury lamp, and the Argon II 4398 Å line from the device itself. Both of these lines should be quite narrow compared to the resolution of the monochromator. In both cases the base of the triangle was found to be 1.2 to 1.3 Å. This increase in instrument broadening appeared to be due to tilting of the monochromator slits, which could not easily be reduced. Using this measured value, the theoretical curves were corrected for instrument broadening. The measured profiles were then fitted to the corrected

theoretical profiles, from which the number density could be obtained. This procedure was followed for the Hydrogen and Argon lines, and the results are tabulated in Table 5.

In Helium, no broadening greater than the instrument resolution could be detected. It was assumed that if the line had a full half-width (FHW) greater than 0.5 Å, it would have been detected. Using 0.5 Å as the maximum FHW for the Helium I 4471 Å line, an upper bound for the number density can be obtained. This is also given in Table 5.

The values of the charged particle number density were not plotted as a function of position in the current sheet. This is because in Hydrogen and Helium no noticeable change in this number density was measured. Therefore the values given in Table 5 for Hydrogen and Helium are the number densities observed anywhere within the current sheet. In Argon there is a marked change through the current sheet, but since there is no line broadening data available for the front portion of the current sheet in Argon, the only indication of the number density variation is given in figure 30. The value of the charged particle number density for Argon given in Table 5 is the result from the line broadening measurement made at the rear of the current sheet.

5. Discussion

The degree of ionization to be expected behind a shock moving with the current sheet velocity is given in Table 1. This table indicates that Helium should be 25% ionized and Argon 80% doubly ionized, if equilibrium is attained behind the shock. It is clear that the measured levels of ionization are considerably below these values. One explanation for this is that equilibrium was not reached, and in order to investigate this possibility it is necessary to obtain some idea of the time required to reach equilibrium.

Petschek and Byron (Ref. 37) have studied the time required to reach equilibrium in Argon, and their results may be extrapolated to give the equilibrium time for the present Mach number. Such an extrapolation indicates that equilibrium should be attained. Hence, the present measurements imply that in this case the extrapolation should not be made. The possibility of attaining equilibrium may also be estimated by using the validity criterion for transient LTE given in reference 18. The conditions assumed are equilibrium conditions behind a shock wave moving at the current sheet speed. This estimate indicates that equilibrium is certainly not reached in Helium (equilibrium time, τ , is 10 μsec), and is probably not attained in Argon (τ = 1.3 μsec). Based on this, it is

concluded that it is likely that equilibrium was not reached in either case.

There is another effect that may be equally important in accounting for the low level of ionization. This is discussed in the Summary (Sec. VI), and it is the lowering of the shock Mach number because it occurs within the current sheet. The Mach number is difficult to estimate when this occurs because the speed of sound ahead of the shock is not known, but this speed must be higher than the ambient speed and hence the Mach number lower. Of course, the lower Mach number will have a lower equilibrium degree of ionization.

If the Mach number is not known, then the equilibrium time cannot be estimated. Hence it is difficult to determine the quantitative affect of either factor. However, it is clear that both of these factors can materially reduce the level of ionization, and these effects are assumed to be the reasons the low levels of ionization are observed.

APPENDIX D

EFFECT OF PISTON LEAKAGE ON CURRENT SHEET SPEED

In the experiment in Argon at 14 KV and 500 μHg, it was observed that after passage of the current sheet the ionized gas number density was found to be relatively large compared to the initial number density (c.f., Sec. 3.4). This leakage must cause some change in the predicted current sheet speed, and it is important to know how large this change will be. In this appendix the effect of this leakage on the current sheet speed is calculated by using the "snowplow" model and the observed amount of leakage.

The amount of mass encountered by a radially expanding sheet is

$$m = A\rho V \qquad (D\text{-}1)$$

where A is the sheet area, ρ is the mass density and V is the radial velocity of the sheet. Hence the change in mass entering and leaving the current sheet is

$$\Delta m = A_1\rho_1 V_1 - A_2\rho_2(V_2 - U_2) \qquad D\text{-}2)$$

where condition 1 is at the leading edge of the current sheet and condition 2 is at the rear edge, and U_2 is the radial velocity of the mass left by the current sheet. Note that Δm is the mass that is accelerated by the current sheet to its speed. If the change in mass is related to

the incoming mass, one has

$$\frac{\Delta m}{m_1} = 1 - \frac{A_2}{A_1}\frac{\rho_2}{\rho_1}\frac{(V_2 - U_2)}{V_1} \qquad \text{(D-3)}$$

Note that $\frac{\Delta m}{m_1}$ should be 1 if the current sheet does not leak, because the value of ρ_2 would then be zero.

The ratio A_2/A_1 is just the ratio of radial positions at the time (2.2 μsec) the measurement was made, and can be taken from the R-t diagram for Argon (Fig. 8), i.e.,

$$\frac{A_2}{A_1} = \frac{R_2}{R_1} = \frac{3}{5} \qquad \text{(D-4)}$$

The ratio of ρ_2/ρ_1 is obtained by using the measured value of the number density as ρ_2 and the initial filling number density as ρ_1.

$$\frac{\rho_2}{\rho_1} = \frac{2 \times 10^{15}}{3.5 \times 10^{15}} \qquad \text{(D-5)}$$

The maximum possible change in current sheet speed occurs when $U_2 = 0$. This is assumed here. The values of V_2 and V_1 are taken from the slopes of the curves in the R-t figure (Fig. 8). These are found to be

$$\frac{V_2}{V_1} = \frac{1.6}{2.5} \qquad \text{(D-6)}$$

When these are put in equation (D-3) the value of $\Delta m/m_1$ is

$$\frac{\Delta m}{m_1} = .785 \qquad \text{(D-7)}$$

The current sheet speed in the case of leakage (U_L) related to the no leakage case (U_{sp}) is given approximately by

$$\frac{U_{sp}}{U_L} = \left(\frac{\Delta m}{m_1}\right)^{\frac{1}{4}}$$

$$= (.785)^{\frac{1}{4}}$$

$$= .94$$

or

$$U_L = 1.06\ U_{sp} \qquad \text{(D-8)}$$

This is under the assumption that the mass left behind is at rest (i.e., $U_2 = 0$). If this mass was moving, that is, it had been accelerated somewhat, but not to current sheet speed ($U_2 \neq 0$), then the difference between the leaking current sheet speed and non-leaking one will be even less. This is probably a more likely situation. The above calculation is felt to show that the measurement of "snowplow" speed for the current sheet and the measured leakage by line broadening are not in disagreement.

APPENDIX E

ELECTRODE LAYERS

A discussion of the layers that may develop on the electrodes of the apparatus is given in this appendix. As previously mentioned, there is the possibility of both viscous and charge layers on the electrodes. Since the presence of either of the layers may influence the manner in which the device performs, the effect of both of these layers should be considered.

First the viscous layer is examined theoretically and shown to have little effect on the operation of the device. Then, since an analytical treatment of the charge layers is difficult, an experimental investigation was made of them. This investigation revealed a rather large charge layer on the anode of the device, which seemed to have a discernible affect on the behavior of the current sheet and shock wave near the anode (c.f., Sec. 3.4). A qualitative discussion of the charge layer and a description of what should be done is an attempt to remove it is given here.

1. Viscous Layers

The approximate thickness of the viscous boundary layer may be calculated by using the theory developed for boundary layers in ordinary shock tubes. According to this theory the Reynolds number behind the shock is (Ref. 38)

$$R_e = \frac{\rho_2 U_p^2}{\mu_2} \frac{U_s}{(U_s - U_p)} \quad t \qquad \text{(E-1)}$$

where ρ_2 is the density behind the shock, μ_2 is the viscosity (absolute) behind the shock, U_p is the piston (current sheet) speed and U_s is the shock speed. t is the time between the shock and piston for a fixed observer. Assuming ideal operation (c.f., Appendix B) the values of U_p and U_s from the similarity theory (Ref. 3) can be used. This gives a value of

$$R_e \simeq 10^5 \qquad \text{(E-2)}$$

For this value of the Reynolds number the flow is laminar (Ref. 39) and a corresponding laminar boundary layer thickness may be calculated. If the displacement thickness for a flat plate (Ref. 40) is used, one obtains

$$\delta = 1.7\ \ell/\sqrt{R_e} = 1.7\ U_p t/\sqrt{R_e} \qquad \text{(E-3)}$$

where ℓ is the distance of the contact surface behind the shock. The value of δ calculated is approximately

$$\delta = 3 \times 10^{-3} \text{cm} \qquad \text{(E-4)}$$

The relative mass accumulated in this boundary layer is approximately

$$\frac{\Delta m}{m} = \frac{\delta}{L} \frac{\rho_{2BL}}{\rho_2} \qquad \text{(E-5)}$$

where L is the spacing of the electrodes (10 cm) and ρ_{2BL} is the mean density of the gas in the boundary layer. As the gas in the boundary layer is at a higher temperature than the wall, but not as hot as that of the discharge, an estimate of it must be made. If this temperature is assumed to be 500° K and the pressure gradient across the layer is neglected, one finds

$$\frac{\Delta m}{m} = 10^{-2} \qquad \text{(E-6)}$$

Thus the amount of mass contained in the viscous boundary layer is quite small. The thickness of the layer is also seen to be small compared to the electrode spacing (Eq.E-4).

2. Charge Layers

Due to the difficulty in treating any charge layer theoretically, only a qualitative description is given here. This description takes as its basis observations made in arc or glow discharges.

In the usual arc or glow discharge the current is carried predominantly by the electrons, due to their higher mobility. In such a case the current tends to be limited by the electron emission from the cathode and a space charge of ions developes on the cathode (Refs. 41, 42). In magnetic devices the electric current due to electrons may be inhibited if the field is sufficiently strong, that is, if $\omega\tau$ for the electrons is much larger than 1. One explanation offered (Ref. 12) for the anode layer is that the mobility of the ions is greater than that of the electrons due to the magnetic field. The role of the ion and electron is thus reversed and a space charge of electrons develops on the anode. This means the current is carried almost entirely by the ions.

For the present device, this type of argument must be considered incorrect for several reasons. First, in most cases $\omega\tau$ for the electrons is not sufficiently large for the electron mobility to be lower than the ions. In these experiments the value of $\omega\tau$ for electrons is at most approximately 10 (Appendix B) and it is only this large at

the very rear of the current sheet. Therefore the current at the front of the current sheet must be predominantly an electron current.

The radial electric field measurements also indicate that the current is carried primarily by the electrons. Following the arguments of section 4.2, one expects a radial electric field of the order of the incoming neutral or ion energy if the electrons are carrying the current. Since the field was measured, even though there is some scatter in the measurement, it lends definite support to the idea that the electrons are carrying the current.

Finally, if the ions were carrying the current, due to the low degree of ionization (Appendix C), their drift velocities would correspond to extremely high values. These velocities would be observable as a doppler shift in the measurement of the Hydrogen spectrum taken in the broadening measurements. It is also unlikely that such velocities of 3 to 4 x 10^5 m/sec would exist for the ions, with the electrons remaining fairly stationary. One thus concludes that the ions cannot be carrying an appreciable part of the current.

A more probable explanation of this effect arises when the external circuit as well as the conditions at the electrodes is considered. If the discharge starts with a sufficiently high voltage and current across the electrodes, and if the cathode emits freely, then the impedance

between the electrodes may be less than that of the connecting circuit. When this develops, a charge sheath must form on the anode to retard the current flowing between the electrodes. If this is the actual case a reduction in the size of the anode to a size smaller than the area of the arc will have the same effect that the anode layer had (Ref. 42), that is, it will retard the current flow to the anode.

Another way of thinking of this is to consider the discharge as a form of non-linear resistor. A high voltage is required to initiate the arc, however, once the arc is started very little voltage is required to draw a large current (under the assumption the cathode emits freely). Before the circuit can readjust the voltage to match this current to that of the external circuit, a charge layer forms on the anode to help retard the current. This charge layer is, of course, one way of readjusting the voltage across the arc.

To determine if this was the correct explanation, and primarily to remove the anode layer, the size of the anode was reduced. This was done by replacing the top electrode (which was previously a conductor) with a glass disk. The center of the disk has a small tungsten or copper button (which is now the electrode) to which the current runs (Fig. 2). The arc forms at the button, runs along the surface of the glass and then across the chamber.

The size of the button is now the size of the anode. In all but one case this removed the anode layer entirely.

A more detailed check can be made to verify that this is indeed what is happening. Due to the varying areas of the arc in different gases, it is possible to reduce the size of the anode to an area considerably less than the area of the Argon arc and still not be appreciably less than the area of the Hydrogen arc. When this was done (at 14 KV) the anode layer disappeared in Argon but remained, although smaller, in Hydrogen. Further reduction of the anode area caused the layer to disappear in Hydrogen in all but one case. Only in Hydrogen at 500 μ did some form of layer remain, and under these conditions it was quite small. It is felt that further reduction in the size of the anode would remove this, but the anode was already so small as to make this difficult. For this reason the anode was left at its present size and no experimental data were taken near the anode at the above condition (Hydrogen 500μ, 14 KV).

APPENDIX F

DETERMINATION OF THE CURRENT DENSITY FROM THE MAGNETIC PROBES

The output of the magnetic probes is the time derivative of the azimuthal (θ) component of the magnetic field. Hence, they are sometimes called $\dot{B}_\theta$ probes. These data are taken at a given radial position (c.f., Fig. 4 for a typical oscillogram signal), and in order to obtain the current density one needs to know the spatial variation of the magnetic field at a given time. To acquire this, the output of the probe is integrated to yield the magnetic field at a fixed radial position as a function of time. This is repeated at different radial positions and all of the data cross plotted to give the spatial variation of the magnetic field at a fixed time. Maxwell's equations can then be used to give the axial current density, J_z, at this time as a spatial derivative of B_θ, i.e.,

$$J_z = \frac{1}{\mu_o} \frac{1}{r} \frac{\partial}{\partial r} (rB_\theta) \qquad \text{(F-1)}$$

where μ_o is the magnetic permeability of free space, r is the radial position and B_θ is the magnetic field taken from the integrated probe traces.

This was done for three to four different times and the peak current density(J_z maximum) was plotted on all the figures of the current sheet trajectory (Figs. 6-24). In

all cases the peak in current density fell so close to the peak in $\dot{B}_\theta$ that no difference could be seen. For this reason the curve designated peak in these figures is the trajectory of the peak in current density and the peak signal of the magnetic probes.

REFERENCES

1. Paul, J. W. M., et al., Nature (1965), 208, No. 5006, pp. 133-135.

2. Vlases, G., Ph.D. Thesis, Caltech (1963).

3. Greifinger, C., and J. D. Cole, Phys. of Fluids (1961), 4, pp. 527-534.

4. Liepmann, H. W. and G. Vlases, Phys. of Fluids (1961), 4, pp. 927-928.

5. Vlases, G. C., J. Fluid Mech. (1963), 16, pp. 82-96.

6. Camac, M., et al., Suppl. Nucl. Fusion (1962), 2, pp. 423-429.

7. Sorrell, F. Y., Bull. Amer. Phys. Soc. (1965), 10, p. 272.

8. Kantrowitz, A., Paper presented at 15th anniversary Solvoy Conference, Brussels, Belgium, Nov. 5-10, 1962. Also Avco Report No. 141 (1962).

9. Vlases, G. C., Joint Institute for Laboratory Astrophysics Report No. 49 (1965).

10. Falk, T. J., and D. L. Turcotte, Phys. of Fluids (1962), 5, pp. 1288-1292.

11. Spitzer, L., Physics of Fully Ionized Gases, Interscience, New York (1956).

12. Johansson, R. B., Phys. of Fluids (1965), 8, pp. 866-871.

13. Lovberg, R. H., IRE International Symposium on Plasma Phenomena and Measurement. San Diego, Oct. 29 - Nov. 1, 1963. Also General Atomic Report GA-4735.

14. Fishman, F. S. and H. E. Petschek, Phys. of Fluids (1962), 5, pp. 632-633.

15. Lovberg, R. H. and L. C. Burkhardt, Phys. of Fluids (1962), 5, pp. 341-347.

16. Longmire, C. L., Elementary Plasma Physics, Interscience, New York (1963).

REFERENCES (cont.)

17. Cooper, J., "A Review of Plasma Spectroscopy", to be published in Reports on Progress in Physics.

18. Griem, H. R., Plasma Spectroscopy, McGraw-Hill, New York (1964).

19. Hoffman, A. L.,"A Concial Model for the Diffusive Piston in an MHD Shock Tube", to be published.

20. Massey, H. S. W., and E. H. S. Burhop, Electronic and Ionic Impact Phenomena, Oxford, London (1956).

21. von Engel, A., Ionized Gases, Oxford, London (1965).

22. De Leew, J. H., Physico-Chemical Diagnostics of Plasmas, pp. 65-95, Edited by T. P. Anderson; R. W. Springer and R. C. Warder, Northwestern University Press, Evanston (1963).

23. Chen, F. F., Plasma Diagnostic Techniques, pp. 113-199, Edited by R. H. Huddlestone and S. L. Leonard. Academic Press, New York (1965).

24. Little, E. M., et al., Phys. of Fluids (1964), 8, pp. 1168-1175.

25. Skalafuris, A. J., Astro. Jour. (1965), 142, pp. 351-368.

26. Lick, W. J., and H. W. Emmons, Thermodynamic Properties of Helium to 30,000° K, Harvard University Press, Cambridge (1962).

27. Sewell, K. G., "The Thermodynamic Properties of High Temperature Argon", Ling-Temco-Vought Report No. Re-IR-26, Oct. 1961.

28. Turner, E. B., "Equilibrium Hydrodynamic Variables Behind a Normal Shock", Space Technology Laboratories Report GM-TR-0165-00460, Aug. 1958.

29. Glasstone, S. and R. H. Lovberg, Controlled Thermonuclear Reactions, D. van Nostrand Co., Princeton (1960).

30. Brown, S. L., Basic Data of Plasma Physics, Wiley, New York, (1954).

REFERENCES (cont.)

31. Fite, W. L., et al., Phy. Rev. (1960), 119, pp. 663-668.

32. Hasted, J. B., Physics of Atomic Collisions, Butterworths and Co., London (1964).

33. Amdur, I., and E. A. Mason, Phys. of Fluids (1958), 1, pp. 370-383.

34. Vanderslice, J. R., et al., Phys. of Fluids (1962), 5, pp. 370-383.

35. Gericke, W. E., Z. Astrophys. (1961), 53, pp. 68-79.

36. Darwin, H. W. and P. Felebok, Data for Plasmas in Local Thermodynamic Equilibrium, Gauthier-Villars, Paris (1965).

37. Petschek, H. E. and S. Byron, Ann. Phys. (1957), 1, pp. 270-315.

38. Hartunian, R. A.; A. L. Russo and P. V. Marrone, Jour. of Aero/Sci. (1960), 27, pp. 587-594.

39. Roshko, A.,and J. A. Smith, AIAA Journal (1964), 2, pp. 186-187.

40. Rosenhead, L., Laminar Boundary Layers, Oxford University Press, London (1963).

41. Penning, F. M., Electrical Discharges in Gases, Macmillian, New York (1957).

42. Cobine, J. D., Gaseous Conductors, Dover, New York (1958).

GAS	INITIAL PRESSURE μ Hg	U_{sp} (cm/μsec)	MEASURED U_{sp} (cm/μsec)	MACH NO.	EQUILIBRIUM TEMPERATURE	DEGREE OF IONIZATION
14 KILOVOLT OPERATION						
Argon	500	1.30	1.32	39	23,500	100%
Argon	100	1.95	2.0	59	30,000	80% A^{++}
Helium	400	2.44	2.40	23.8	20,000	25%
Hydrogen	500	2.78	2.70	19	6,500	0
Hydrogen	100	4.12	4.0	28	12,000	15%
25 KILOVOLT OPERATION						
Argon	500	1.61	1.63	48	30,000	70% A^{++}
Argon	100	2.41	2.40	72	41,000	50% A^{+++}
Hydrogen	500	3.44	3.50	23	10,000	5%
Hydrogen	100	5.10	5.60	35	14,000	32%

TABLE 1. OPERATING CONDITIONS

GAS	INITIAL PRESSURE μ Hg	TIME OF MEASUREMENT (μsec)	MEASURED WIDTH (cm)	CALCULATED WIDTH (cm)	IDEAL SEPARATION (cm)
14 KILOVOLT OPERATION					
Argon	500	3.5	3.25	1.75	0.90
Argon	100	3.0	2.24	1.29	1.0
Helium	400	2.75	2.28	1.70	1.15
Hydrogen	500	2.5	1.52	3.87	0.83
Hydrogen	100	1.6	1.78	2.42	1.25
25 KILOVOLT OPERATION					
Argon	500	2.5	3.05	1.23	0.69
Argon	100	2.25	2.92	0.93	0.92
Hydrogen	500	2.0	1.65	2.5	0.82
Hydrogen	100	1.3	1.78	1.57	0.80

TABLE 2. CURRENT SHEET WIDTHS

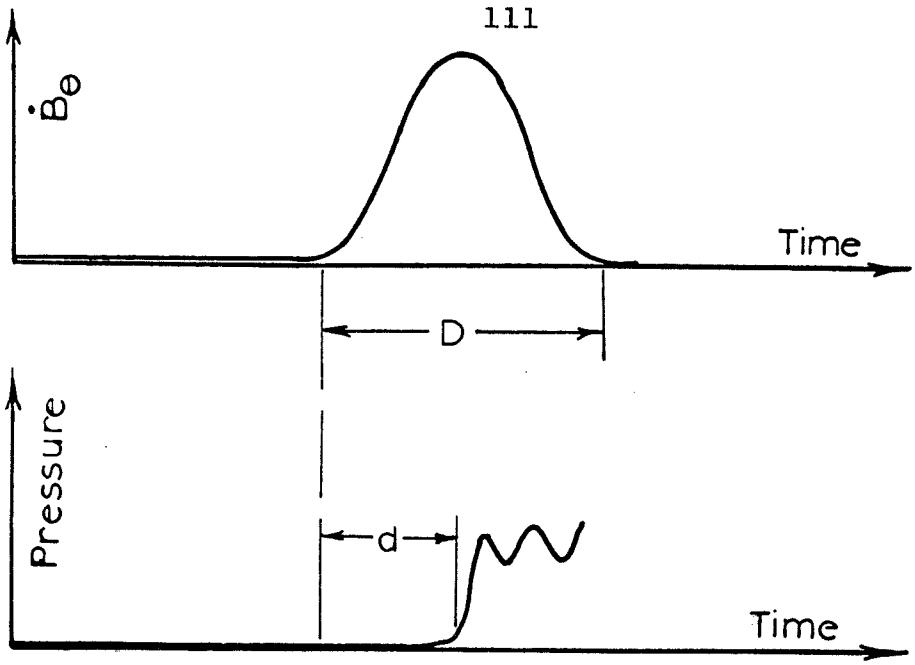

GAS	INITAL PRESSURE	R = d/D
14 KILOVOLT OPERATION		
Argon	500μ	.95
Argon	100μ	.90
Helium	400μ	.50
Hydrogen	500μ	.08
Hydrogen	100μ	.20
25 KILOVOLT OPERATION		
Argon	500μ	.88
Argon	100μ	.72

TABLE 3. PARAMETER R

14 KILOVOLT OPERATION					
GAS	INITAL PRESSURE μ Hg	$\frac{1}{2}MU^2_{sp}$ (ev)	MEASURED POTENTIAL (volts)	PERCENT IONIZED	ESTIMATED KT_E (ev)
Argon	500	35	82	42.5	1.95
Argon	100	79	184	45.7	2.60
Helium	400	12.8	182	6.8	1.70
Hydrogen	500	4.1	110	3.63	0.55
Hydrogen	100	9.0	207	4.4	1.00

TABLE 4. SUMMARY OF ELECTRIC FIELD MEASUREMENTS

14 KILOVOLT OPERATION					
GAS	INITIAL PRESSURE μ Hg	MEAN FREE PATH (mm)		de BROGLIE WAVELENGTH (Å)	ELECTRON NUMBER DENSITY/cm^3
		N - N	N - I		
Argon	500	0.24	3.4	7.5×10^{-3}	- - -
Argon	100	1.2	8.4	5.0×10^{-3}	2×10^{15}
Helium	400	0.80	7.1	3.9×10^{-2}	$\leq 10^{15}$
Hydrogen	500	0.46	2.9	.15	5×10^{14}
Hydrogen	100	2.3	9.5	.10	- - -

TABLE 5. COLLISION PARAMETERS

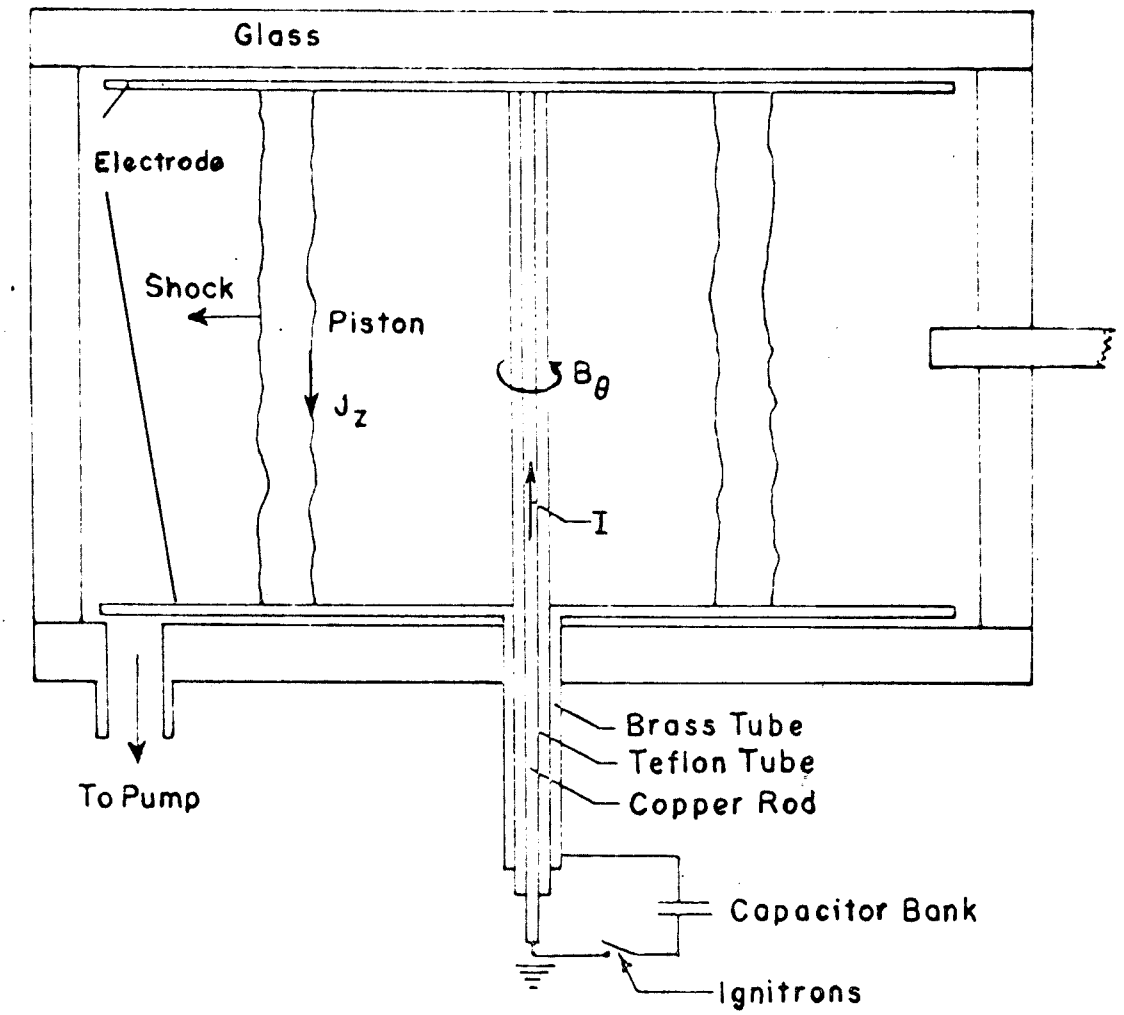

Figure 1. Schematic View of the Inverse Pinch Shock Tube

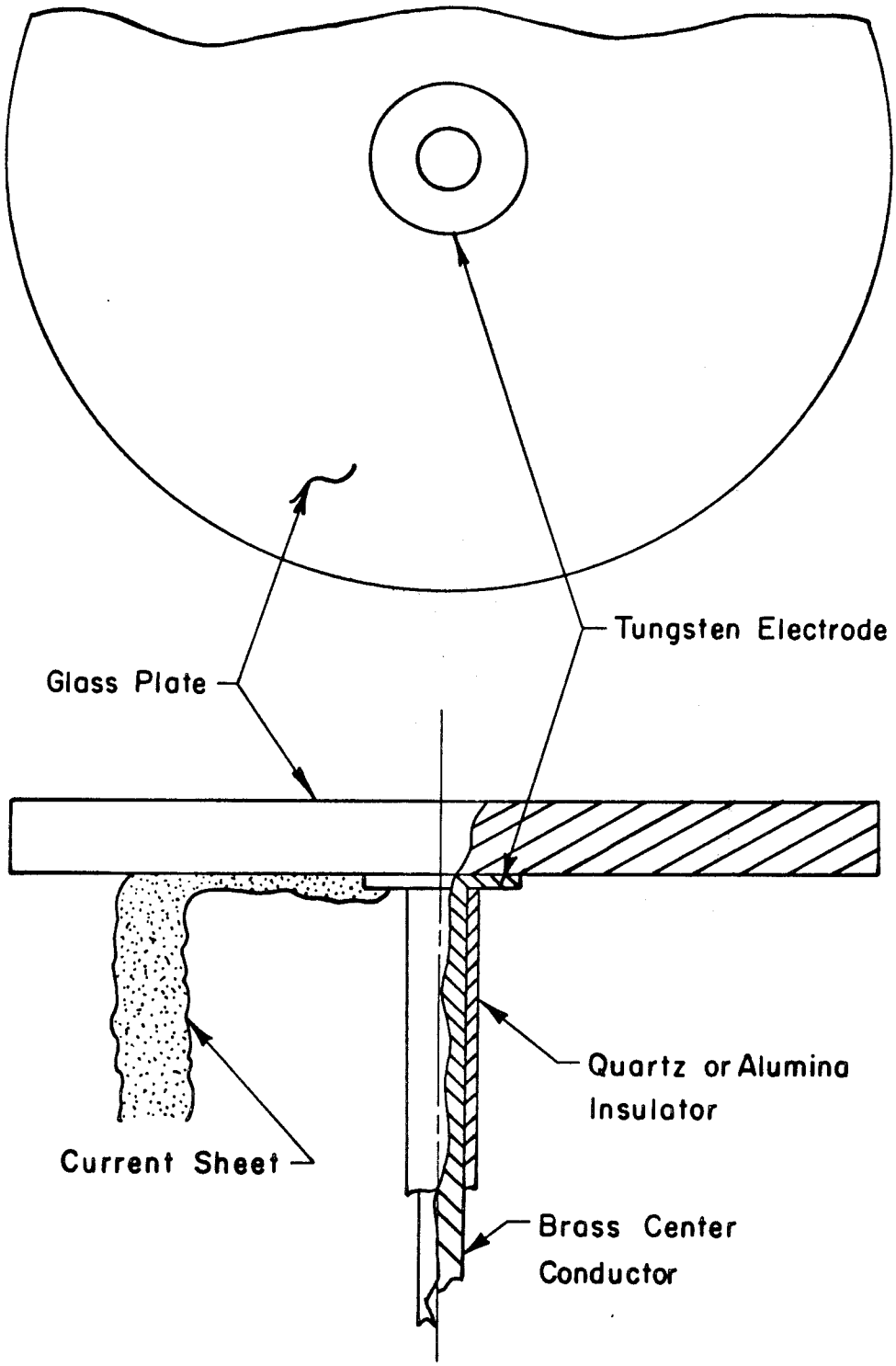

Figure 2. Anode Detail of the Inverse Pinch

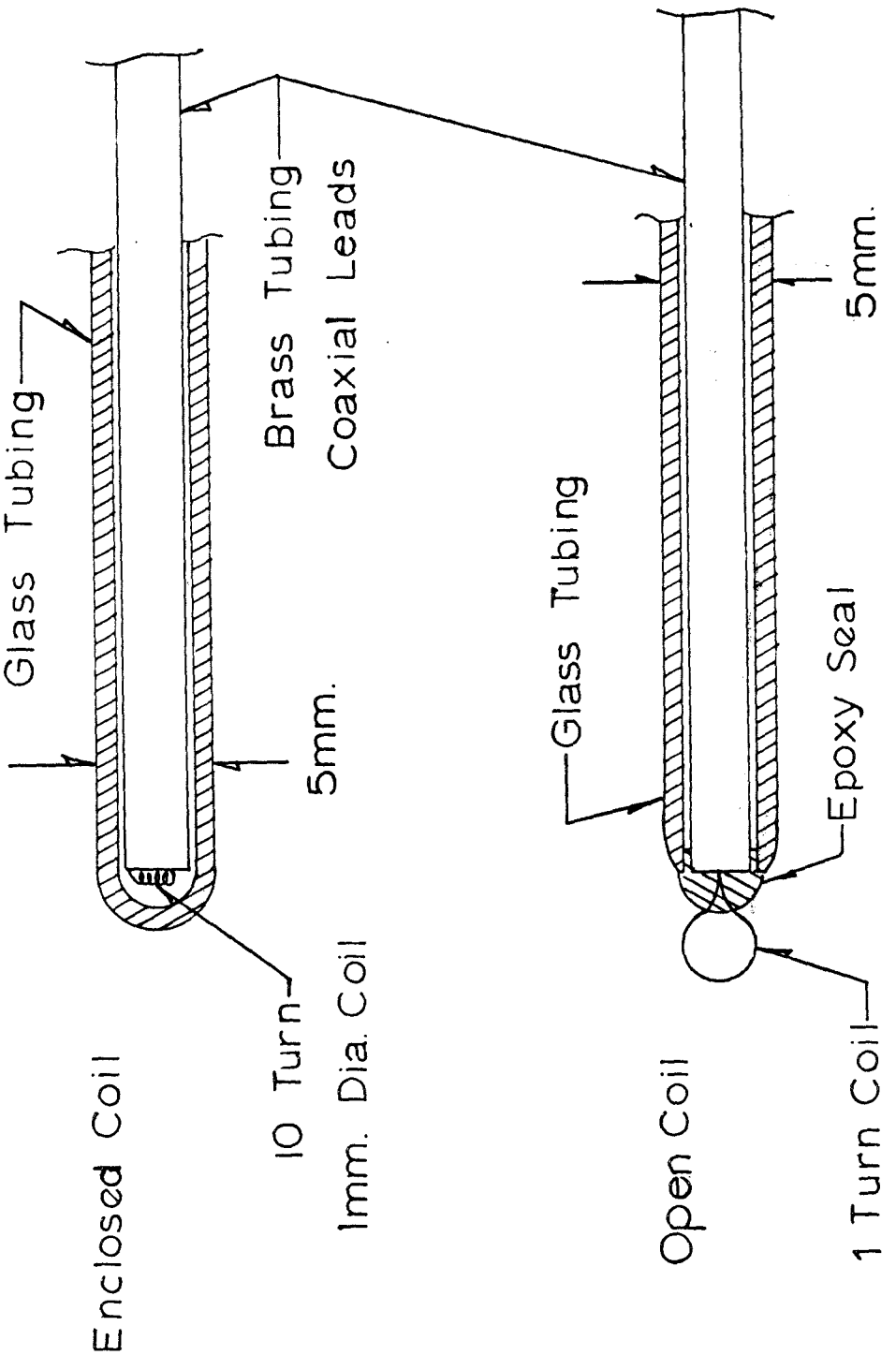

Figure 3. Magnetic Probes

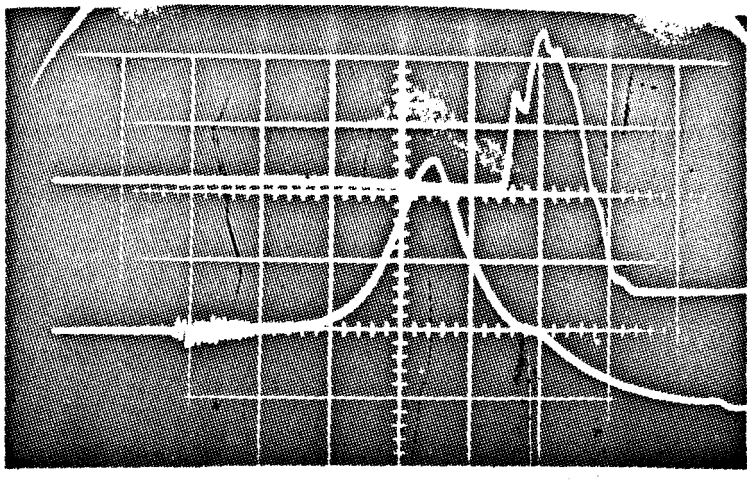

(a) Upper Beam: Pressure Probe
Lower Beam: Magnetic Probe

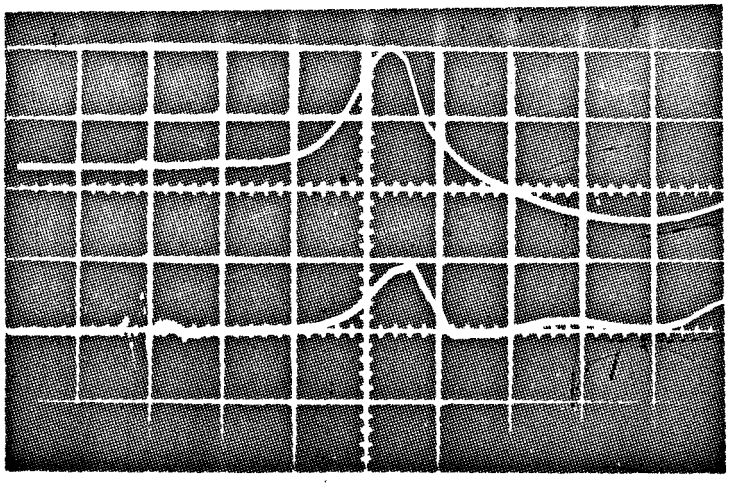

(b) Upper Beam: Magnetic Probe
Lower Beam: Radial Electric Field Probe

Figure 4. Oscillograms for Argon, 14 KV, 500μ, Sweep rate 1 μs/cm left to right. Probes approximately 4.9 cm from the center of the chamber.

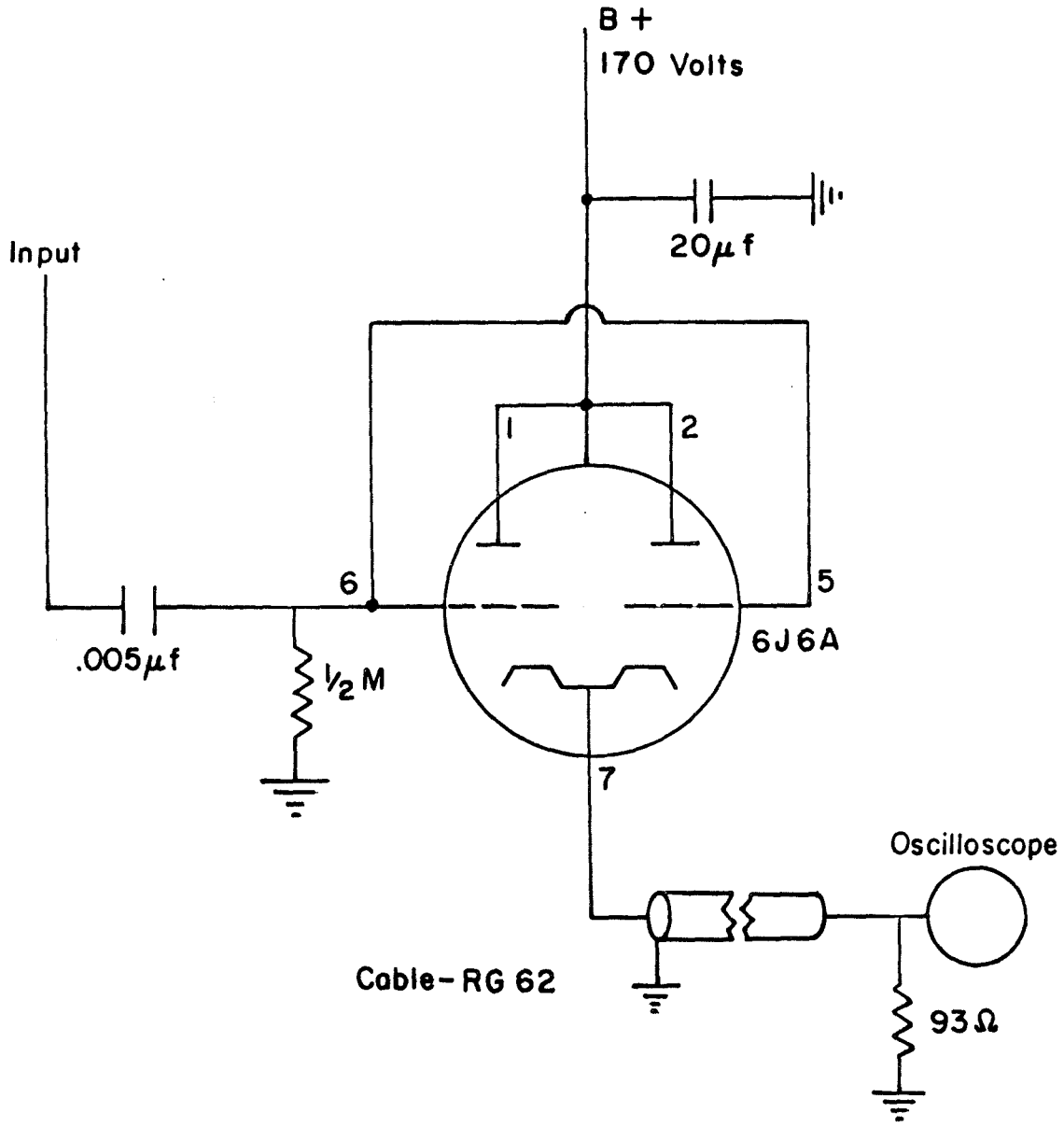

Figure 5. Cathode Follower Circuit

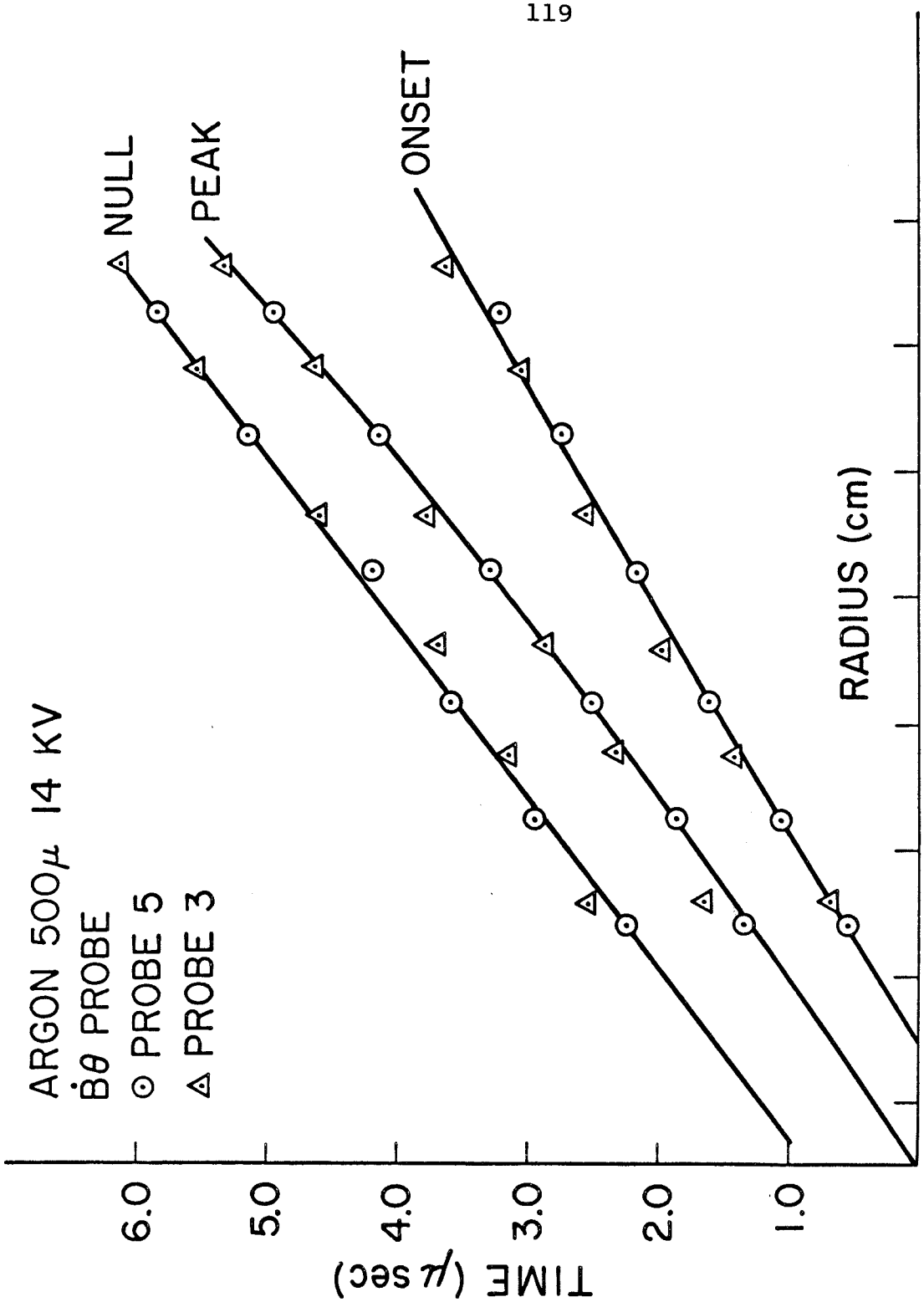

Figure 6. Magnetic Probe Data, Argon, 14 KV, 500μ

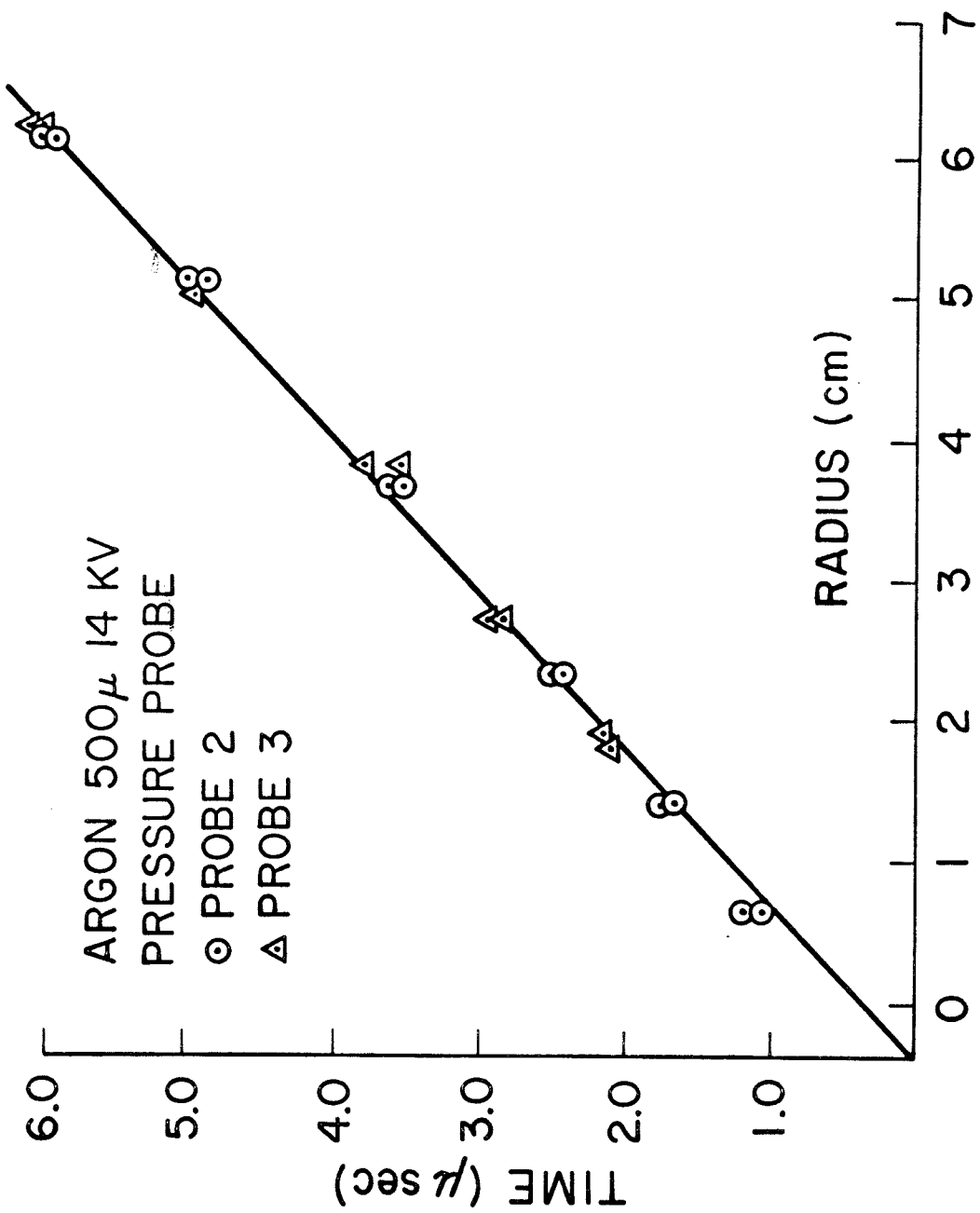

Figure 7. Pressure Probe Data, Argon, 14 KV, 500μ

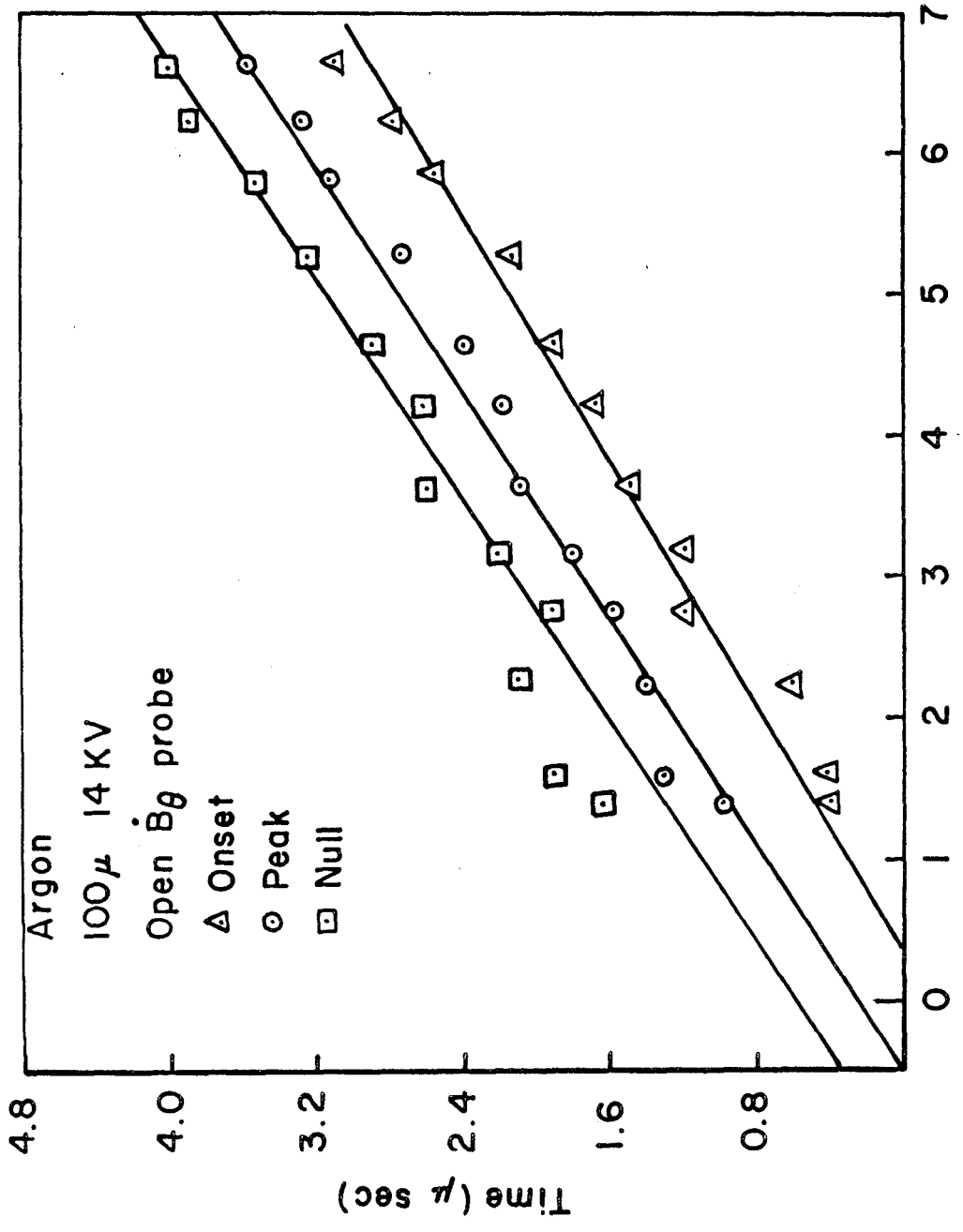

Figure 8. Magnetic Probe Data, Argon, 14 KV, 100μ

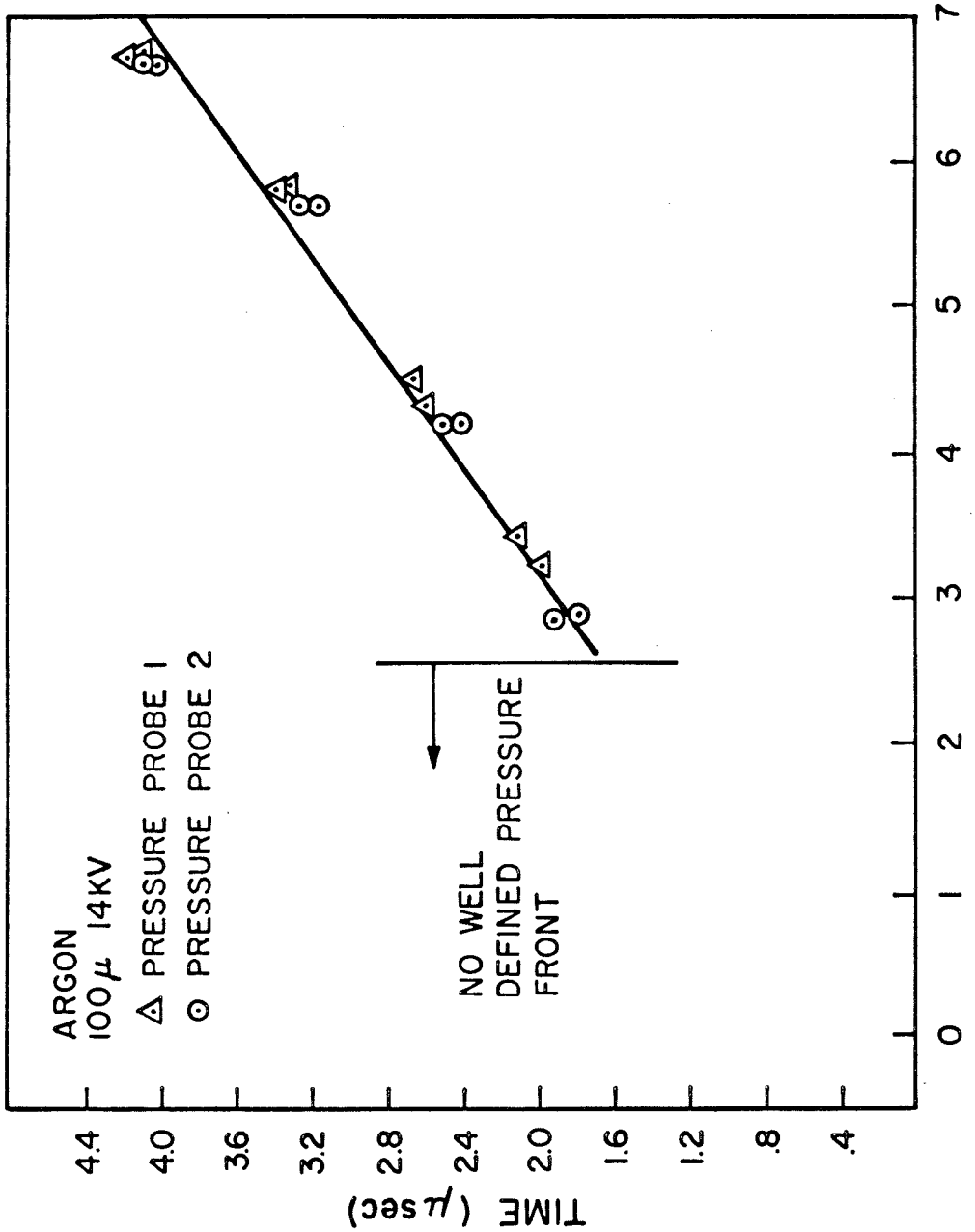

Figure 9. Pressure Probe Data, Argon, 14 KV, 100μ

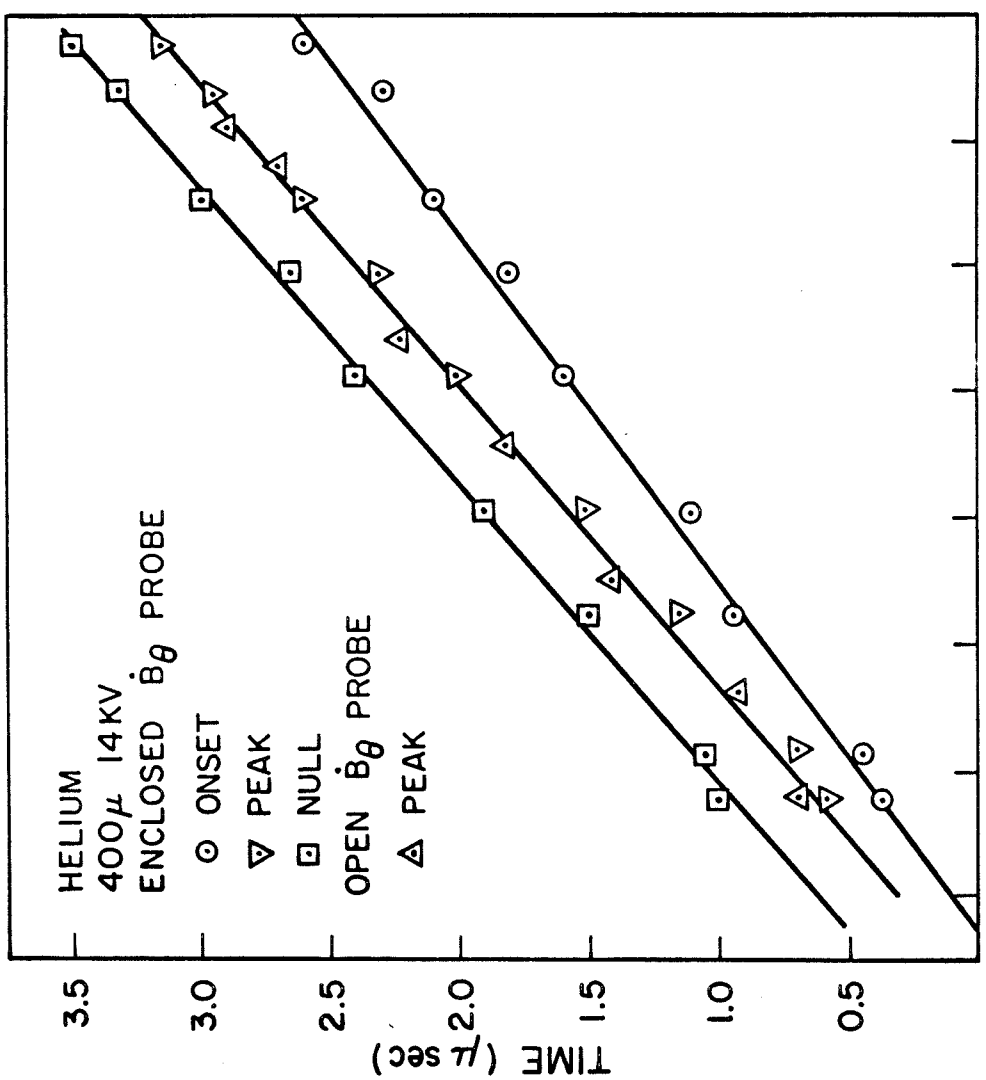

Figure 10. Magnetic Probe Data, Helium, 14 KV, 400μ

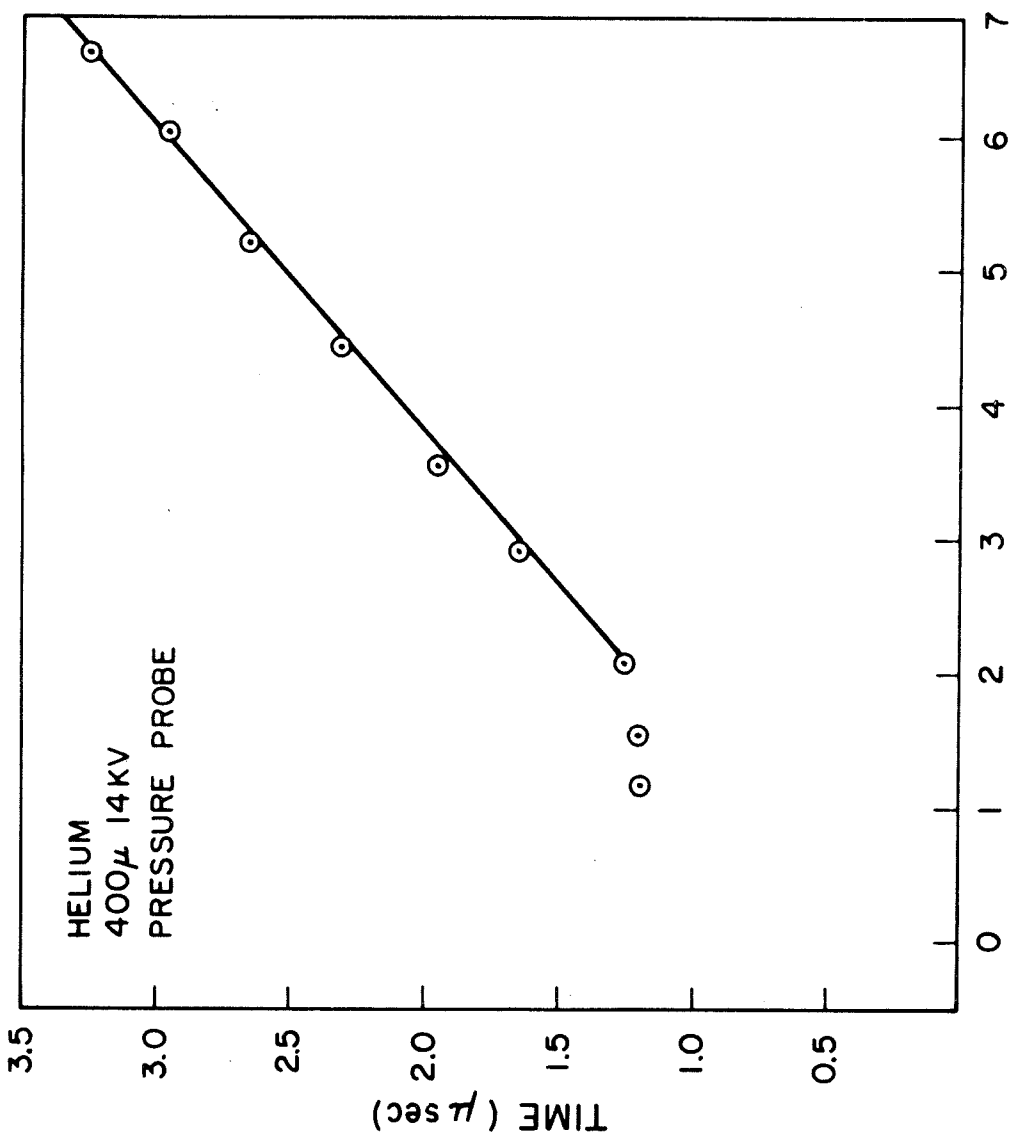

Figure 11. Pressure Probe Data, Helium, 14 KV, 400μ

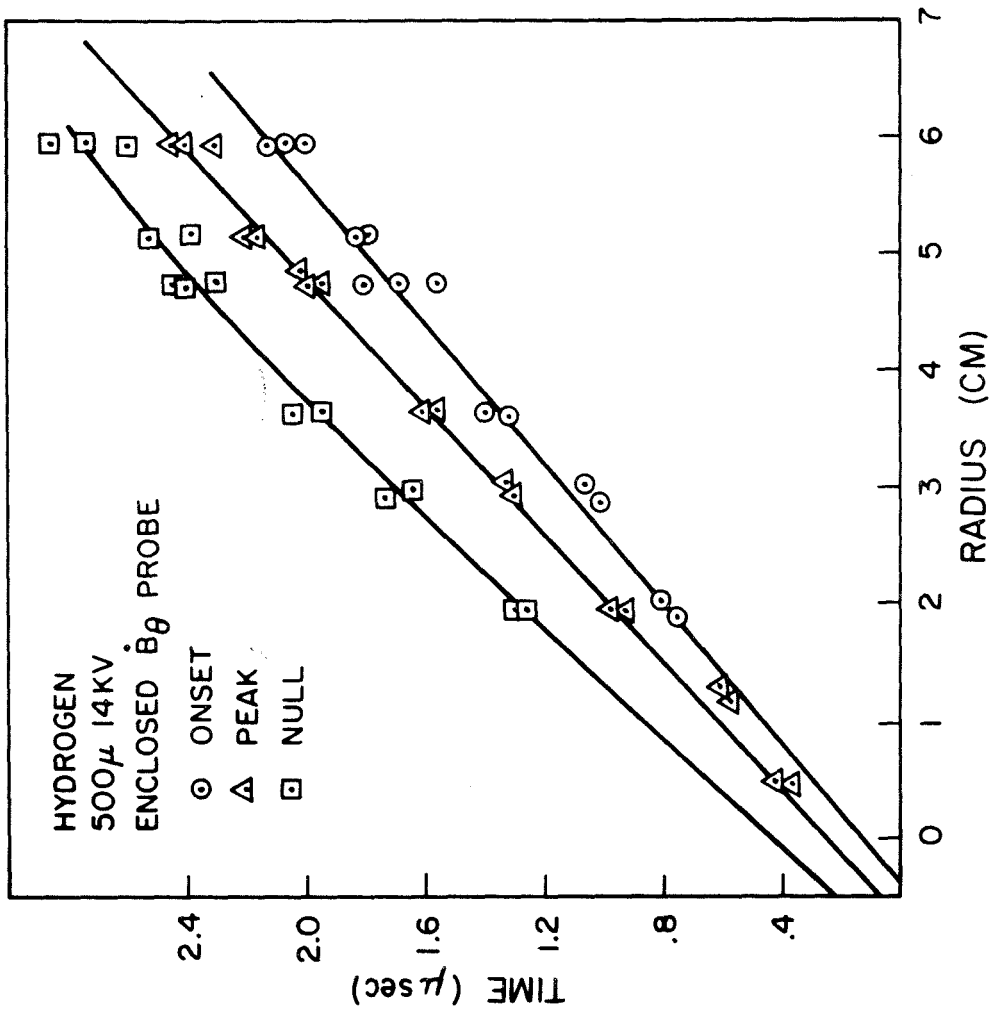

Figure 12. Enclosed Magnetic Probe Data, Hydrogen, 14 KV, 500μ

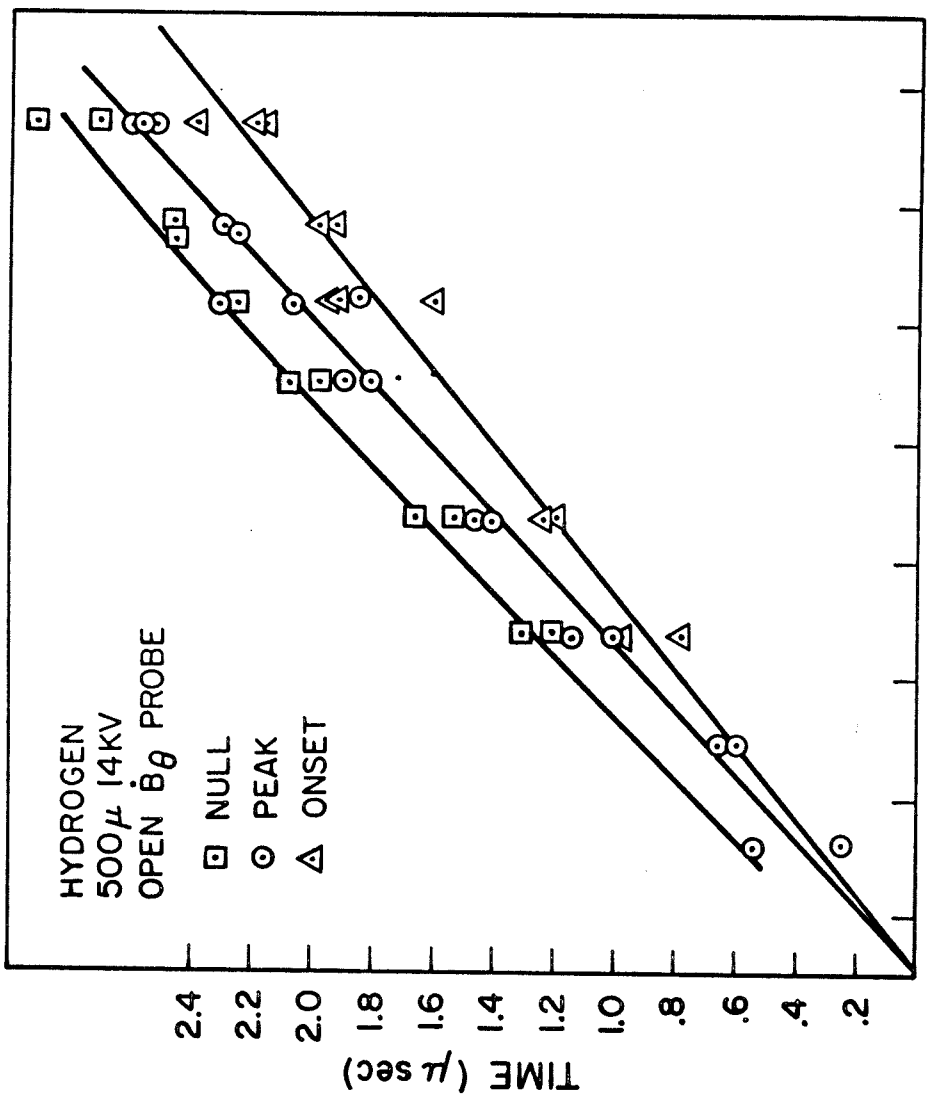

Figure 13. Open Magnetic Probe Data, Hydrogen, 14 KV, 500μ

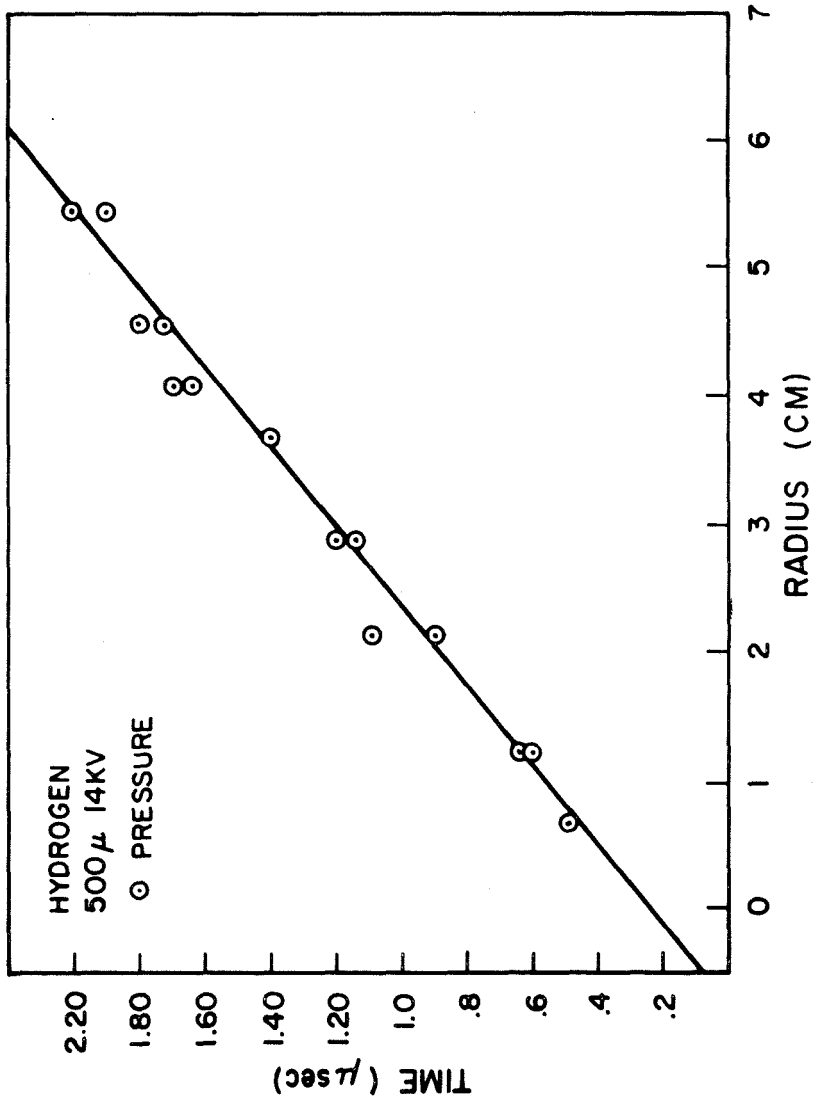

Figure 14. Pressure Probe Data, Hydrogen, 14 KV, 500μ

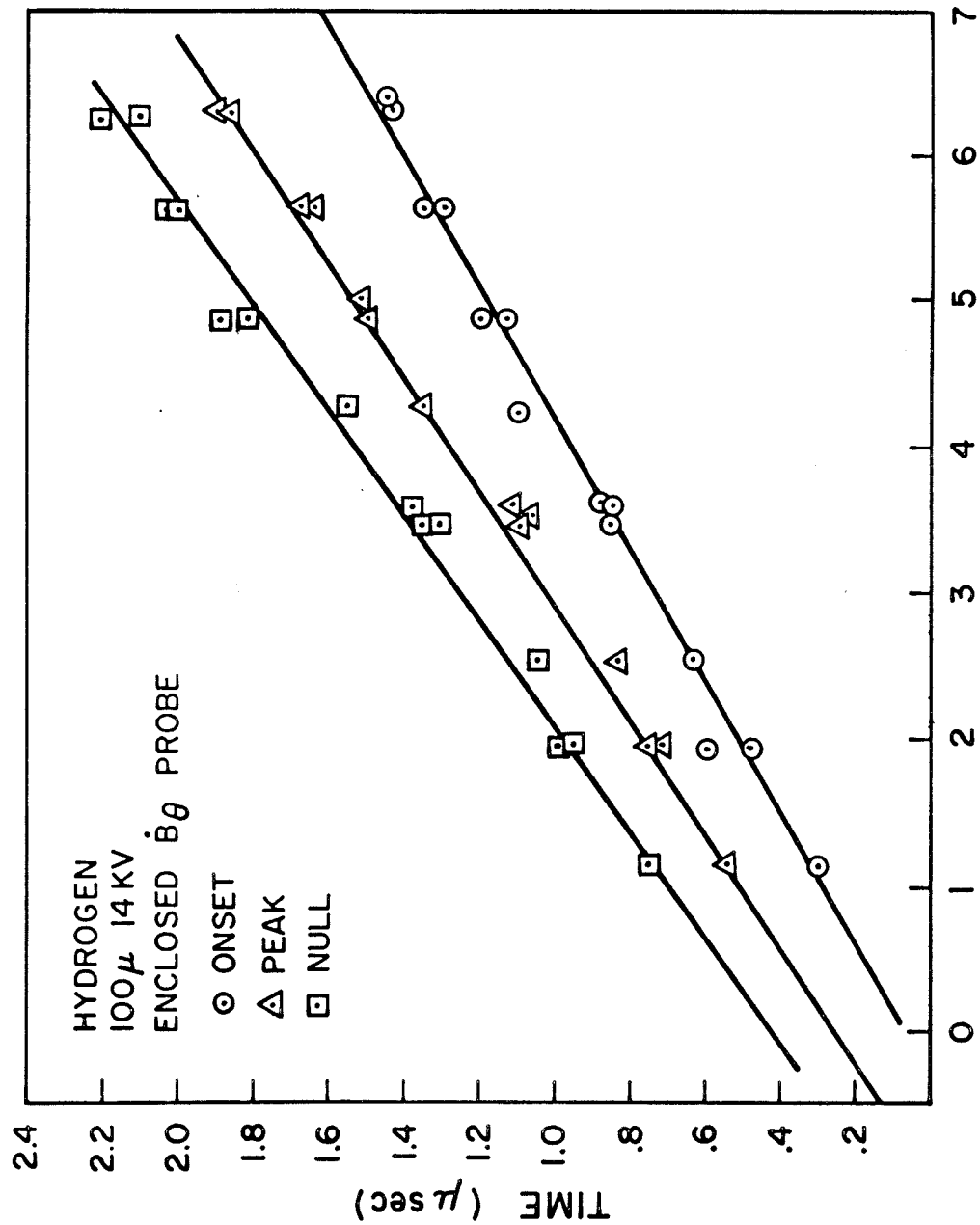

Figure 15. Enclosed Magnetic Probe Data, Hydrogen, 14 KV, 100μ

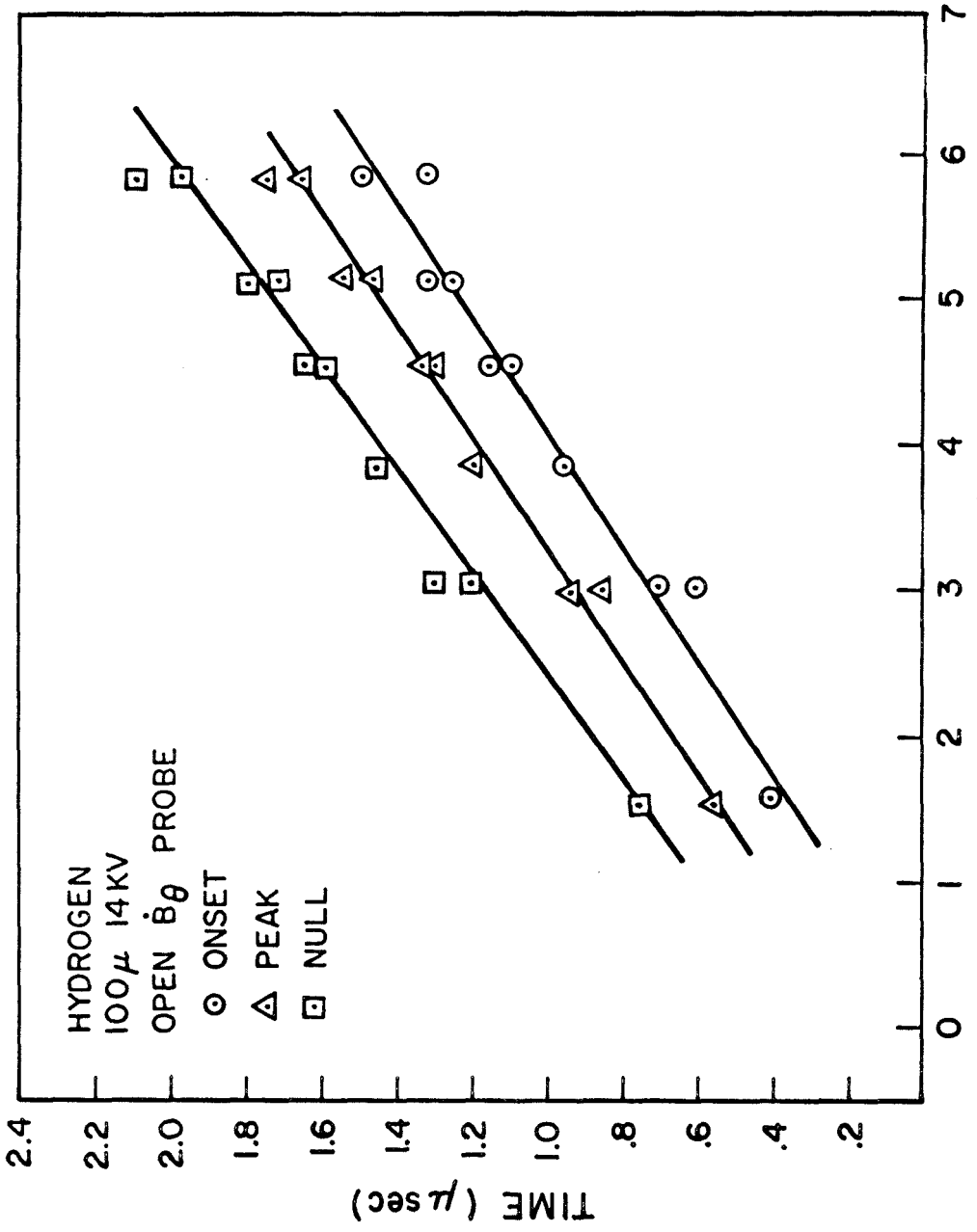

Figure 16. Open Magnetic Probe Data, Hydrogen, 14 KV, 100μ

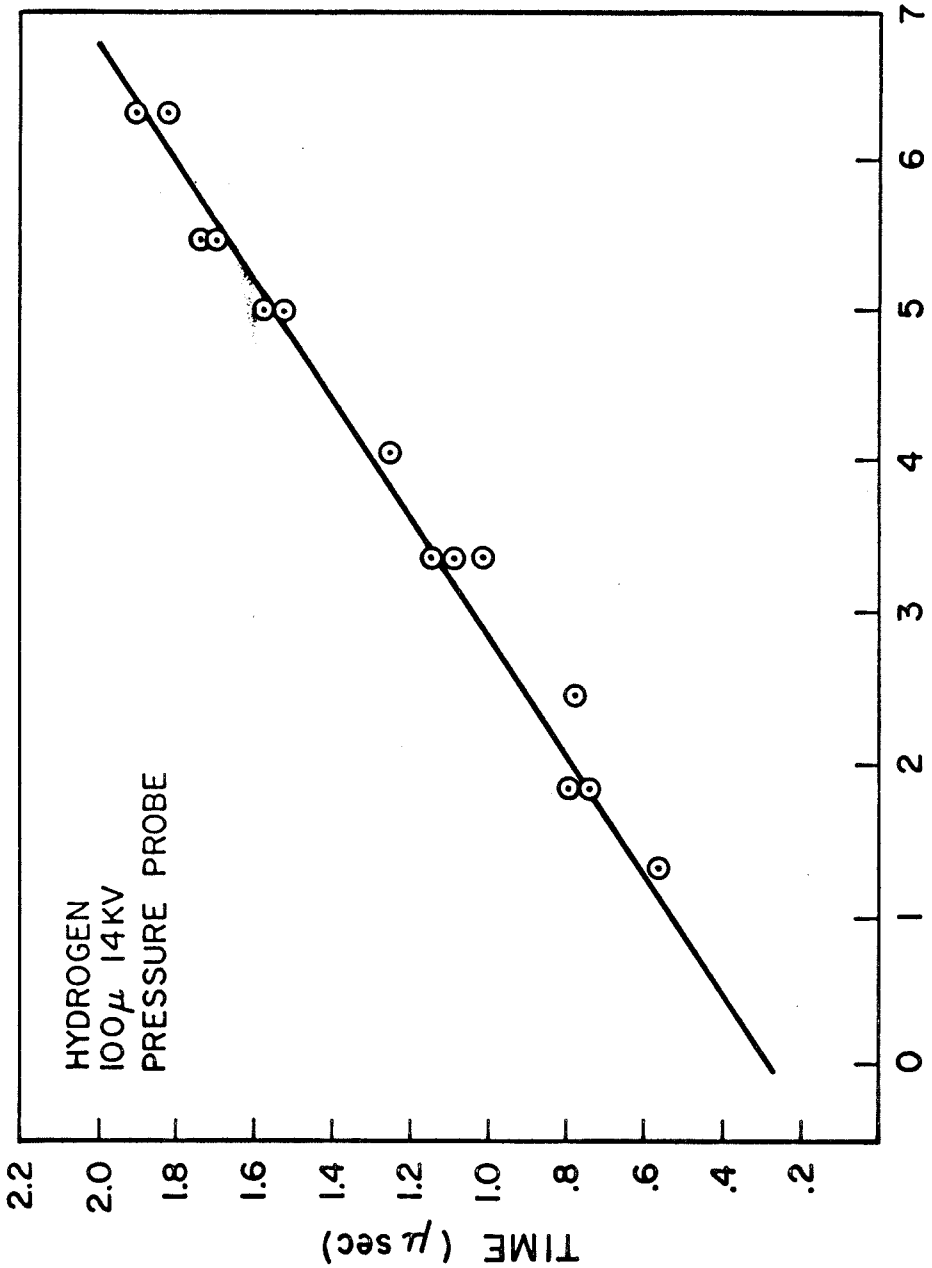

Figure 17. Pressure Probe Data, Hydrogen, 14 KV, 100μ

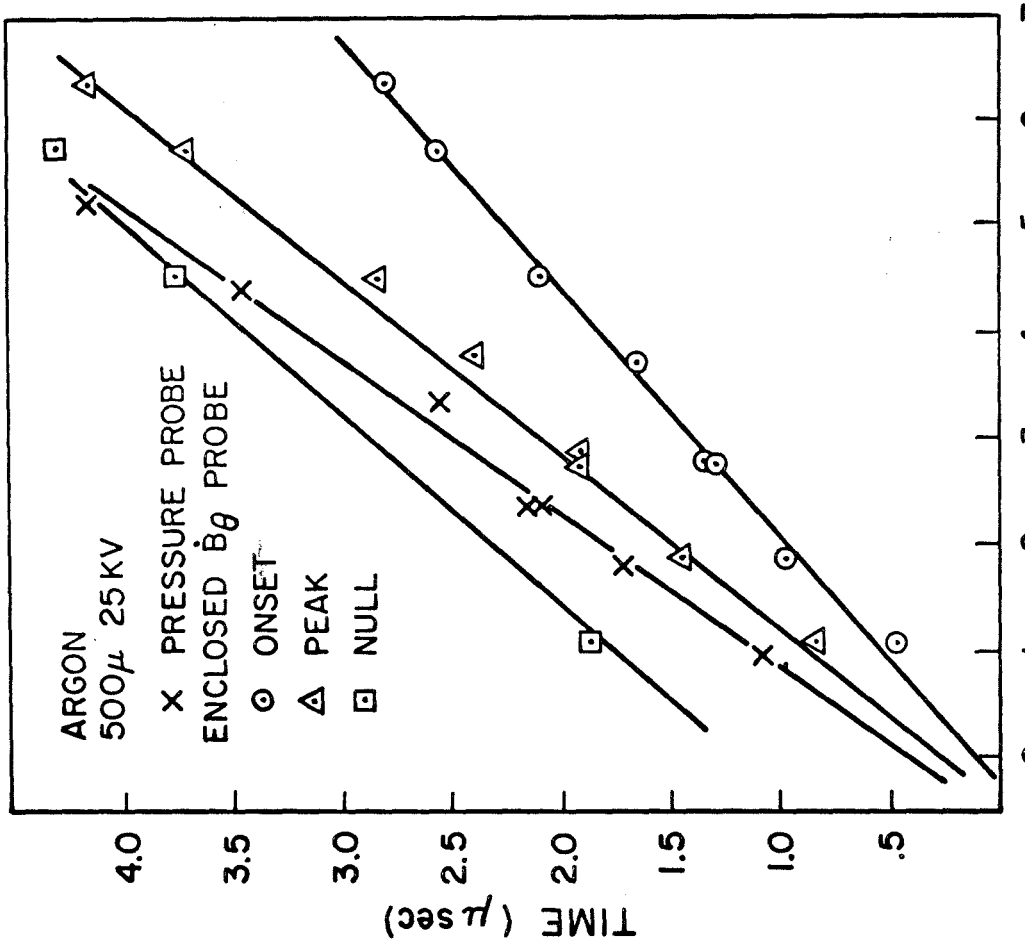

Figure 18. Magnetic and Pressure Probe Data, Argon, 25 KV, 500μ

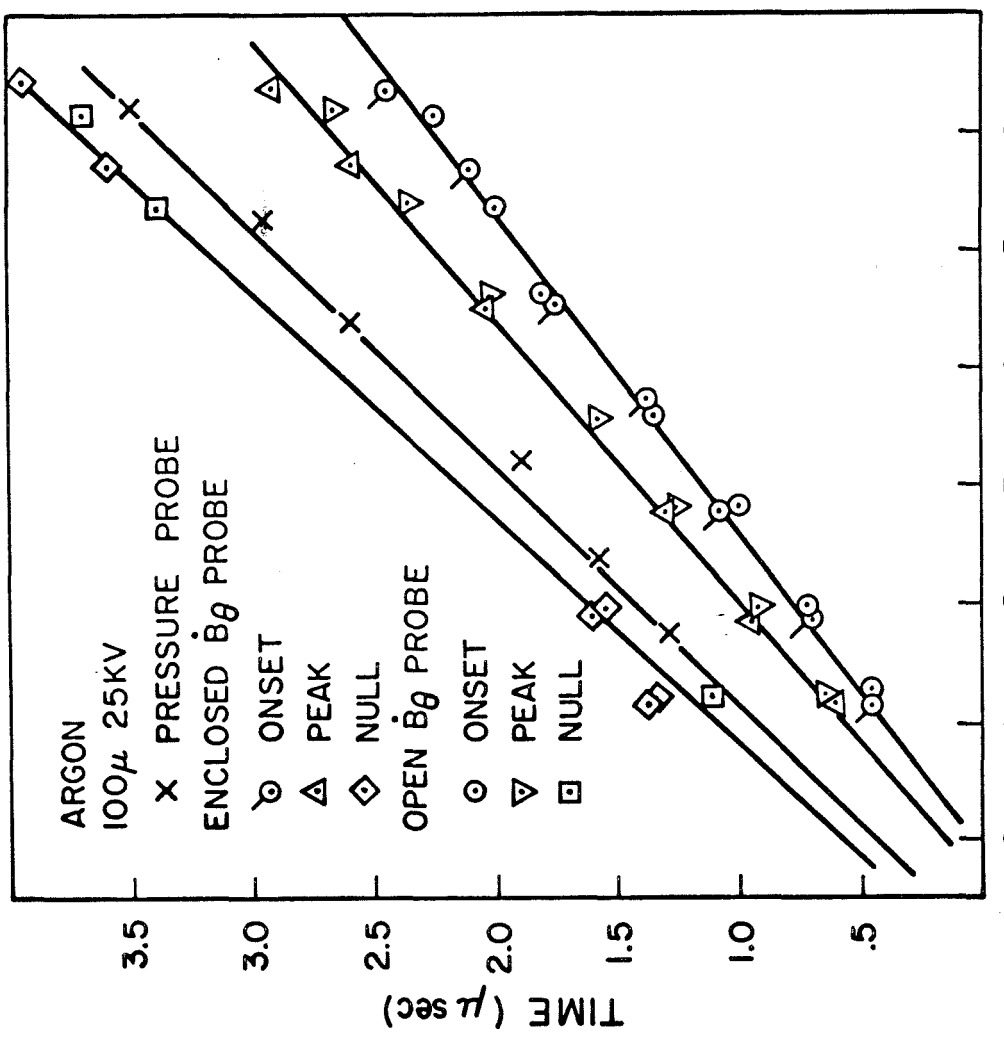

Figure 19. Magnetic and Pressure Probe Data, Argon, 25 KV, 100μ

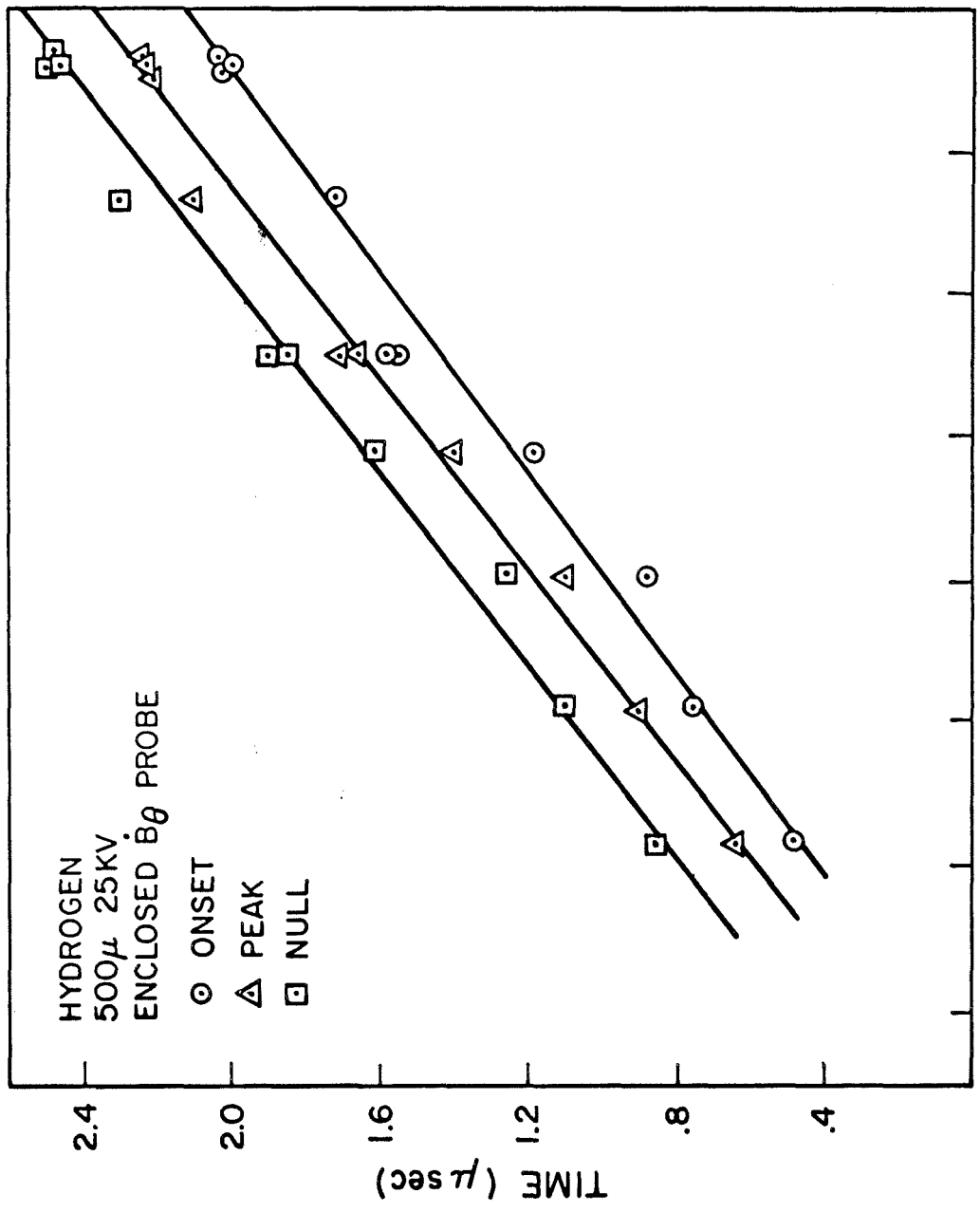

Figure 20. Enclosed Magnetic Probe Data, Hydrogen, 25 KV, 500μ

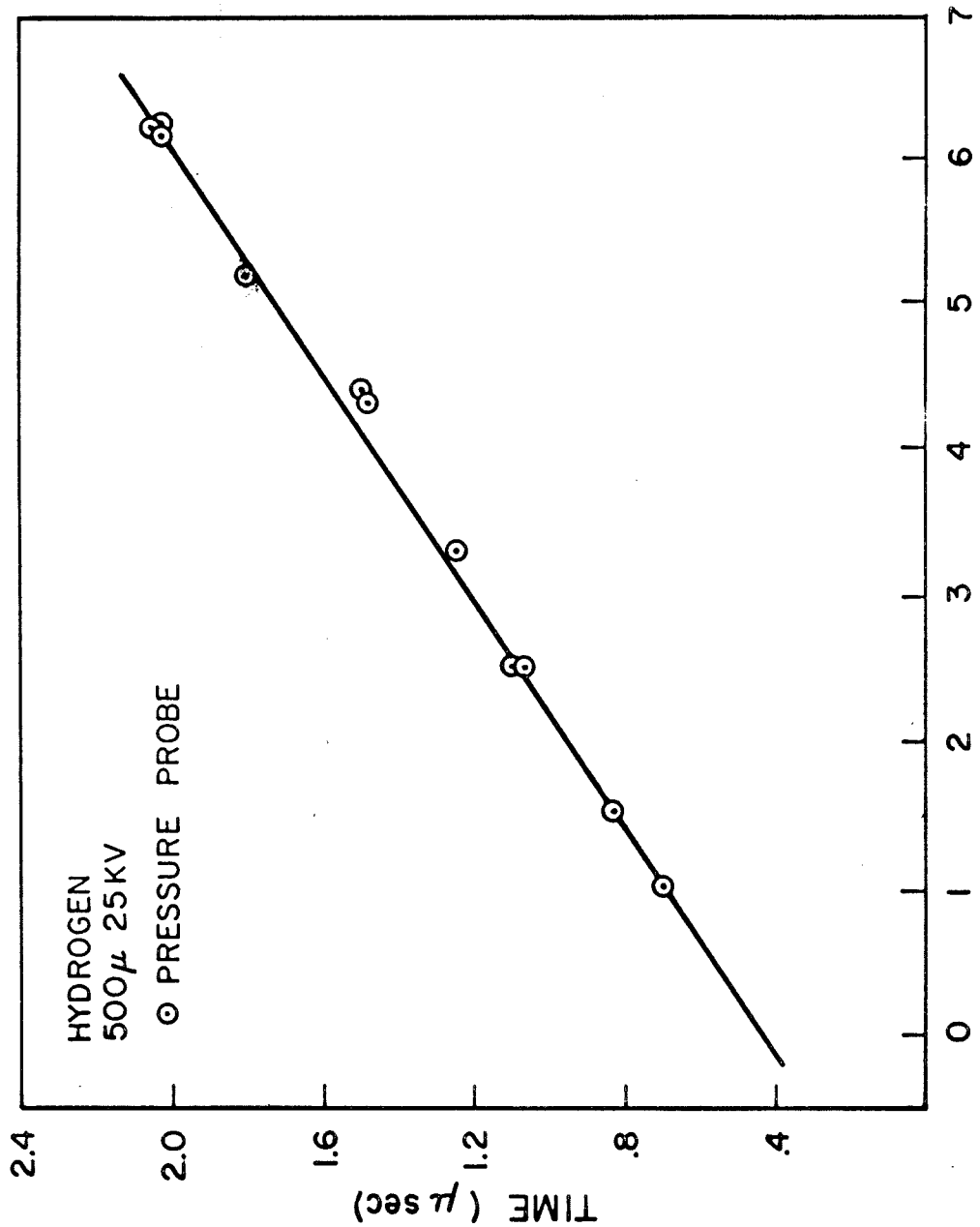

Figure 21. Pressure Probe Data, Hydrogen, 25 KV, 500μ

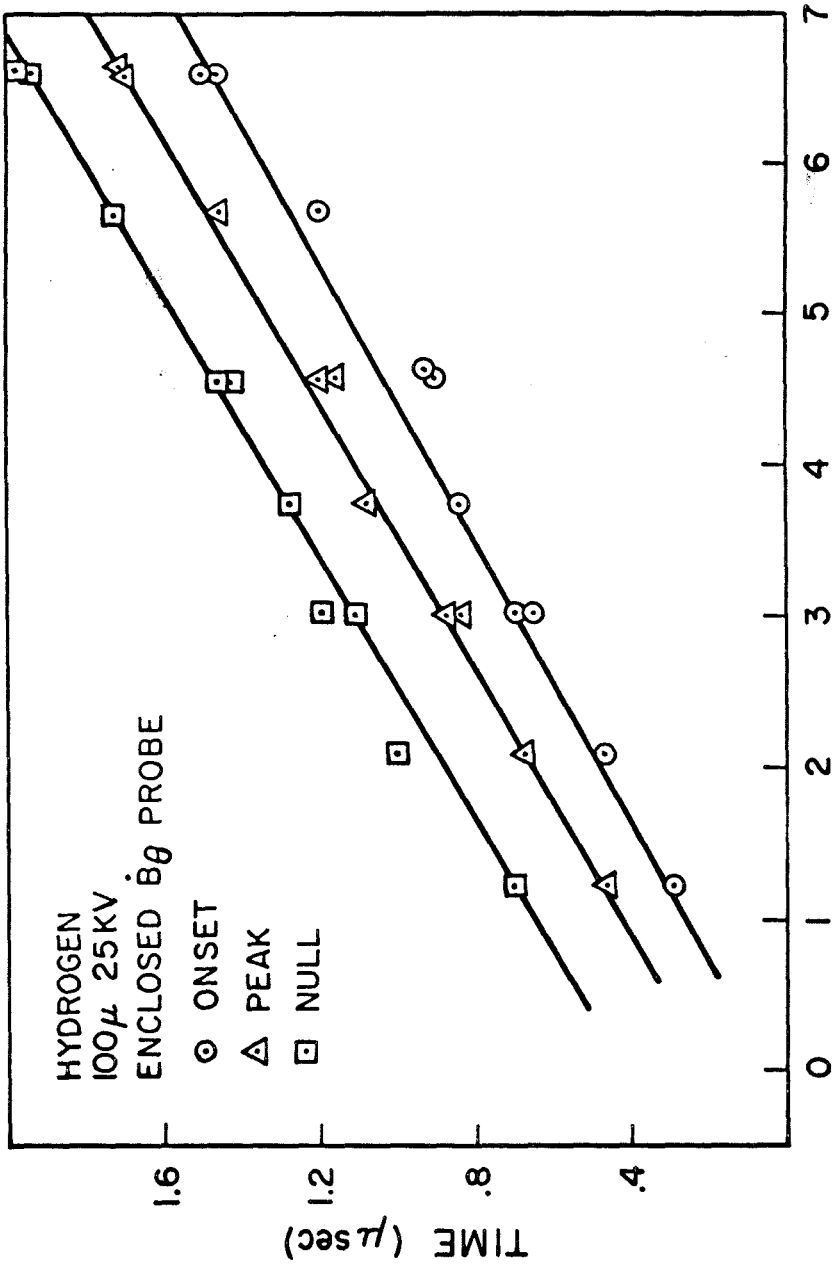

Figure 22. Enclosed Magnetic Probe Data, Hydrogen, 25 KV, 100μ

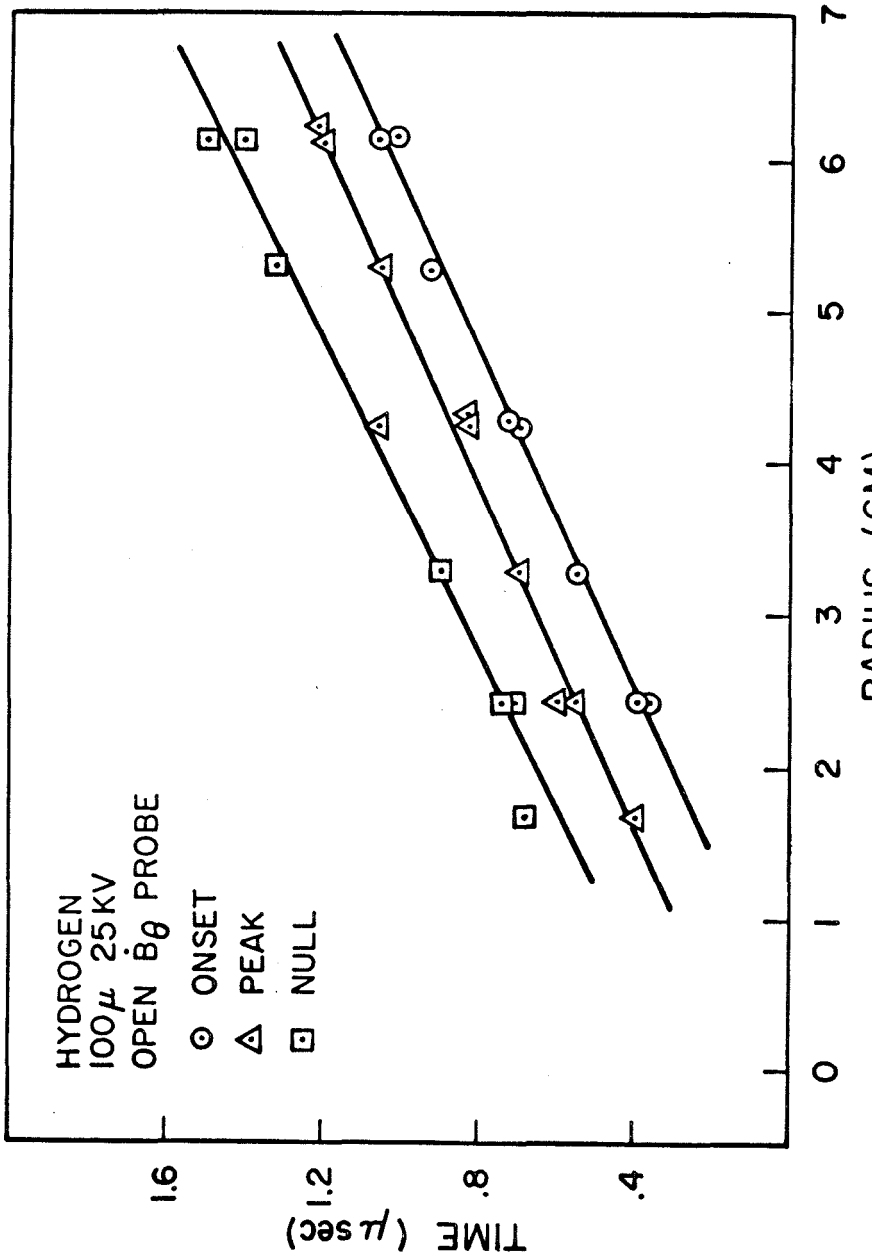

Figure 23. Open Magnetic Probe Data, Hydrogen, 25 KV, 100μ

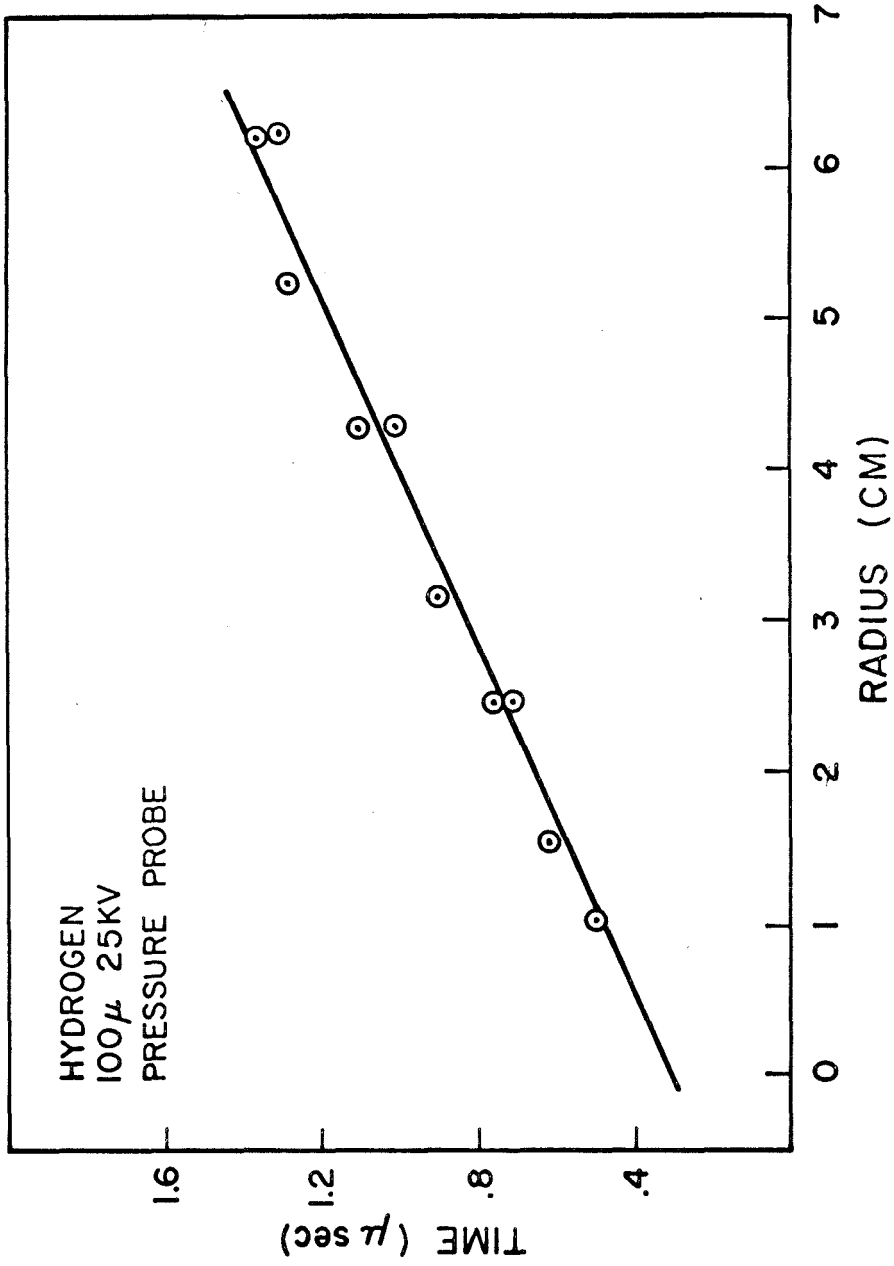

Figure 24. Pressure Probe Data, Hydrogen, 25 KV, 100μ

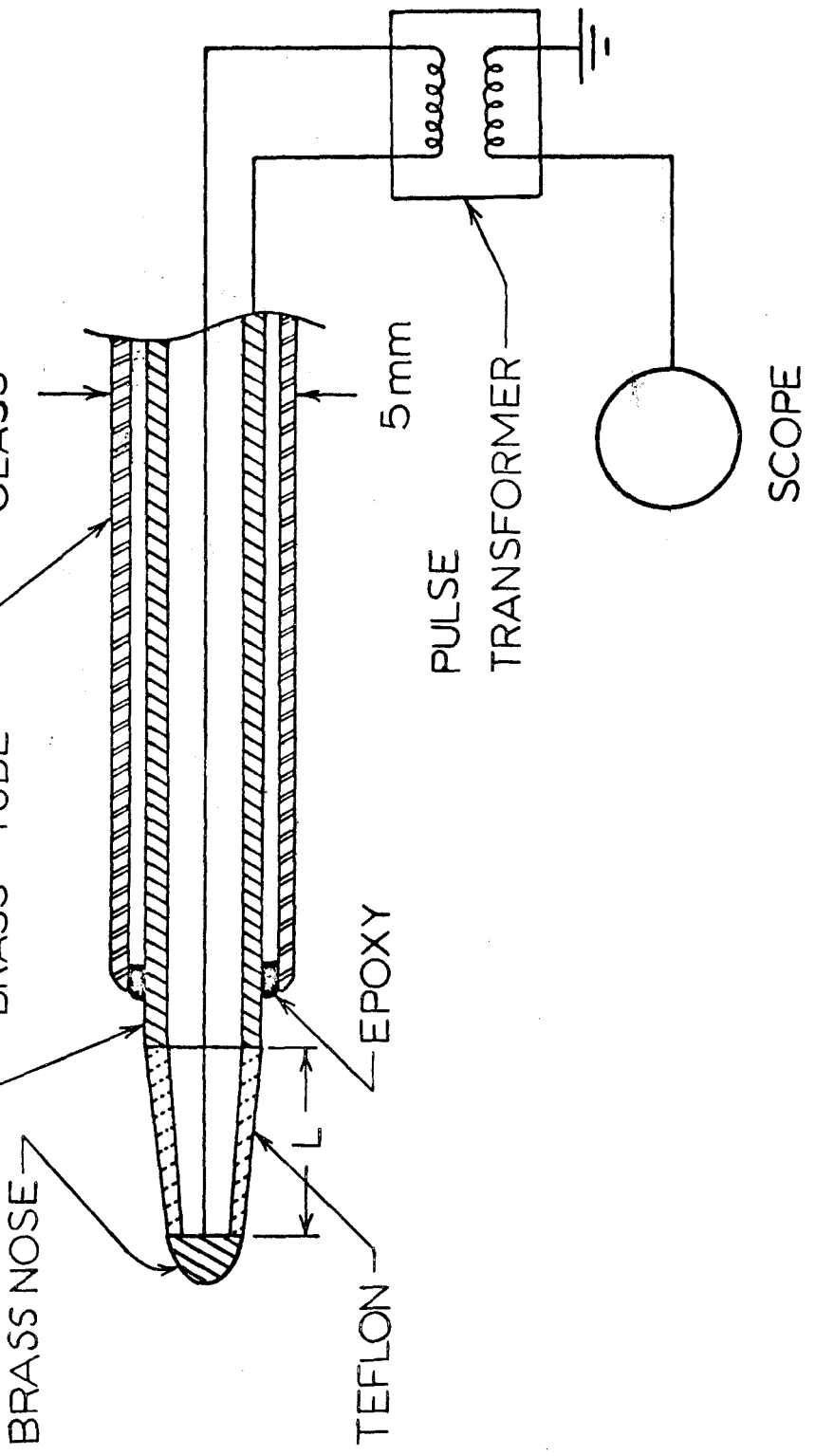

Figure 25. Basic Radial Electric Field Probe

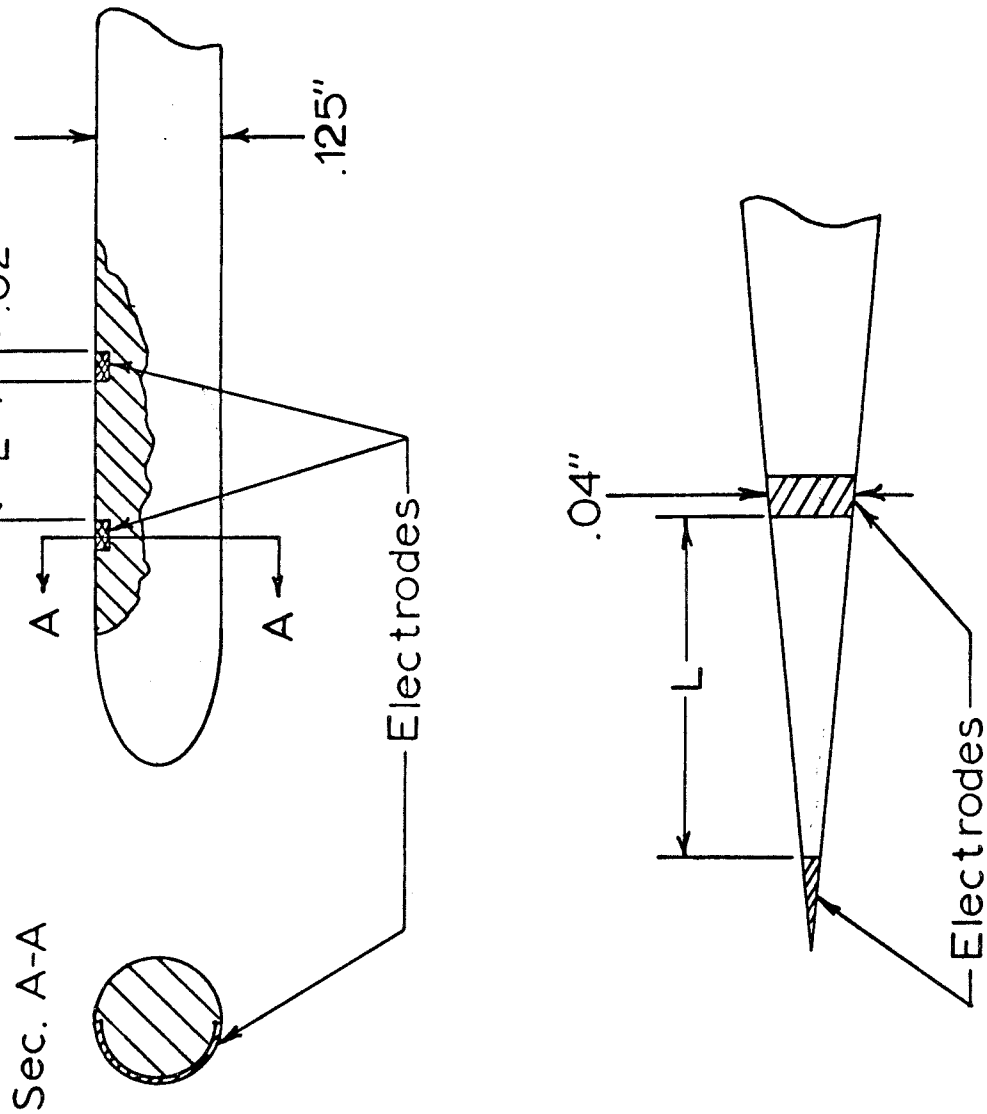

Figure 26. Different Shaped Radial Electric Field Probes

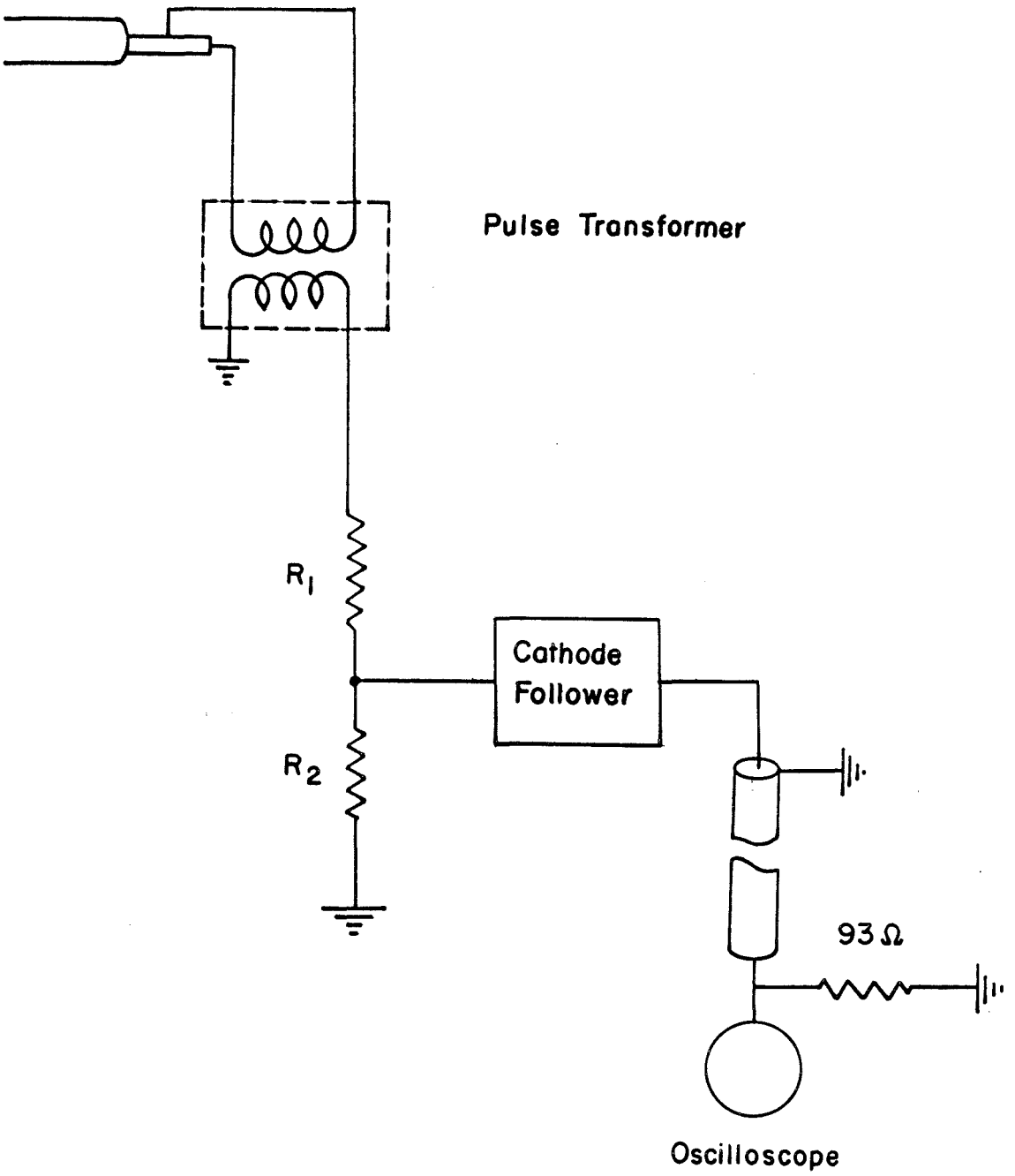

Figure 27. Circuit for the Radial Electric Field Probes

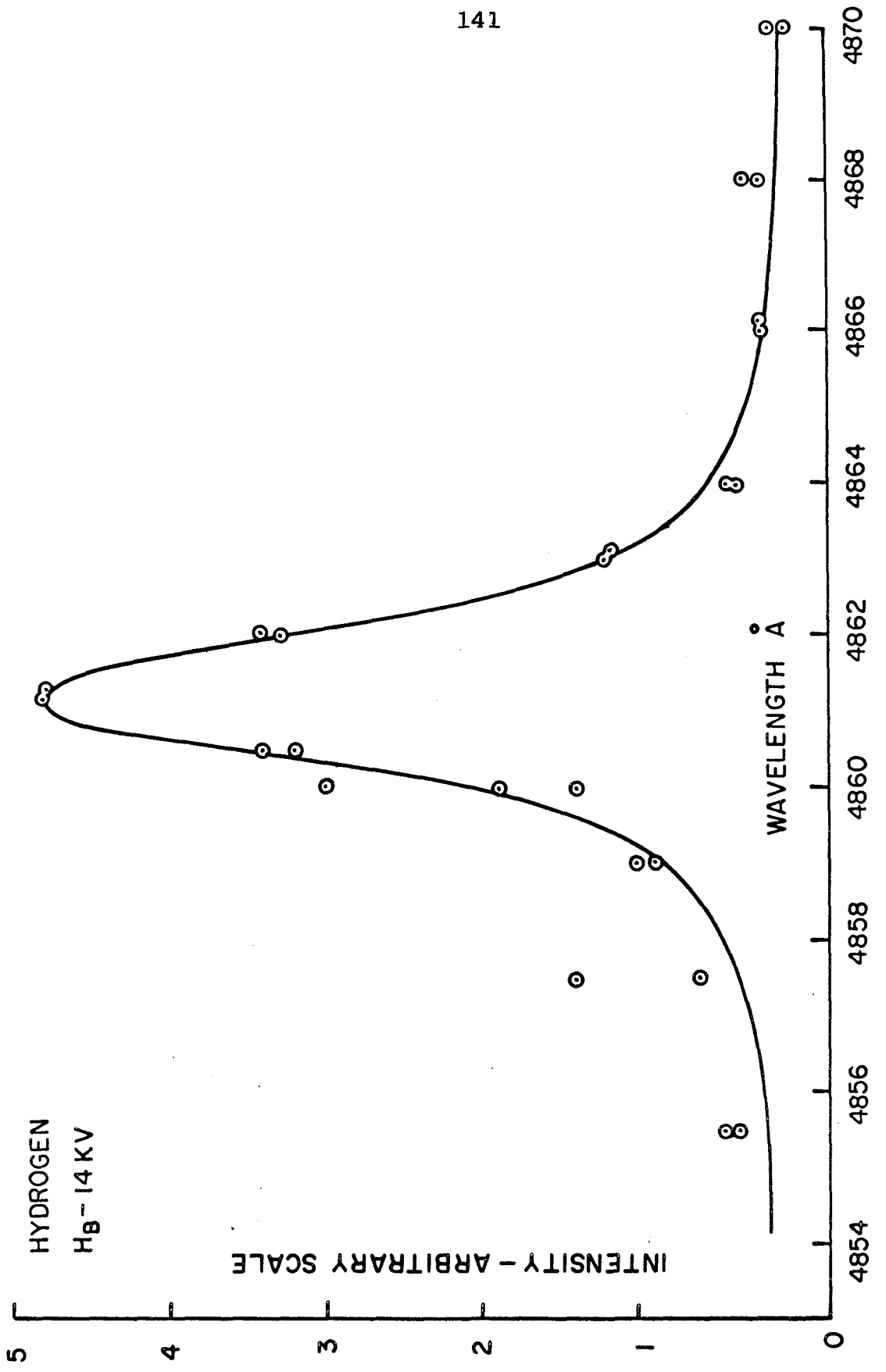

Figure 28. Line Profile for Hydrogen, H_β

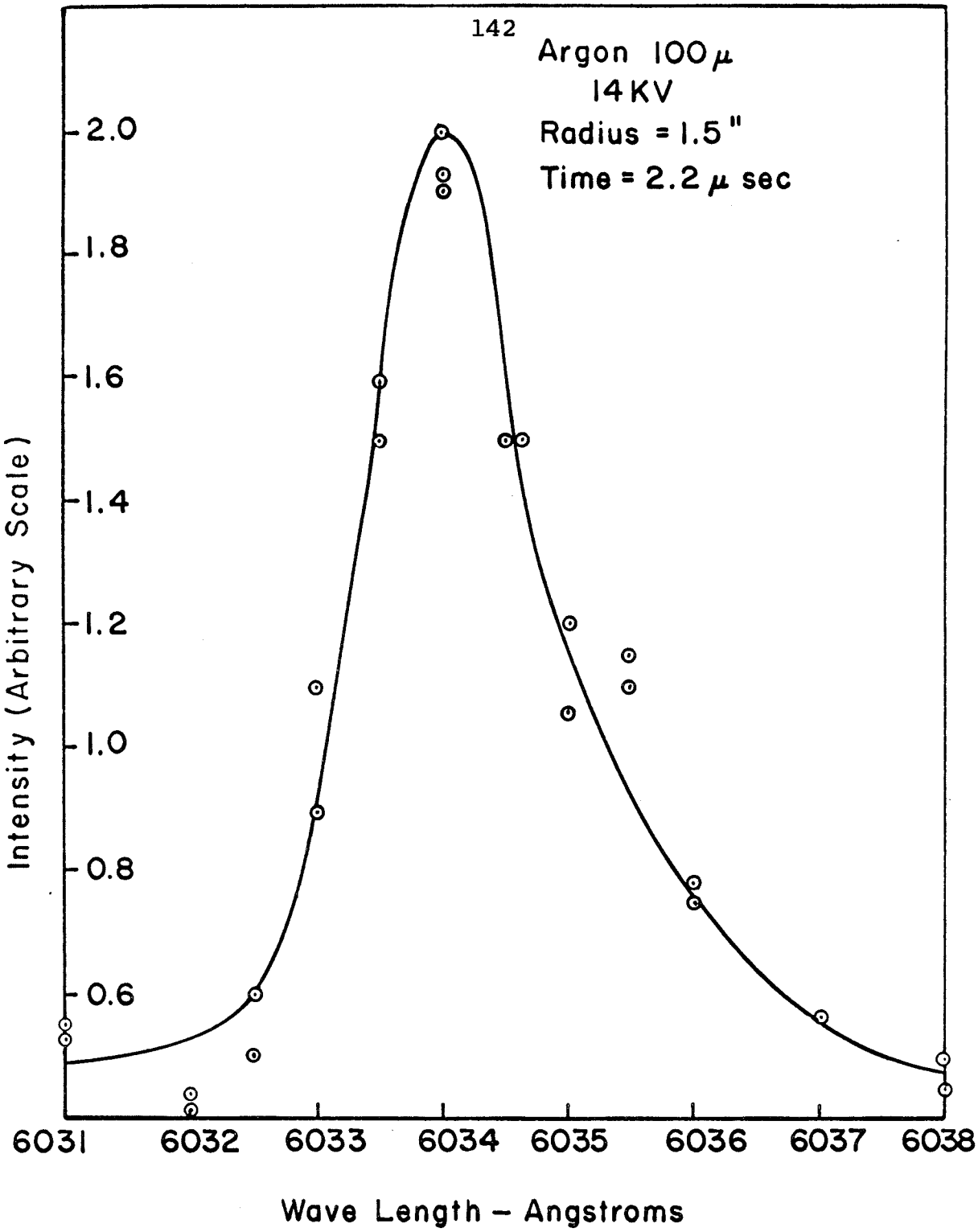

Figure 29. Line Profile for Argon I, 6032 Å

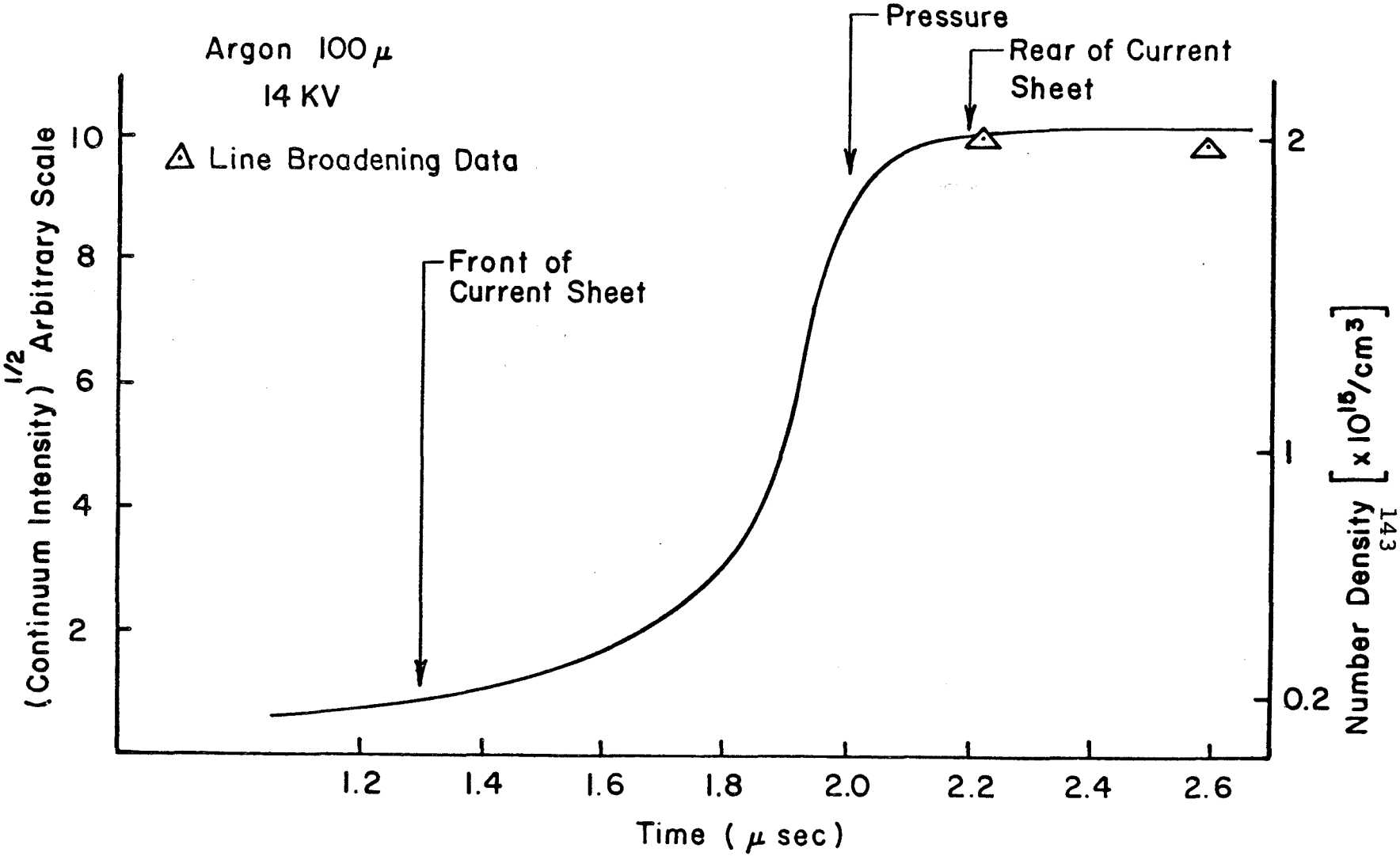

Figure 30. Continuum Intensity for Argon